Aus dem Pathologischen Institut der Ludwig-Maximilians-Universität München

Direktor: Prof. Dr. med. Thomas Kirchner

In der Arbeitsgruppe Experimentelle und Molekulare Pathologie

Leiter: Prof. Dr. rer. nat. Heiko Hermeking

Role of the p53/miR-34a Pathway in the Response to Tumor Hypoxia

---

Dissertation zum Erwerb des Doktorgrades der Naturwissenschaften (Dr. rer. nat.) an der Medizinischen Fakultät der Ludwig-Maximilians-Universität München

vorgelegt von

Huihui Li

aus Shandong, Volksrepublik China

2017

Gedruckt mit der Genehmigung der Medizinischen Fakultät

der Ludwig-Maximilians-Universität München

Erstgutachter: Prof. Dr. rer. nat. Heiko Hermeking

Zweitgutachter: Professor Dr. Peter Jon Nelson

Dekan: Prof. Dr. med. dent. Reinhard Hickel

Tag der mündlichen Prüfung: 14.12.2017

To my family.

Eidesstattliche Versicherung

Huihui Li

Ich erkläre hiermit an Eides statt, dass ich die vorliegende Dissertation mit dem Thema

“Role of the p53/miR-34a pathway in the response to tumor hypoxia”

selbständig verfasst, mich außer der angegebenen keiner weiteren Hilfsmittel bedient und alle Erkenntnisse, die aus dem Schrifttum ganz oder annähernd übernommen sind, als solche kenntlich gemacht und nach ihrer Herkunft unter Bezeichnung der Fundstelle einzeln nachgewiesen habe.

Ich erkläre des Weiteren, dass die hier vorgelegte Dissertation nicht in gleicher oder in ähnlicher Form bei einer anderen Stelle zur Erlangung eines akademischen Grades eingereicht wurde.

Ort, Datum:_____ Unterschrift:_____

Publications

The results of this thesis have been published in the following articles:

Original article:

Li H., Rokavec M., Jiang L., Horst D., Hermeking H. (2017). Antagonistic Effects of p53 and HIF1A on microRNA-34a Regulation of PPP1R11 and STAT3 and Hypoxia-induced Epithelial to Mesenchymal Transition in Colorectal Cancer Cells. Gastroenterology.

DOI: http://dx.doi.org/10.1053/j.gastro.2017.04.017

Reviews:

Rokavec M., **Li H.**, Jiang L., and Hermeking H. (2014). The p53/miR-34 axis in development and disease. J Mol Cell Biol 6, 214-230.

Rokavec M., **Li H.**, Jiang L., and Hermeking H. (2014). The p53/microRNA connection in gastrointestinal cancer. Clin Exp Gastroenterol 7, 395-413.

In addition, I made contributions to the following articles, which are not further described here:

Original articles:

***Equal contribution**

Li H.*, Rokavec M. *, and Hermeking H. (2015). Soluble IL6R represents a miR-34a target: potential implications for the recently identified IL-6R/STAT3/miR-34a feed-back loop. Oncotarget 6, 14026-14032.

Rokavec M.*, Öner M.G.*, **Li H.***, Jackstadt R.*, Jiang L, Lodygin D., Kaller M., Horst D., Ziegler P.K., Schwitalla S., Slotta-Huspenina J., Bader F.G., Greten F.R., Hermeking H. (2014). IL-6R/STAT3/miR-34a feedback loop promotes EMT-mediated colorectal cancer invasion and metastasis. J Clin Invest. 124(4):1853-67.

Shi L.*, Jackstadt R.*, Siemens H., **Li H.**, Kirchner T., Hermeking H. (2014). p53-induced miR-15a/16-1 and AP4 form a double-negative feedback loop to regulate epithelial-mesenchymal transition and metastasis in colorectal cancer. Cancer Res. 74(2):532-42.

Abbreviations

CRC	colorectal cancer
CIN	chromosomal instability
CIMP	CpG island methylator phenotype
MSI	microsatellite instability
TSS	transcriptional start site
HRE	hypoxia-response element
EMT	epithelial-mesenchymal transition
MET	mesenchymal-epithelial transition
miRNAs	microRNAs
EMT-TF	EMT-inducing transcription factor
IL-6	interleukin-6
IL-6R	IL-6 receptor
ZEB	zinc finger E-box-binding homeobox protein
bHLH-PAS	basic helix–loop–helix-PER-ARNT-SIM
HIF1A	hypoxia-inducible factor-1A
VHL	von-Hippel–Lindau
STAT3	signal transducers and activators of transcription 3
PP1	protein phosphatase 1
S727	serine 727
Y705	tyrosine 705
FCS	fetal calf serum
5-FU	5-fluorouracil
DMSO	dimethyl-sulfoxide
APC	adenomatous polyposis coli
APS	ammonium peroxodisulfate
TEMED	tetramethylethylendiamin,1,2-bis (dimethylamino) –ethan
SDS	sodium dodecyl sulfate
PFA	paraformaldehyde
DAPI	2-(4-Amidinophenyl)-6-indolecarbamidine-dihydrochloride
dNTPs	deoxynucleotides triphosphate
WB	Western blot analysis
IF	indirect immunofluorescence
ChIP	chromatin immuno-precipitation
Co-IP	co-immunoprecipitation
IHC	immunohistochemical analysis
bp	base pair
kbp	kilo base pairs
Cy3	cyanine 3
cDNA	complementary DNA
E.coli	*Escherichia coli*

Abbreviations

DNA	deoxyribonucleic acid
DOX	doxycycline
gDNA	genomic DNA
HBSS	Hank's balanced salt solution
eGFP	enhanced green fluorescent protein
HDF	human diploid fibroblast
HRP	horseradish peroxidase
IgG	immunoglobulin
DMEM	Dulbecco`s modified Eagles medium
LB	lysogeny broth
PCR	Polymerase chain reaction
MEF	mouse embryonic fibroblast
$CoCl_2$	Cobalt (II) chloride
FACS	fluorescence-activated cell sorting
qPCR	quantitative real-time PCR
ECL	enhanced chemiluminescence
CLSM	confocal laser scanning microscopy
ORF	open reading frame
PAGE	polyacrylamide gel electrophoresis
P/C	phase contrast
IVC	individually ventilated cages
FFPE	formalin-fixed, paraffin-embedded
TMA	tissue microarray
PBS	phosphate buffered saline
UTR	untranslated region
VSV	vesicular stomatitis virus (tag)
SD	standard deviation
SDS	sodium dodecyl sulfate
siRNA	small interfering RNA

Table of contents

1. Introduction

1.1 Cancer and colorectal cancer

1.1.1 The hallmark of cancer

Cancer is the second most common cause of death globally, and was responsible for 8.2 million deaths in 2012 [1]. Approximately 14 million new cases were diagnosed with cancer in the world in 2012 [1]. Cancer is a heterogeneous disease caused by mutations and epigenetic changes [2]. Ten fundamental hallmark features common to most cancer cells were described by Hanahan and Weinberg [3, 4] (**Figure 1.1**):

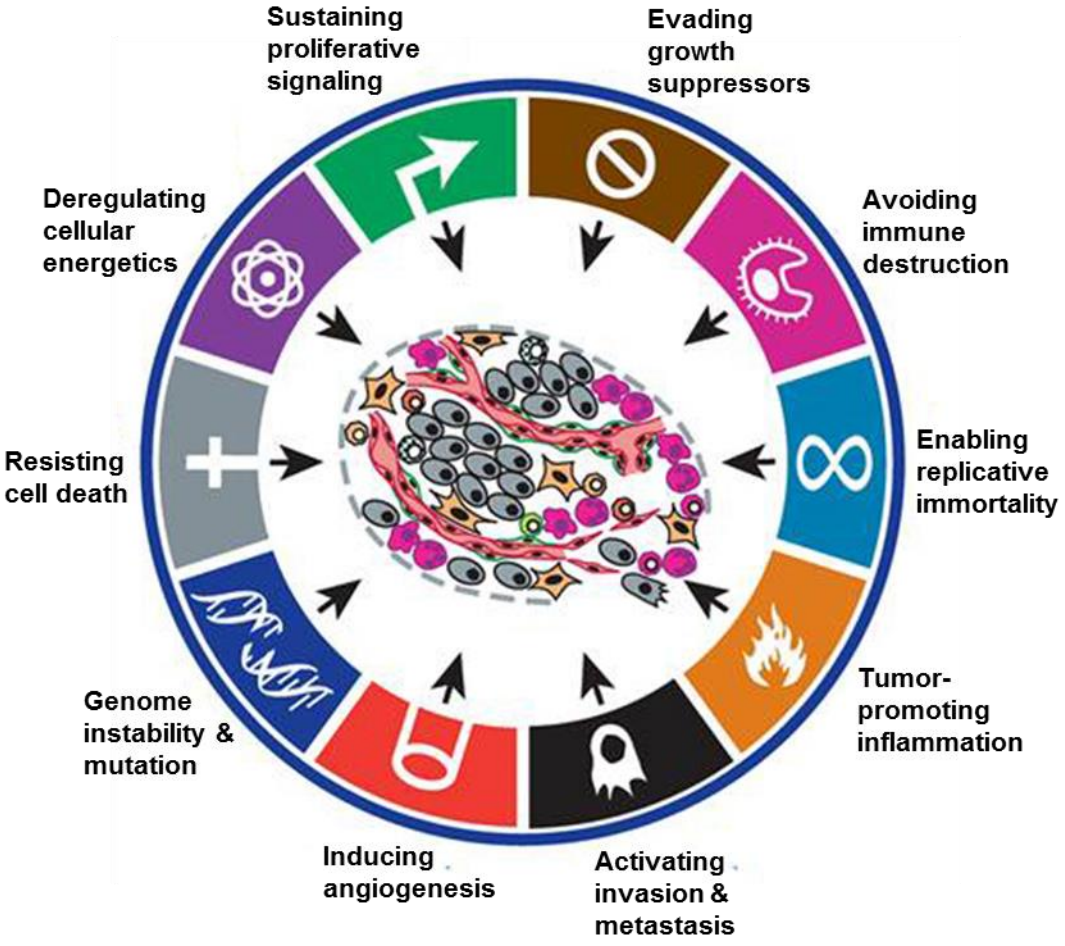

Figure 1.1 The hallmarks of cancer. Ten fundamental hallmark features acquired during tumor development. Figure from [3].

1.1.2 Colorectal cancer

Colorectal cancer (CRC) is the third most common cancer diagnosed and the fourth most common cancer cause of death globally [1]. The progressive accumulation of genetic and epigenetic alterations results in the transformation from normal epithelial cells to colorectal adenocarcinomas [5]. The molecular pathogenesis of colorectal cancer is heterogeneous. Three different mechanisms underlying CRC etiology, namely chromosomal instability (CIN), CpG island methylator phenotype (CIMP), and microsatellite instability (MSI), were described [6]. A classification of the molecular mechanisms underlying the development of CRC may be useful for determining the treatment response of patients [7, 8].

Cancer develops in a stepwise manner and each step is associated with changes at the molecular level. A widely accepted model of colorectal cancer progression was proposed by Fearon and Vogelstein [9]. Vogelstein and colleagues demonstrated that most colorectal cancers begin with mutations in the *adenomatous polyposis coli (APC)* gene. Subsequently, additional mutations of the RAS-pathway promote the transition from breakthrough phase to expansion phase (see also **Figure 1.2**). These two mutations lead to the abnormal proliferation and disordered cellular architecture that defines benign tumors [10]. Subsequent mutations in *SMAD4, TP53, PIK3CA,* and *FBXW7,* enable colorectal cancer cells to invade normal tissues and grow in otherwise hostile environments; such cells are defined as malignant [10]. However, so far no genetic alterations have been shown to be required to convert a malignant primary tumor into a metastatic lesion [10]. Therefore, malignant tumor cells may already possess the capacity to metastasize [10].

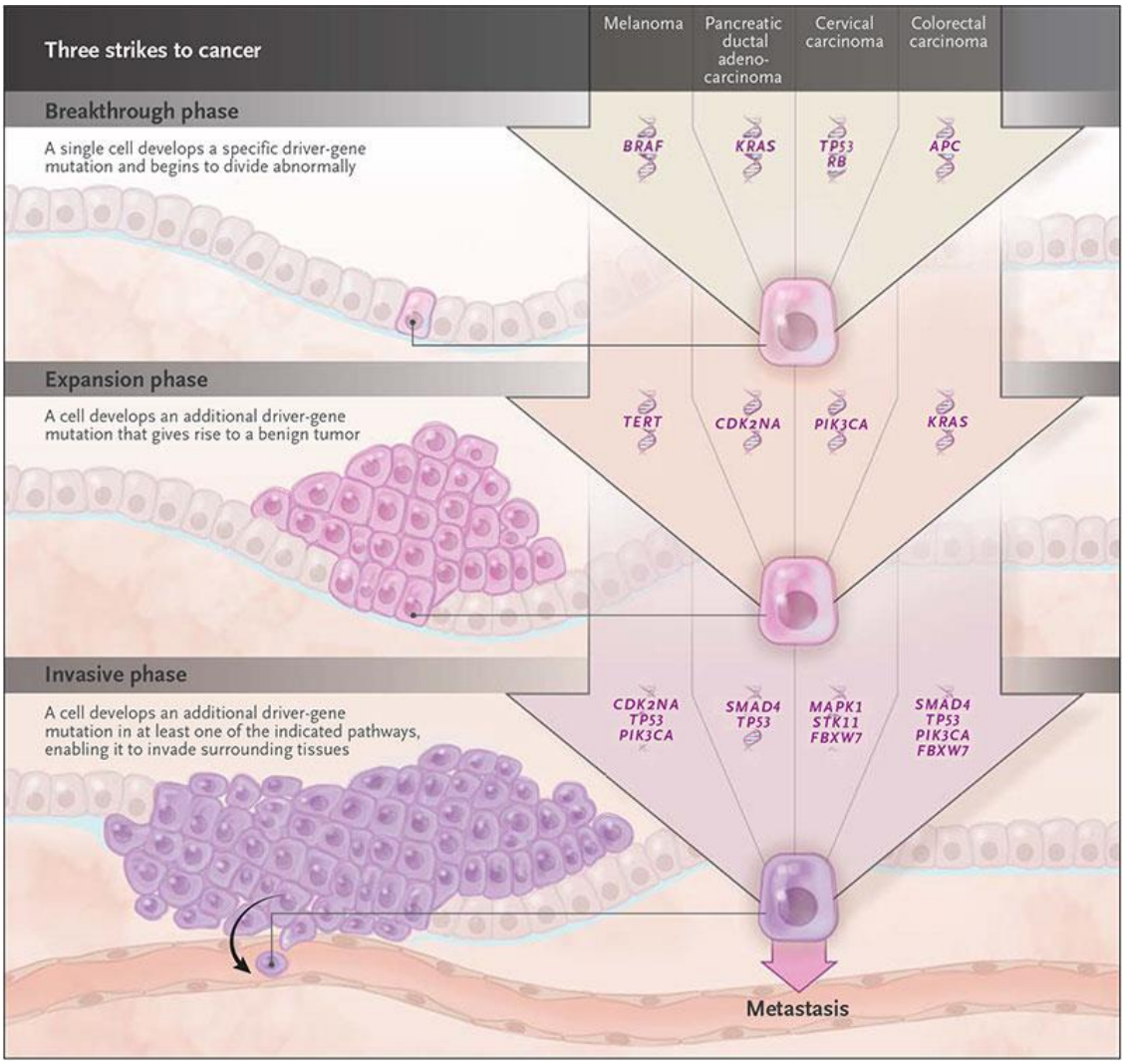

Figure 1.2 Three Strikes to Cancer. Examples of the genetic alterations leading to four representative cancer types are shown. Each gene symbol denotes a pathway. For example, *APC* denotes the pathway regulated by *APC*. A "mutation" in a pathway can be achieved by genetic or epigenetic inactivation of both alleles of a tumor-suppressor gene or by genetic activation of an oncogene in that pathway. Pathogenic strains of human papillomavirus initiate the breakthrough phase by disabling both the *TP53* and *RB* pathways. Legend and figure from [10].

Approximately 90% of all cancer-related deaths are caused by metastases [11]. About one-fifth of CRC patients present with metastasis and after surgical treatment, 30 to 50% develop metastasis [12, 13]. In CRC, primary cancer cells spread via blood or lymph circulation to distant organs, such as the liver, peritoneum, lungs, bone and brain. The liver represents the most frequent site of CRC metastases. Approximately 55% of CRC patients develop liver metastasis.

1.2 Epithelial-Mesenchymal Transition

Epithelial-Mesenchymal Transition (EMT) is a cellular program that is important for the formation of tissues and organs during embryonic development and during wound healing [14]. During EMT, epithelial cells lose cell-cell adhesion and cell polarity and acquire properties of mesenchymal cells, such as enhanced migratory and invasive capacities.

1.2.1 EMT in tumor progression

EMT not only occurs during embryonic development, but also is an essential element in tumor progression and metastasis [15]. Cancer cells at the primary site acquire a mesenchymal phenotype, which allows them to invade surrounding tissues, intravasate into and extravasate from blood-vessels, and colonialize distant organs and tissues [15, 16] (**Figure 1.3**). After seeding, these cells switch back to an epithelial phenotype and proliferate to form metastases [15]. The processes by which cells switch between epithelial and mesenchymal phenotypes are known as the epithelial-to-mesenchymal transition (EMT) and its counterpart, the mesenchymal-to-epithelial transition (MET) [17] (**Figure 1.3**). During metastasis formation, primary tumor cells accumulate genetic and epigenetic changes, which enable these to escape from the tumor mass and invade into surrounding tissue [18, 19]. Alterations of gene expression in the tumor microenvironment may also contribute to this process [20, 21]. In patient samples, EMT is observed in the invasive front of various tumor types, indicating that micro-environmental signals trigger and control EMT [22-24]. EMT also contributes to tumor stemness, escape from senescence, evasion of the immune system, chemo-resistance as well as tumor relapse [19].

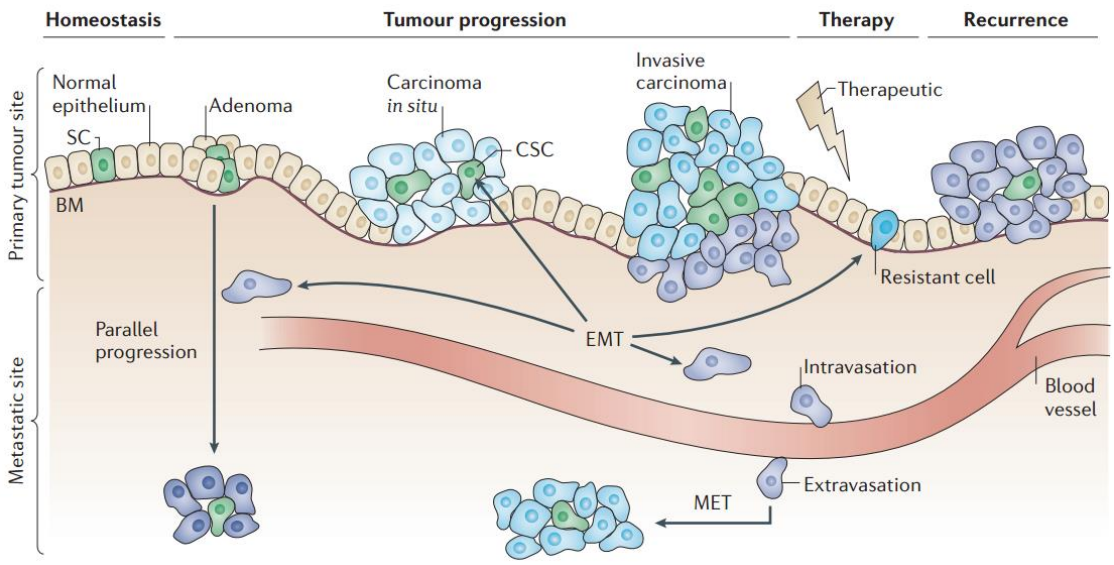

Figure 1.3 Role of EMT during cancer progression. In tumor cells, EMT transcription factors (EMT-TFs) may primarily redefine the epithelial status of the cell, potentially - but not necessarily - assigning stem cell (SC) characteristics to dedifferentiated tumor cells, or they may redefine resident genetically altered stem cells to be cancer stem cells (CSCs). The dissemination of tumor cells from the solid tumor and subsequent migration after breakdown of the basement membrane (BM) - the classical view of the role of EMT in cancer — can only be achieved when all component pathways of the network are activated and fully parallels the process that is seen in development: if the cancer cell has acquired the necessary genetic aberrations and receives the appropriate signals at the tumor-host interface, the cell is ready to move towards metastasis. At this point, the active contribution of the EMT-associated programme is probably to give survival signals and to maintain the mesenchymal status of the metastasizing cell. It is likely that EMT also has a role in parallel progression, in which tumor cells escape early and metastasis progresses in parallel to the primary tumor. EMT features may further promote resistance during tumor therapy, leading to recurrence and a poor prognosis. The degree of EMT during the different steps in cancer progression probably depends on the imbalance of several associated regulatory networks with activated oncogenic pathways. Legend and figure from [25].

1.2.2 Regulation of EMT

Much effort has been devoted to understanding the regulatory mechanism of EMT. A number of distinct signaling pathways regulate EMT [14]. The best studied regulatory network controlling EMT is the transcriptional control. EMT transcription factors (EMT-TFs) are up-regulated in many different tumors [15]. EMT-TFs are central regulators of EMT [26, 27]. The zinc-finger transcription factor SNAIL is the best studied TF that regulates EMT [28]. The expression of SNAIL inversely correlates with the

expression of E-cadherin [26]. Indeed, SNAIL directly binds to an E-box (CACCTG) in the promoter of *CDH1* [28]. Peinado *et al.* also showed that the expression of SNAIL is associated with poor prognosis, tumor recurrence, and metastasis in breast carcinomas [26]. The transfection factor ZEB (zinc finger E-box-binding homeobox protein) induces EMT and directly binds to an E-box of *CDH1* [29]. The EMT transcription factor TWIST is also a key regulator of EMT [26]. As described below in **chapter 1.3.3**, ZNF281 represents a new EMT-promoting transcription factor that participates in these regulatory networks [30]. Moreover, the transfection factor STAT3 that mediates EMT induced by the pro-inflammatory cytokine IL-6, and thereby promotes invasion and metastasis of CRC cell lines [31].

Some other epithelium-specific transcription factors, such as GRHL2, ELF3 and ELF5, are decreased during EMT and actively drive MET when overexpressed in mesenchymal cells. All these findings suggest the concept of a tightly controlled balance between the epithelial and the mesenchymal status [25].

Besides EMT-TFs, epigenetic changes also contribute to EMT [32]. The epigenetic regulation of *CDH1* promoter has been recognized as part of the program that results in EMT [33, 34]. For example, it has been shown that the hyper-methylation of *CDH1* correlates with the expression of SNAIL [35] and that ZEB1 modifies chromatin at the *CDH1* promoter via recruiting SIRT1 deacetylase [36].

1.3 The p53/microRNA-34 axis in colorectal cancer

1.3.1 The p53 tumor suppressor protein

TP53, which encodes the p53 protein, is one of the most frequently mutated genes in human cancers. It has been reported that more than 80% of CRCs show inactivation of *TP53* by mutation [37]. The p53 protein represents a transcription factor, that is activated by diverse cellular stresses, such as DNA damage, ribosomal stress, oncogene activation and lack of oxygen or other nutrients and exerts multiple tumor suppressive functions through regulating the expression of its target genes [38]. For example, p53 promotes cell cycle arrest, senescence, and apoptosis [39, 40]. Under

conditions of stress and damage, p53 suppresses tumorigenesis either by supporting the repair of cells or eliminating damaged cells that cannot be repaired [41].

Recently, microRNAs have been added to the list of p53 targets that mediate its tumor suppressive function [42]. p53 regulates the expression of its target miRNAs by direct binding to their promoters, as shown for *miR-34a/b/c, miR-200, miR-15a/16*-1, *miR-192/194/215*, *miR-145* and *miR-107*. Alternatively, p53 regulates the processing of miRNA precursors, which has been shown for *miR-16-1*, *miR-145*, and *miR-199a-3p* [43]. p53 also directly controls the transcription of genes that are involved in canonical metastasis pathways [44]. Therefore, loss the function of p53 promotes migratory and invasive properties [44], which allows tumor cells to invade into surrounding tissues, enter into circulation and extravasate into secondary sites [45]. The suppression of metastasis by p53 is mediated via the inhibition of factors [46, 47], which initiate and maintain EMT programs [25]. Numerous EMT-TFs are repressed by p53-induced miRNAs. In colorectal cancer, p53 negatively regulates EMT by suppressing the expression of SNAIL and ZEB1 [48, 49]. In addition, our lab recently showed that the zinc finger 281 protein (ZNF281) and the STAT3 pathway are integrated into the p53 regulatory network via miR-34a [30, 31]. Despite abundant evidence showing that metastatic processes are repressed by p53, *TP53* knockout mice tumors do not metastasize frequently or display invasive physiologic characteristics [50, 51], suggesting that p53 loss alone is not sufficient to drive invasive cellular migration *in vivo*.

1.3.2 microRNAs and miR-34 family

microRNAs (miRNAs), a subset of non-coding RNAs, are ~22 nucleotides long, single-stranded RNAs that exert biological functions by repressing the translation of target protein-encoding genes [52]. miRNAs were first discovered as regulators of development in the nematode *Caenorhabditis elegans* [53, 54]. Afterward, thousands of miRNA genes have been identified in animal and plant genomes [55]. miRNAs are involved in many human diseases [56] and participate in the regulation of almost every

cellular process, such as proliferation, cell cycle control, apoptosis, differentiation, angiogenesis, migration, metabolism, autophagy, and stemness [57-61]. Currently, miRNAs are being tested as targets and therapeutics to combat diseases and infections [62, 63].

Since the first demonstration of an involvement of miRNAs in lymphomas in 2002 [64], the role of miRNAs has been investigated in various tumor entities [65]. Deregulation of miRNAs expression has been shown in all types of human cancer [66, 67]. Various roles of miRNAs were shown in cancer development and progression [59]. About 50% of annotated human miRNAs are located within fragile regions of chromosomes, which are frequently lost in various human cancers [68].

The *miR-34a* and *miR-34b/c* genes are directly activated by p53 [69, 70]. miR-34a is transcribed from a unique gene located on chromosome 1p36.22, which is commonly deleted in neuroblastoma [71], whereas miR-34b and miR-34c are encoded by a common host-gene located on chromosome 11q23.1. Interestingly, miR-34a and miR-34c have identical seed sequences, whereas the miR-34b seed sequence is similar, but not identical, suggesting that miR-34a and miR-34c share similar mRNA targets, whereas miR-34b targets might be slightly different from these. Moreover, miR-449a/b/c belongs to the miR-34 family as well due to similarities in the seed sequence. It is located in a highly conserved region within the second intron of the *CDC20B* gene on chromosome 5 [72]. The expression of miR-34 is also induced by the ETS family transcription factors ELK1 and Foxo3a, which bind to the promoter regions of *miR-34a* and *miR-34b/c*, respectively [73, 74]. Moreover, all members of the miR-34 family are frequently down-regulated by epigenetic silencing in many tumor types [75, 76]. The promoter of *miR-34* harbors a CpG island, which represents a site of hyper-methylation causing transcriptional silencing either through affecting the binding of transcription factors or by influencing the chromatin status.

In addition, it has been shown that the EMT-TFs SNAIL and ZEB1 repress *miR-34a* and *miR-34b/c* by directly binding to E-boxes in the *miR-34* promoters [48]. This repression may be converted into permanent silencing by CpG-methylation. In mice,

miR-34a is ubiquitously expressed, with highest levels in the brain and testes, whereas miR-34b and miR-34c are expressed mainly in brain, lungs, and testes [77, 78]. Thus, miR-34a is expressed at higher levels than miR-34b/c in most tissues, except in lungs, where miR-34b and miR-34c are predominant.

Recently, it was shown that miR-34a/b/c has an important role in the response to chemotherapeutic agents [79] and may act as a tumor suppressor [80]. The miR-34 family suppresses tumor growth and metastasis through targeting multiple oncogenic target mRNAs [79].

The roles of the miR-34 family identified in cell culture based analyses suggested that it can also suppress tumor formation *in vivo* [79]. Accordingly, re-expression of miR-34a caused 20% to 83% inhibition of tumor growth in xenograft mouse models of lymphoma, prostate, pancreatic or non-small cell lung cancer, as well as melanoma, [81-83]. In 2013, MRX34, a liposome-based miR-34 mimic, the first cancer-targeted miRNA-based drug, was used in phase I clinical trial in patients with advanced hepatocellular carcinoma [82, 84]. Furthermore, co-treatment with miR-34 mimics may enhance the beneficial effects of conventional cancer therapies. It has been shown that in various cancer models, that ectopic expression of miR-34a precursors attenuates chemo-resistance to different chemotherapeutic drugs [82]. Besides, hyper-methylation of the *miR-34a/b/c* promoters is frequently found in different primary tumors and various cancer cell lines and causes a significant reduction of endogenous miR-34a/b/c levels [85-87]. Thus, de-methylating drugs may lead to re-expression of *miR-34a/b/c* and facilitate anti-cancer therapies in the future. Indeed, treatment of prostate cancer patients with BioResponse 3/3'-Diindolylmethane (BR-DIM) prior to radical prostatectomy in a phase II clinical trial led to the re-expression of *miR-34a*, which resulted in repression and nuclear exclusion of its target, the androgen receptor [88, 89]. Moreover, natural compounds, such as Resveratrol, Rhamnetin, Genistein, and difluorinated Curcumin (CDF), cause re-expression of *miR-34a* in tumors, thus could be an important focus for future anti-cancer research studies [79]. Therefore, development of efficient delivery system

for miR-34 into tumors or re-expression of miR-34 may be an efficient strategy for anticancer therapy.

1.3.3 The p53/miR-34 axis in tumor development

As described above, p53 directly regulates miRNA expression or regulates the processing of miRNA precursors, but is also thought to be repressed by several miRNAs [43]. This thesis focuses on the function of the p53/miR-34 axis in colorectal cancer. The miR-34 family encodes the first miRNAs found to be directly activated by p53 and suppress tumor growth and metastasis [79]. The p53/miR-34 axis and its targets are often connected through positive or negative feedback loops that either reinforce the p53/miR-34 signaling or suppress it. For example, MDM4 binds to p53 and inhibits its transcriptional activity, but MDM4 is also a target of miR-34a [90, 91] (**Figure 1.4A**). Therefore, p53, miR-34a and MDM4 form a positive feed-back loop. Interestingly, the expression of miR-34 family can also be regulated by c-Myc via a miR-34a/c-Myc/ARF/HDM2/p53 negative feedback loop [92] (**Figure 1.4A**). Furthermore, SIRT1, which represses p53 activity by deacetylation of the p53 protein, is a direct target of miR-34a [93] (**Figure 1.4B**). miR-34a also directly targets nicotinamide phosphoribosyltransferase (NAMPT) [94]. In addition, a positive feedback loop was found between SIRT1 and MYC [95, 96]. Therefore, by repressing the c-Myc/SIRT1 axis, miR-34 may represent a central mediator of cell cycle suppression by p53. Moreover, the p53/miR-34 axis has also been implicated in the regulation of EMT, invasion and migration processes. miR-34a directly targets and suppresses the EMT-TF SNAIL [48, 49], whereas SNAIL represses all members of the miR-34 family by directly binding to their promoters in CRC cell lines, thereby forming a double-negative feedback loop [48] (**Figure 1.4C**). Furthermore, p53 induces members of the miR-200 family [97], which also represent EMT-regulating miRNAs that suppress EMT by a similar double-negative feedback loop involving the EMT-TFs ZEB1 and ZEB2 [98, 99]. These miRNAs form two double-negative feedback loops with their targets SNAIL, ZEB1, and ZEB2 that act as bimodal switches to stabilize either the epithelial

or the mesenchymal state [48]. Moreover, ZEB1 was shown to repress miR-34a by binding to the same E-boxes in *miR-34* promoters as SNAIL, thereby adding more complexity and further connecting the miR-34/SNAIL and miR-200/ZEB loops [48]. Hahn *et al.* recently showed that the zinc finger 281 protein (ZNF281) is an important miR-34 target with respect to EMT [30]. SNAIL and ZNF281 were directly targeted by miR-34a, which is repressed by SNAIL and ZNF281 [30, 48, 100]. Thereby, these factors form a negative feedback loop.

Recently, we found that exposure to pro-inflammatory cytokine interleukin-6 (IL-6) results in repression of *miR-34a* via direct binding of STAT3 to the promoter of *miR-34a* [31]. Furthermore, miR-34 directly targets IL-6 receptor (IL-6R), which together forms an IL-6R/STAT3/miR-34a feedback loop (**Figure 1.4D**). The activation of this loop is required for EMT, invasion, and metastasis of CRC cell lines and is associated with nodal and distant metastasis in CRC patients. In addition, deregulation of this regulatory loop by deletion of *miR-34a* was shown to promote invasion in a mouse model of colitis-associated-colon cancer [31].

Among other direct miR-34a targets that promote cancer cell EMT, invasion and migration are c-kit [101], the RAS-oncogene homolog RRAS [102], Axl [103], Arhgap1 [104], PDGFR-α/β [105], Fra-1 [106, 107], and c-Met [108].

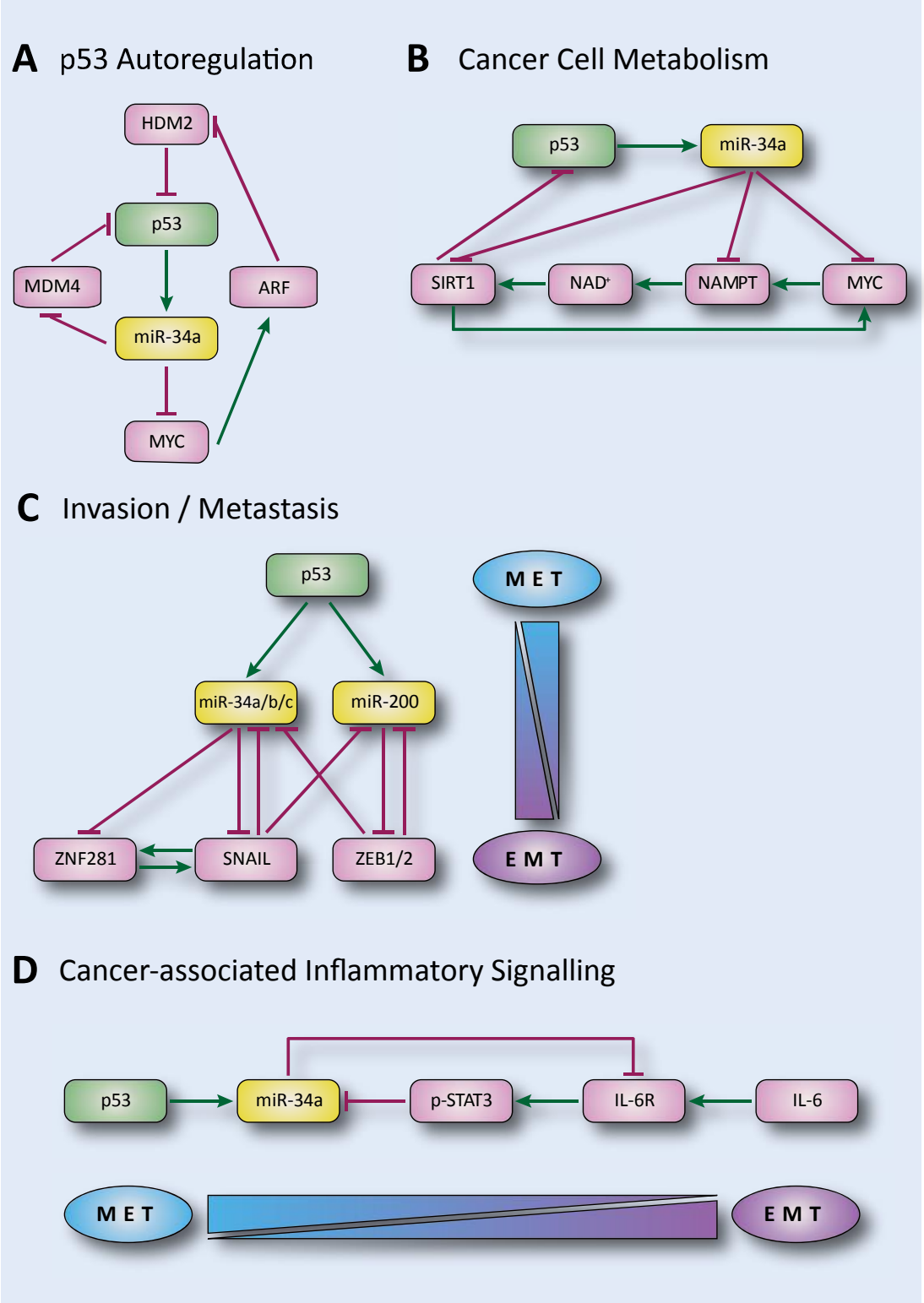

Figure 1.4 The role of p53/miR-34 axis in (A) p53 autoregulation, (B) cancer cell metabolism, (C) invasion and metastasis, (D) cancer-associated inflammatory signaling. Modified from [43, 79].

1.4 Hypoxia and cancer

The tumor microenvironment promotes cell proliferation, motility, and adhesion [109]. However, the normal cellular microenvironment by suppresses malignant cell growth [109]. Hypoxia, i.e. low oxygen concentration, is an essential aspect of tumor microenvironment. Hypoxia is a hallmark of tumors caused by their insufficient vascularization [110]. Also human colorectal carcinomas (CRC) display hypoxic areas [111]. Clinically, hypoxia is associated with tumor progression, resistance to chemotherapy and radiotherapy and poor clinical prognosis [112-114].

The definition of hypoxia depends on the type of tissue and tumor that is studied [115]. However, it is generally accepted that hypoxic tumors exhibit median oxygen levels below 2% [115]. The phenotypic variability of cancer cells is partially related to their oxygen requirement and tolerance towards hypoxia [115]. Cancer cells undergo genetic and epigenetic changes that allow them to survive in the hypoxic microenvironment [116]. Cancer cells exposed to hypoxia display an elevated mutation frequency [117]. And hypoxia was shown to promote chromosomal rearrangements, gene amplification, and reintegration into chromosomal fragile sites [118, 119]. This accelerated genetic instability may lead to an aggressive, invasive and metastatic phenotype [120]. In addition, mutation of the tumor suppressor *TP53* provides cancer cells with a selective advantage under conditions of hypoxia [121]. Indeed, hypoxia may influence most the hallmarks of tumorigenesis [122] (**Figure 1.4**).

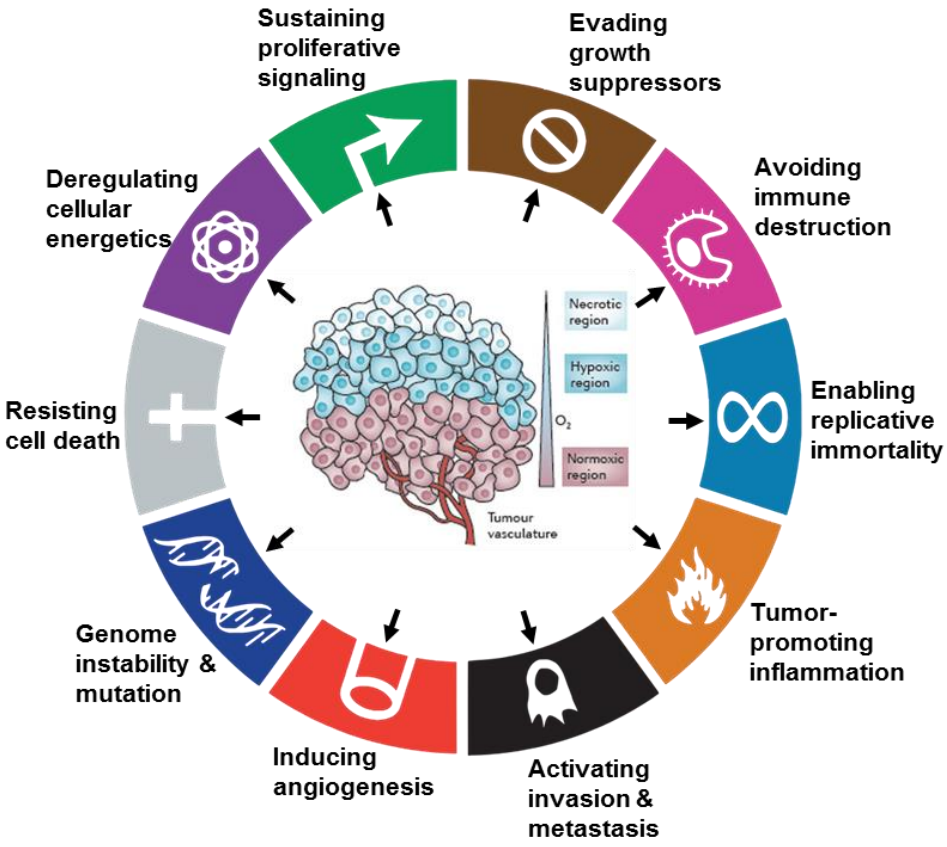

Figure 1.4 The effects of hypoxia on the hallmarks of human cancers. Modified from [3, 123].

1.4.1 The role of HIF transcription factors in cancer

HIF (hypoxia inducible factor) transcription factors belong to the basic helix–loop–helix-PER-ARNT-SIM (bHLH-PAS) family and represent important mediators of the transcriptional response to hypoxia [124-126]. HIF1A, which was first identified in studies of the human *EPO* gene [127], is a heterodimer consisting of an O_2-regulated HIF1A subunit and a constitutively expressed HIF1B subunit. HIF1 binds to the hypoxia-response element (HRE), a consensus sequence 5'-RCGTG-3' in the promoter region of its target genes. HIF1A protein levels increase dramatically when the cellular O_2 concentration is reduced [128]. HIF1A protein stability is negatively regulated by O_2-dependent prolyl-hydroxylation, which enables binding of E3 ubiquitin ligase von-Hippel–Lindau (VHL), leading to ubiquitination and thereby proteasomal degradation of HIF1A. Elevated levels of HIF1A protein have been associated with

progression and poor clinical outcome for many different tumor entities [125, 129] including CRC [130, 131].

HIF1A directly regulates genes that are related to the regulation of multiple adaptive responses to hypoxia [124, 132]. HIF1A induces EMT through regulating EMT-TFs, activating EMT-associated signaling pathways, modulating EMT-associated inflammatory cytokines, as well as by influencing epigenetic regulators [133]. Dependent on the cellular contexts, hypoxia induces a set of miRNAs, such as miR-21, 23, 24, 26, 103/107, 210 and 373. miR-210 is directly induced by HIF1A and HIF1A is a direct target of miR-210 [134]. Therefore, these factors form a negative feed-back loop. Moreover, a large number of miRNAs are down-regulated under hypoxia [135]. For example, miR-16-1, which is a prototypical tumor suppressor miRNA in leukemia and lymphoma, is down-regulated by HIF1A, and thereby contributes to the overexpression of VEGF in anaplastic large-cell lymphomas [136].

Initial work suggested that hypoxia has a minimal effect on the miRNA processing machinery [137], but more recent evidence suggests that hypoxia regulates miRNA processing. Several components of the microRNA processing machinery, such as Exportin 5 and AGO2, have been found to be regulated by hypoxia [138]. In addition, hypoxia potentiates miRNA-mediated gene silencing through post-translational modification of AGO2 [139]. Very recently, EGFR was shown to suppress the maturation of specific tumor suppressive miRNAs in response to hypoxic stress through phosphorylation of AGO2. The association between EGFR and AGO2 was enhanced by hypoxia, leading to a reduction in the binding of Dicer to AGO2 and the inhibition of the processing from precursor to mature miRNAs [140]. In breast cancer, Dicer was significantly reduced in a HIF-hydroxylase PHD2 dependent manner when exposed to hypoxia [141]. In addition, hypoxia promotes stem cell phenotypes and poor prognosis through epigenetic regulation of DICER [142]. Moreover, hypoxia-mediated down-regulation of the microRNA processing component Drosha is dependent on ETS1/ELK1 transcription factors [142].

1.4.2 Hypoxia and the p53 family

Hypoxia activates p53 via the activation of ATM (ataxia-telangiectasia mutated) or ataxia-telangiectasia mutated and Rad3-related kinases [143-145], PNUTS [146], mitochondrial generation of reactive oxygen species (ROS) [147] or enhancement of translation and mRNA half-life [148]. Moreover, activation of p53 by hypoxia acts as a selective pressure during tumor growth, which results in the clonal expansion of cells with mutant or inactive p53 [121]. This mechanism may explain the more aggressive nature of hypoxic tumors and the frequent occurrence of p53 mutations in advanced stages of tumor development. However, the nature and function of p53 targets that are affected by loss of p53 function is largely unknown. Moreover, p53 represses the activation of HIF1-dependent signaling [149]. The amplification of HIF1-dependent responses to hypoxia via loss of p53 contributes to the angiogenic switch, promoting cancer progression [150]. Accordingly, p53-deficient tumors exhibit a poor response to combinations of anti-angiogenic treatments and chemotherapy [151].

Changes in HIFs and p53 activity allow cancer cells to survive through affecting angiogenesis, tumor microenvironment, metabolism, stemness, metastasis and recurrence [152]. For example, the transcriptional reprogramming mediated by HIF1 modulates the expression of genes involved in ECM degradation within the primary tissues and at distant sites of metastasis [152]. Loss or mutant p53 affects the ability of invasion and metastasis [153]. Remarkably, the interaction of mutant p53 with TAp63 promotes the stability of HIF, resulting in enhanced metastatic potential [154, 155]. Therefore, altered interactions within the p53 family affect the activation of HIF signaling, thus facilitates HIF-dependent pro-metastatic activities [152].

The p53-miRNA network has been extensively examined in the context of oncogenesis and tumor biology [156]. Recent work indicates that p53 may also regulate specific miRNA transcription during hypoxia independent of HIF signaling. Under hypoxic conditions (0.5% O_2), p53 accumulates in aryl hydrocarbon nuclear translocator (ARNT) knockout mouse embryonic fibroblasts (MEFs) that lack intact HIF signaling and directly induces miR-210 [157]. The p53-mediated expression of

miR-210 protects cardiomyocytes exposed to hypoxia [157]. Notably, p53 also induces other miRNAs, such as miR-107 and miR-192, during tumorigenesis that have also been implicated as hypoxia-regulated miRNAs [156]. However, direct experimental evidence demonstrating a functional link between p53 and induction of these miRNAs in the context of hypoxia is currently lacking [158].

1.4.3 Hypoxia and STAT3

Hypoxia activates the transcription factor STAT3 via phosphorylation of STAT3 at serine 727 (S727) and tyrosine 705 (Tyr705) residues [159]. Phosphorylation at S727 is required for the maximal transcriptional activity of STAT3 [160], and has been implicated in the promotion of tumor growth and invasion [161-163]. Furthermore, the activation of STAT3 by S727 phosphorylation was observed in various human cancer stem cells and is associated with poor overall survival [164]. Interestingly, protein phosphatase 1/PP1, which negatively regulates STAT3 by de-phosphorylation of S727, is inhibited by hypoxia [165]. Phosphorylation of STAT3 at S727 is sufficient to activate STAT3 and enhances prostate tumorigenesis independent of Y705 phosphorylation [163, 166].

1.4.4 Hypoxia and chemo-resistance

Hypoxia induces chemo-resistance to Cisplatin, 5-fluoro-uracil, Doxorubicin, Etoposide, Gemcitabine, Melphalan, and Docetaxel in various types of tumors [167]. Also in colorectal cancer hypoxia induces chemo-resistance to 5-fluoro-uracil [168]. Notably, HIF1A represents the main mediator of hypoxia-induced chemo-resistance [167]. Accordingly, inhibition of HIF1A reverses multidrug resistance in colon cancer [169] and tumor cells expressing HIF1A are more resistant to Cytostatics than *HIF1A*-defective cells [170]. HIF1A may mediate chemo-resistance via affecting drug transporters, drug targets or via changing the response to drugs [167]. However, there are also HIF1A-independent mechanisms of hypoxia-induced chemo-resistance, such as acidosis and nutrient starvation, which inhibit cell proliferation and increase interstitial fluid pressure [171-173]. Recently, several studies suggested that EMT plays a

central role in chemo-resistance by enhancing cancer cell survival, cell fate transition, and the induction of drug resistance-mediating factors [174-176]. Some studies showed that hypoxia-induced EMT and chemo-resistance are frequently associated in diverse types of cancer [177-179].

2. Aims of the study

The present study had the following aims:

- Characterization of the role of the p53/miR-34a pathway in hypoxia-mediated effects during CRC progression
- Characterization of miR-34a targets relevant for hypoxia-induced EMT in CRC cells
- Determination of the prognostic and therapeutic value of the identified regulations and components for CRC

3. Materials

3.1 Chemicals and reagents

Application	Chemical compound	Supplier
Cell culture	FCS	Life Technologies
	Penicillin-Streptomycin (10,000 U/mL)	Life Technologies
	DMEM medium	Life Technologies
	Mc Coy's medium	Life Technologies
	HBSS, no calcium, no magnesium, no phenol red	Life Technologies
	etopside	Sigma-Aldrich
	5-FU	Sigma-Aldrich
	DMSO	Carl Roth
qPCR	Fast SYBR® Green Master Mix	Applied Biosystems
	Fast SYBR Green Master Mix Universal RT	Exiqon A/S
WB	Protein A-Sepharose® from Staphylococcus aureus	Sigma-Aldrich
	Rotiphorese gel 30 (37,5:1)	Carl Roth
	APS	Carl Roth
	TEMED	Carl Roth
	Nonidet®P40 substitute	Sigma-Aldrich
	sodium deoxycholate	Carl Roth
	SDS	Carl Roth
	β-mercaptoethanol	Sigma-Aldrich
	glycerol	Carl Roth
	bromophenol blue	Carl Roth
	complete mini protease inhibitor cocktail	Roche
	PhosSTOP Phosphatase Inhibitor Cocktail	Roche
	Bradford reagent	Bio-Rad
	PageRuler™ Prestained Protein Ladder	Fermentas
	Immobilon-P PVDF,0.45µm Membrane	Merck Millipore
	skim milk powder	Sigma-Aldrich
	Methanol	Carl Roth
	ECL/HRP substrate	Merck Millipore
IF	PFA	Merck KgaA
	FCS	Life Technologies
	DAPI	Carl Roth
	Triton X 100	Carl Roth
	Tween 20	Sigma-Aldrich
	ProLong Gold antifade	Invitrogen
Modified Boyden-chamber assay	DAPI	Carl Roth
	BD Matrigel™ Basement Membrane Matrix	BD Bioscience
	Triton X 100	Carl Roth

Application	Chemical compound	Supplier
ChIP	Protein G Sepharose®, Fast Flow	Sigma-Aldrich
	BSA fatty acid free	Sigma-Aldrich
	Salmon Sperm DNA	Promega
	37% formaldehyde	Merck Millipore
Luciferase reporter assays	ampicillin	Sigma-Aldrich
	water (molecular biological grade)	Life Technologies
	LB-Agar (Lennox)	Carl Roth
	LB-Medium (Luria/Miller)	Carl Roth
	Hi-Di™ Formamide	Applied Biosystems
	sea plaque® agarose	Lonza
	O'Gene Ruler 1kb DNA ladder	Fermentas
	ethidium bromide	Carl Roth
	HiPerFect Transfection Reagent	Qiagen
	Opti-MEM® Reduced Serum Medium	Life Technologies
Generation of vectors	ampicillin	Sigma-Aldrich
	water (molecular biological grade)	Life Technologies
	LB-Agar (Lennox)	Carl Roth
	LB-Medium (Luria/Miller)	Carl Roth
	Hi-Di™ Formamide	Applied Biosystems
	sea plaque® agarose	Lonza
	O'Gene Ruler 1kb DNA ladder	Fermentas
	ethidium bromide	Carl Roth
	Lipofectamine® 2000 Transfection Reagent	Invitrogen
	Chloroquine	Sigma-Aldrich
	Opti-MEM® Reduced Serum Medium	Life Technologies
	puromycin dihydrochloride	Sigma-Aldrich
	doxycycline hyclate	Sigma-Aldrich
IHC	H_2O_2	Carl Roth
	Hematoxylin	vector laboratories
	xylol	Carl Roth
	Goat Serum	Invitrogen
	Rabbit Serum	Invitrogen
Colony formation assay	Crystal violet	Carl Roth
	Acetic acid	Carl Roth
	Methanol	Carl Roth
Wound healing	Mitomycin C	Sigma-Aldrich
Xenograft	D-luciferin	Caliper Life Sciences
Tumoroid	BD Matrigel™ Basement Membrane Matrix	BD Bioscience

3.2 Buffers and solutions

2x Laemmli buffer:

125 mM TrisHCl (pH 6.8); 4% SDS; 20% glycerol; 0.05% bromophenol blue (in H_2O); 10% β-mercaptoethanol (added right before use)

10x 'Vogelstein' PCR buffer:

166 mM NH_4SO_4; 670 mM Tris (pH 8.8); 67 mM $MgCl_2$; 100 mM β-mercaptoethanol

RIPA buffer (for protein lysates):

1% NP40; 0.5% sodium deoxycholate; 0.1% SDS; 250 mM NaCl; 50 mM TrisHCl (pH 8.0)

SDS buffer:

50 mM Tris (pH 8.1); 100 mM NaCl; 0.5% SDS; 5 mM EDTA

10x Tris-glycine-SDS running buffer (5l, for SDS-PAGE):

720 g Glycin; 150 g Tris base; 50 g SDS; pH 8.3-8.7; ad 5 l ddH_2O

Towbin buffer (for Western blotting):

200 mM glycine; 20% methanol; 25 mM Tris base (pH 8.6)

10x TBS-T (5l):

500 ml 1M Tris (pH 8.0); 438.3 g NaCl; 50 ml Tween20; ad 5 l ddH_2O

10x PBS (1l):

80g NaCl; 1g KCl; 14.42g $Na_2HPO_4*2H_2O$; 2g KH_2PO_4; ad 1 l ddH_2O

3.3 Kits

Application	Kit	Supplier
qPCR	High Pure RNA Isolation Kit	Roche
	High Pure miRNA Isolation Kit	Roche
	miRCURY LNATM Universal RT microRNA PCR – Universal cDNA Synthesis Kit II	Exiqon A/S
	Verso cDNA Kit	Thermo Fisher Scientific
WB	BCA Protein Assay Kit	Thermo Fisher Scientific
IHC	Dakocytomation Target Retrieval Solution citrate (10×)	Agilent
	DAB	vector laboratories
Generation of vectors	QIAamp DNA Micro Kit	QIAGEN
	High Pure RNA Isolation Kit	Roche
	Verso cDNA Kit	Thermo Fisher Scientific
	QIAquick Gel Extraction Kit	QIAGEN
	QIAquick PCR Purification Kit	QIAGEN
	Pure Yield™ Plasmid Midiprep System	Promega
	QIAprep Spin Miniprep Kit	QIAGEN
	BigDye® Terminator v3.1 Cycle Sequencing Kit	Life Technologies
	DyeEx® 2.0 Spin Kit	QIAGEN
	QuikChange II XL Site-Directed Mutagenesis Kit	Agilent Technologies
DNA isolation	DNeasy Blood & Tissue Kit	Qiagen
Luciferase reporter assays	Dual-Luciferase® Reporter Assay System	Promega

3.4 Enzymes

Application	Enzyme	Supplier
Cell culture	Trypsin-EDTA (0.5%, 10x, phenol-red free)	Invitrogen
qPCR	DNase I (RNase-free)	Sigma-Aldrich
Generation of vectors	restriction endonucleases	New England Biolabs
	Platinum® *Taq* DNA polymerase	Invitrogen
	Pfu polymerase	Thermo Fisher Scientific
	FIREPol® DNA Polymerase	Solis BioDyne
	T4 DNA ligase	Thermo Fisher Scientific

3.5 Antibodies

3.5.1 Primary antibodies

epitope	species	catalog no.	company	use	dilution	source
Vimentin	human	# 2707-1	Epitomics	WB	1:500	rabbit
E-cadherin	human	# 334000	Invitrogen	WB; IF	1:1000; 1:50	mouse
β-actin	human	# A2066	Sigma-Aldrich	WB	1:1000	rabbit
p53	human	# sc-126	Santa Cruz	WB	1:1000	mouse
α-tubulin	human	# T-9026	Sigma-Aldrich	WB	1:1000	mouse
SNAIL	human	# 3879S	Cell Signaling	WB	1:500	rabbit
STAT3	human	# sc-482	Santa Cruz	WB	1:1000	rabbit
$STAT3^{pS727}$	human	# 9134	Cell Signaling	WB	1:1000	rabbit
$STAT3^{pY705}$	human	# 9131	Cell Signaling	WB	1:1000	rabbit
VSV	human	# V4888	Sigma-Aldrich	WB; co-IP	1:1000	rabbit
GLUT1	human	# sc-377228	Santa Cruz	IHC	1:100	mouse
Laminin 5γ2	human	# MAB19562	Merck Millipore	IHC	1:100	mouse
HIF1A	human	# NB100-105	Novus Biologicals	WB; CHIP	1: 1000	mouse
INH3	Human	# sc-376034	Santa Cruz	WB; IHC; co-IP	1: 1000; 1:100	mouse
HIF1A	mouse	# LS-B12555	LSBio	WB; IHC	1: 500	rabbit
INH3	mouse	# SAB4502938	Sigma-Aldrich	WB; IHC	1:500	rabbit
Cleaved caspase-3	mouse	# 9661	Cell Signaling	IHC	1:400	rabbit

3.5.2 Secondary antibodies

Secondary antibodies or conjugates

name	ordering no.	company	use	dilution	source
anti-mouse HRP	# W4021	Promega	WB	1:10.000	goat
anti-rabbit HRP	# A0545	Sigma	WB	1:10.000	goat
Anti-Rabbit-Cy3	# 715-165-150	Jackson Immuno-Research	IF	1:100	donkey
Alexa Flour 555-conjugated anti-mouse	# A21422	Invitrogen	IF	1:500	goat
Phalloidin-conjugated Alexa-647	# A22287	Invitrogen	IF	1:40	--
Alexa Flour 555-conjugated anti-rabbit	# A-11034	Invitrogen	IF	1:1000	goat

3.6 Oligonucleotides

3.6.1 Oligonucleotides used for qPCR

gene	forward (5'-3')	reverse (5'-3')
human:		
β-actin	TGACATTAAGGAGAAGCTGTGCTAC	GAGTTGAAGGTAGTTTCGTGGATG
VIM	TACAGGAAGCTGCTGGAAGG	ACCAGAGGGAGTGAATCCAG
CDH1	CCCGGGACAACGTTTATTAC	GCTGGCTCAAGTCAAAGTCC
pri-miR-34a	CGTCACCTCTTAGGCTTGGA	CATTGGTGTCGTTGTGCT
SLUG	GGGGAGAAGCCTTTTTCTTG	TCCTCATGTTTGTGCAGGAG
STAT3	GGGAAGAATCACGCCTTCTAC	ATCTGCTGCTTCTCCGTCAC
SNAIL	GCACATCCGAAGCCACAC	GGAGAAGGTCCGAGCACAC
FN	CTTTGGTGCAGCACAACTTC	TCCTCCTCGAGTCTGAACCA
Inh3	CTGTGTCTGTCTGGCCCTAA	GGGTGGGTATTGGGAGGAAA
ZEB1	TCAAAAGGAAGTCAATGGACAA	GTGCAGGAGGGACCTCTTTA
murine:		
β-actin	CTAAGGCCAACCGTGAAAAG	ACCAGAGGCATACAGGGACA
VIM	ATCGACAAGGTGCGCTTCC	TTGCCCTGGCCCTTGA
CDH1	GATTTGAGCCAGCTGCACAG	GGGTGGGAGCCACATCATT
pri-miR-34a	CTGTGCCCTCTTGCAAAAGG	GGACATTCAGGTGAGGGTCTTG
SLUG	ATCCTCACCTCGGGAGCAT	GGTAGAGGAGAGTGGAGTGGAGC
SNAIL	CACACGCTGCCTTGTGTCT	GGTCAGCAAAAGCACGGTT
FN	AGTGCTTCATGCCGCTAGAT	GGGTGAAAGGACCACTCAAA
Inh3	ACAACCGAGCCAGAGAATCA	AAGGCCCGAGGCTTCTCATA
ZEB1	GCATGTGACCTGTGTGACAA	GATAGGGCTTTTCCCCAGAG
ZEB2	ATTGCACATCAGACTTTGAGGAA	ATAATGGCCGTGTCGCTTCG
Twist	CCCACCCCACTTTTTGACGA	GGGATGCCTTTCCTGTCAGT

3.6.2 Oligonucleotides used for cloning and mutagenesis of *Inh3* 3'-UTRs

gene	forward (5'-3')	reverse (5'-3')
human:		
Inh3 3'-UTR	TCCCTCTCTCCTCCAGCATT	CCGGATCCCAGTAAGGGGTA
Inh3 3'-UTR site1 mutant	CCAGTGTCTTCCTTTTGTTCTCA GTCGGAAACTGCCTGTCCTGGG	CCCAGGACAGGCAGTTTCCGACT GAGAACAAAAGGAAGACACTGG
Inh3 3'-UTR site2 mutant	CAACAGTCCCAGCTTTCAGTCG GAGGGTCCCAGTCAGATTCC	GGAATCTGACTGGGACCCTCCGA CTGAAAGCTGGGACTGTTG
murine:		
Inh3 3'-UTR	TCACCATTCATGTGTCTGCCT	AAGTGGTGCCATGGGTTTTG
Inh3 3'-UTR site1 mutant	CTATCCCTTTTGTTCTCAGTCGG AAACTACCTGTCCTGGGATCC	GGATCCCAGGACAGGTAGTTTCC GACTGAGAACAAAAGGGATAG
Inh3 3'-UTR site2 mutant	CAACGGTCCCAGCTTTCAGTCG GAGGGCTCCAATCAGATGCC	GGCATCTGATTGGAGCCCTCCGA CTGAAAGCTGGGACCGTTG

3.6.3 Oligonucleotides used for qCHIP

gene	forward (5'-3')	reverse (5'-3')
16q22	CTACTCACTTATCCATCCAGGCT AC	ATTTCACACACTCAGACATCAC AG
miR-34a HRE1	ATAATGGTTGGGGCAGGAGG	TAAAGGTTCCCAGAGACGCA
miR-34a HRE2	TCGCATCTTGTTGAATCCGG	AGGGCCTCTCGCCTGGA
miR-34a HRE3	CGGTGAAGGGGATGAGGACCAG	GCGGCATCTCCTCCACCTGAAA
Inh3 HRE1	AACCTACTTGTCGGCCTTCC	ATTCGTTCTCTCTGGGGTGA
Inh3 HRE2	TTACGCGCCTCCATCTTCAA	AAGTGGGAGCAGTTGGAAAC
Inh3 HRE3	GCTTGGTGCACACAACTCC	AACAAATTTGGCGGAAGGGG
Inh3 HRE4	CCCCTTCCGCCAAATTTGTT	AGGCGTCGCTGGATTAGTT
Inh3 HRE5	CTCCCTGTCCTGAGCCTTAG	GCCTAGCTCCTCCAACAACT
VEGF	CCTTTGGGTTTTGCCAGA	CCAAGTTTGTGGAGCTGA

3.6.4 Oligonucleotides used for cloning and mutagenesis of human *miR-34a* promoter

gene	forward (5'-3')	reverse (5'-3')
miR-34a promoter	CTGAGAGTGGGTATGGGATTGCC	GCAGGACTCCCGCAAAATCTCCAAATG
miR-34a HRE2 mutant	CACACCCGCGTCCAGGAAAGGGGTTTCTTCCCTCTTC	GAAGAGGGAAGAAACCCCTTTCCTGGACGCGGGTGTG

3.6.5 Oligonucleotides used for cloning of human *Inh3*

gene	forward (5'-3')	reverse (5'-3')
Inh3	CGGGATCCTCCCTGTCCTGAGCCTTAGC	ACGCGTCGACGTGCTGCATTGGCCCTGGAG

3.6.6 microRNA mimics and antagomiRs

The following pre-microRNA mimics and antagomiRs were purchased from Ambion: pre-miR miRNA Precursor Negative Control # 1 (# AM17110); pre-miR-34a (# PM11030); pre-miR-34c (# PM11039); anti-miR Negative Control # 1 (# AM17010); has-miR-34a-5p anti-miR miRNA Inhibitor(# AM11030)

3.6.7 siRNAs

The following siRNAs were purchased from Ambion:

Negative control (ID # 4611), STAT3 (ID # 6880), INH3 (ID # s13943), and HIF1A (ID # s6539).

3.7 Search Algorithms

application	internet	Supplier
miR-34 binding site prediction	miRwalk	http://zmf.umm.uni-heidelberg.de/apps/zmf/mirwalk2/
miR-34 binding site prediction	targetscan	http://www.targetscan.org/vert_71/

3.8 Vectors

Name	Insert	Reference
pRTR	--	[180]
pRTR-p53-VSV	human *TP53*	[181]
pCDNA3.1-p53-VSV	human *TP53*	
pRTR-pri-miR-34a	human *miR-34a*	[182]
tTA-p53	human *TP53*	[183]
pGL3-control-MCS	--	[71]
pGL3-Inh3 wt	human *Inh3* 3'UTR	
pGL3-Inh3 mut1	human *Inh3* 3'UTR	
pGL3-Inh3 mut2	human *Inh3* 3'UTR	
pGL3-Inh3 mut1 + 2	human *Inh3* 3'UTR	
pGL3-mInh3 wt	mouse *Inh3* 3'UTR	
pGL3-mInh3 mut1	mouse *Inh3* 3'UTR	
pGL3-mInh3 mut2	mouse *Inh3* 3'UTR	
pGL3-mInh3 mut1 + 2	mouse *Inh3* 3'UTR	
pRL	Renilla	[184]
pBV	--	[185]
pBV-miR-34a	human *miR-34a* promoter	
HA-HIF1A	human *HIF1A* with activating mutation	[186]

3.9 Mice

application	Mice	Supplier
Xenograft	NOD/SCID mice	Jackson Laboratory
IHC	*miR-34a*$^{-/-}$; *miR-34bc*$^{-/-}$; *Apc*$^{Min/+}$ and *miR-34a*$^{+/+}$; *miR-34bc*$^{+/+}$; *Apc*$^{Min/+}$ mice	Dr. Alexander Nikitin ; Dr. Marlon Schneider
Tumoroid	*miR-34a*$^{-/-}$; *miR-34bc*$^{-/-}$; *Apc*$^{Min/+}$ and *miR-34a*$^{+/+}$; *miR-34bc*$^{+/+}$; *Apc*$^{Min/+}$ mice	Dr. Alexander Nikitin ; Dr. Marlon Schneider

3.10 Cell lines

Species	Cell lines	Medium	Supplier
Human CRC cell lines	SW480	DMEM Medium + 10% FBS	--
	SW620		--
	DLD-1	McCoy`s 5A Medium + 10% FBS	--
	HT29		--
	HCT15		--
	HCT116 *TP53*$^{-/-}$		Bert Vogelstein (Johns Hopkins University, Baltimore)
	HCT116 *TP53*$^{+/+}$		
	RKO *TP53*$^{-/-}$		
	RKO *TP53*$^{+/+}$		
	SW48 *TP53*$^{-/-}$		
	SW48 *TP53*$^{+/+}$		
Murine CRC cell line	CT26		Gabriele Multhoff (Technical University, Munich)
Human kidney cell line	HEK293	DMEM Medium + 5% FBS	--

3.11 Software

application	software	Supplier
Data analysis	SPSS Statistics 23.0	IBM
Data analysis and figure generation	Prism5 program	Graph Pad Software Inc.
WB	Varioskan Flash Multimode Reader	Thermo Scientific
	KODAK MI SE software	Carestream Health
qPCR	ND 1000 NanoDrop Spectrophotometer	NanoDrop products
Sequencing analysis	DNA Sequencing Analysis Software v5	Applied Biosystems
	BioEdit	BioEdit
qPCR	LightCycler 480	Roche
IF	ZEN 2009	Zeiss
Wound healing assay	Axiovision	Zeiss
Morphology	Axiovision	Zeiss
IHC	Axiovision	Zeiss
Luciferase reporter assays	SIMPLICITY software package	DLR
Modified Boyden-chamber	Axiovision	Zeiss
Xenograft	IVIS Illumina System	Caliper Life Sciences
Ectopic expression	BD ACCURI C6	bdbiosciences

3.12 Laboratory equipment

application	Device	Supplier
qPCR	ND 1000 NanoDrop Spectrophotometer	NanoDrop
	LightCycler 480	Roche
WB	Mini-PROTEAN®-electrophoresis system	Bio-Rad
	HTU SONI130	G. Heinemann Ultraschall- und Labortechnik
	Varioskan Flash Multimode Reader	Thermo Scientific
	PerfectBlue™ SEDEC 'Semi-Dry' blotting system	Peqlab Biotechnologie
	Mini Trans-Blot® Electrophoretic Transfer Cell	Bio-Rad
	Powerpac 300 Power Supply	Bio-Rad
	biophotometer plus	eppendorf
	EPS 600 power supply	Pharmacia Biotech
	440CF imaging system	Eastman Kodak
Modified Boyden-chamber assay	Boyden chamber transwell membranes (pore size 8.0 µm)	Corning
	Axiovert 25 microscope	Carl Zeiss
Cell culture	Herasafe KS class II safety cabinet	Thermo Fisher Scientific
	Neubauer counting chamber	Carl Roth
Sequencing	ABI 3130 genetic analyzer capillary sequencer	Applied Biosystems
IF	Axiovert 25 microscope	Carl Zeiss
IHC	Axiovert 25 microscope	Carl Zeiss
Ectopic expression	Fisherbrand FT-20E/365 transilluminator	Fisher Scientific
	GeneAmp® PCR System 9700	Applied Biosystems
	MultiImage Light Cabinet	Alpha Innotech
	BD AccuriTM C6 Flow Cytometer Instrument	BD Accuri

application	Device	Supplier
Wound healing assay	Culture-Insert 2 Well	ibidi
	Axiovert 25 microscope	Carl Zeiss
Luciferase reporter assays	Orion II luminometer	Berthold Technologies
Xenograft	IVIS Illumina System	Caliper Life Sciences
Colony formation assay	Varioskan Flash Multimode Reader	Thermo Scientific
Cell proliferation	real-time cell analyzer (RTCA)	Roche
Common used	Forma scientific CO2 water jacketed incubator	Thermo Fisher Scientific
	Falcons, dishes and cell culture materials	Schubert & Weiss OMNILAB
	5417C table-top centrifuge	Eppendorf
	waterbath	Memmert
	Biofuge pico table top centrifuge	Thermo Fisher Scientific
	Megafuge 1.0R	Thermo Fisher Scientific
	Biofuge fresco	Thermo Fisher Scientific

4. Methods

4.1 Bacterial culture

4.1.1 Propagation and seeding

For replication of plasmids harboring an ampicillin or kanamycin resistance, bacterial *E.coli* XL1-blue strain was used. The bacterial cells were cultured either in liquid LB-medium by agitation (225 rpm) or on LB agar plates at 37°C overnight. LB-medium or LB agar plates were supplemented with 100 µg/ml ampicillin or 50 µg/ml kanamycin.

4.1.2 Transformation

In order to transform the plasmids harboring an ampicillin or kanamycin resistance, competent bacterial *E.coli* XL1-blue strain was used. In general, approximately 100 ng of plasmid DNA was added to 200 µl aliquots of competent bacterial *E.coli* XL1-blue and incubated on ice for thirty minutes. The competent cells were subjected to a heat -shock at 42°C for ninety seconds and then placed on ice for additional two minutes. Subsequently, 1 ml of antibiotic-free LB-medium was added and pre-incubated at 37°C for one hour. Next, the cells were plated on LB-agar plates containing ampicillin or kanamycin and cultured at 37°C overnight. For further propagation of the plasmid a transformed single cell clone was used to inoculate the respective amount of LB-medium containing the corresponded antibiotics, and then was incubated at 37°C overnight and subjected to the procedure of plasmid DNA purification.

4.1.3 Purification of plasmid DNA from *E.coli*

In order to prepare small amounts of plasmid DNA, bacterial, transformed with plasmids, were incubated in a volume of 5 ml of LB-medium supplemented with ampicillin or kanamycin. The plasmid DNA was isolated according to the manufacturer's instructions of the QIAprep Spin Miniprep Kit (Qiagen). The method

was preferentially used due to the better yield and quality of DNA for high transfection efficiency.

In order to prepare large amounts of plasmid DNA, bacterial cells were incubated in a volume of 150 ml of LB-medium containing ampicillin or kanamycin. Pure Yield™ Plasmid Midiprep System (Promega) was used according to the protocol of the manufacturer for DNA purification.

4.1.4 Sequence inserts DNA in plasmid

In order to verify DNA sequences introduced into plasmid, DNA sequencing was conducted according to the manufacturer's instructions of BigDye Terminator v1.1 Cycle Sequencing Kit (Life Technologies). Briefly, master mix was prepared containing Big Dye Terminator V1.1, 5×Sequencing buffer, primer (10 µM), plasmid (1 µg/ml). And then the PCR program was conducted by 15 cycles of each ten seconds at 96°C and ninety seconds at 60°C. Subsequently, the DyeEx 2.0 Spin Kit (Qiagen) was used according to the manufacturer's protocol in a 5417C centrifuge (Eppendorf). After that, purified DNA was mixed with Hi-Di Formamide (Applied Biosystems), and loaded into to ABI3130 genetic analyzer capillary sequencer (Applied Biosystems) for sequencing. Data was analyzed by applying the 3130 Data Collection Software v3.0 and the sequencing analysis software 5.2 (Applied Biosystems).

4.2 Polymerase Chain Reaction (PCR) methods

4.2.1 Colony PCR

To verify the identity and orientation of DNA inserts colony PCR was conducted. For this, 20 µl PCR master mix containing vector and/or insert specific primers, dNTPs, 10x Vogelstein PCR buffer and FIREPol® DNA polymerase was prepared. Single colonies were picked from the LB-agar plate and transferred into correspond PCR tube. The PCR cycling conditions were the following: 95°C for five minutes, followed by 25 cycles of 95°C for twenty seconds, 55°C for thirty seconds and 72°C

for X minute/s (1 minute per 1 kb length of the expected PCR product), and then another 72°C for seven minutes. PCR fragment length was analyzed by supplementing the sample with loading dye and loading it into agarose gel (percentage of the gel adjusted to the fragment length) for electrophoresis.

4.2.2 Cloning of the human *miR-34a* promoter

The promoter region 2 kbp upstream of the transcriptional start site of human *miR-34a* gene was PCR-amplified from genomic DNA of human diploid fibroblasts (HDFs). The PCR product was cloned into the shuttle vector pGEM-T-Easy (Promega), then transferred into the pBV-MCS vector and verified by sequencing. Mutagenesis of the promoter sequence was achieved using the QuikChange II XL Site-Directed Mutagenesis Kit (Stratagene) according to manufacturer's instructions and verified by sequencing. The sequences of oligonucleotides used as cloning and mutagenesis of human *miR-34a* promoter primers are listed in **Table 3.6.4**.

4.2.3 Cloning of 3´-UTR sequences

The full-length 3'-UTRs of the human and mouse *Inh3* mRNAs were PCR-amplified from cDNA of human diploid fibroblasts (HDFs) and mouse embryonic fibroblasts (MEFs), respectively. The PCR product was cloned into the shuttle vector pGEM-T-Easy (Promega), and then transferred into the pGL3-control-MCS vector [71] and verified by sequencing. Mutagenesis of the *miR-34a* seed-matching sequences in human and mouse was achieved using the QuikChange II XL Site-Directed Mutagenesis Kit (Stratagene) according to manufacturer's instructions and verified by sequencing. The sequences of oligonucleotides used as cloning and mutagenesis of human and mouse 3'-UTR primers are listed in **Table 3.6.2**.

4.2.4 Episomal vectors for ectopic expression of proteins

The generation of the pRTR vector, which is an improved version of the pRTS vector is described in [180]. To generate the episomal pRTR-Inh3-VSV vector, the *Inh3* ORF was isolated from cDNA of HDFs, and ligated into the modified pUC19-SfiI shuttle vector pUC19-SfiI-CVSV, in which a VSV-tag was inserted via XhoI and XbaI restriction sites (**Figure 4.1**), via BamHI and SalI restriction sites, released with SfiI, and the resulting fragment was ligated into pRTR. The insert orientation and the ORFs were verified by sequencing. The sequences of oligonucleotides used as cloning human *Inh3* primers are listed in **Table 3.6.5.** More detailed information on the generation of p53 or the pri-miR-34a pRTR vectors is provided in [48, 182]. Other expression plasmids are listed in **Table 3.8**.

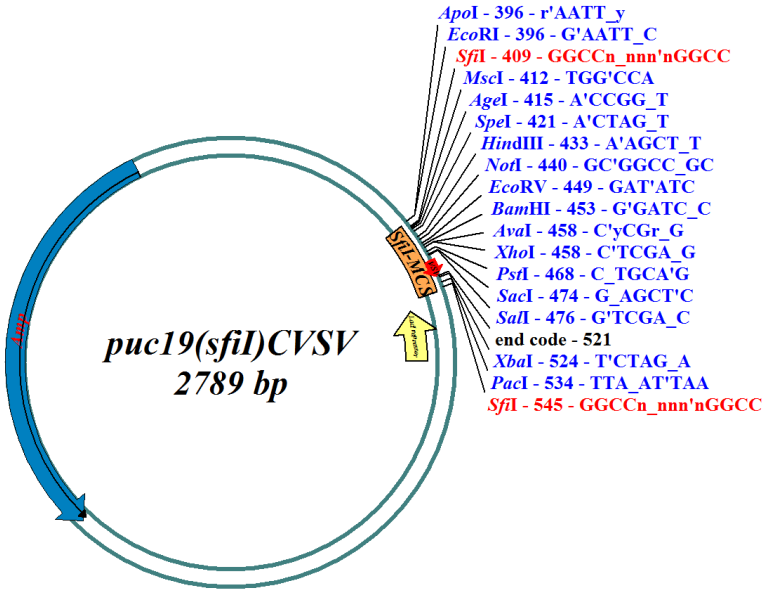

Figure 4.1 Schematic map of pUC19(sfiI)-CVSV.

4.3 Cell culture of human cells

4.3.1 Propagation of human cell lines

The human colorectal cancer cell lines SW480 and SW620, as well as human diploid fibroblasts (HDFs) were maintained in high glucose Dulbecco`s modified

Eagles medium (DMEM, Invitrogen) containing 10% fetal bovine serum (FBS). Human breast cancer cell line HEK293T was cultured in high glucose Dulbecco`s modified Eagles medium (DMEM, Invitrogen) containing 5% FBS. The human colorectal cancer cell lines HCT-15, HT29, DLD-1, HCT116, RKO, SW48 and CT26 and their derivatives were cultured in McCoys medium (Invitrogen) containing 10% FBS. *TP53*$^{-/-}$ and *TP53*$^{+/+}$ HCT116, RKO and SW48 lines were kindly provided by Bert Vogelstein (Johns Hopkins University, Baltimore) and CT26 cells by Gabriele Multhoff (Technical University, Munich). All cells were cultivated in presence of 100 units/ml penicillin and 0.1 mg/ml streptomycin at 20% O_2, 5% CO_2 and 37°C. Cells used are listed in **Table 3.10**. Hypoxia was achieved using a CD210 incubator (Binder). In order to avoid any confluency of the cells, they were passaged every two to four days and seeded into fresh culturing flasks. Doxycycline (DOX; Sigma) was dissolved in water (100 µg/ml stock solution) and used at a final concentration of 100 ng/ml. $CoCl_2$ (Cobalt (II) chloride) was dissolved in water and used at a final concentration of 40 ng/ml. Etoposide (Sigma) was used at a concentration of 20 µM and 5-FU (Sigma) at 25 µg/ml. SiRNAs (silencer siRNA (Ambion): negative control (ID # 4611), STAT3 (ID # 6880), INH3 (ID # s13943), and HIF1A (ID # s6539)) were transfected at a final concentration of 10 nM using HiPerfect transfection reagent (Qiagen).

4.3.2 Transfection of oligonucleotides and vector constructs

Transfections of oligonucleotides and vector constructs were carried out using freshly trypsinized and seeded cells in the medium and cell culturing format of choice, preferentially into a six- or twelve-well format.

In order to transfect oligonucleotides HiPerFect (Qiagen) was used. For six-well format, the transfection reagent mix contained 100 µl Opti-MEM (Invitrogen), 10 µl HiPerFect (Qiagen) and 10 µl of the respective oligonucleotide (10 µM) (Ambion – Applied Biosystems, final concentration (100 nM)).

In order to transfect plasmid DNA, the transfection mix consisted of 150 µl Opti-MEM, 5 µl Lipofectamine® 2000 Transfection Reagent (Invitrogen) and incubated at room temperature for five minutes. In the meanwhile, prepare the mix consisted of 150 µl Opti-MEM, 4 µg DNA. Mix these two mixtures. Before adding the mix drop-wise to the cells, it was incubated at room temperature for fifteen to twenty minutes. After incubation, the respective assays were carried out. Selection of plasmid containing cells was started twenty four hours after transfection using appropriate antibiotics.

4.3.3 Generation of cell pools stably expressing conditional alleles

Stable transfection cells were generated as described previously [48]. Briefly, cells were transfected with pRTR plasmids using FuGene reagent (Roche). After 24 hours, cells were transferred into media containing 4 µg/ml puromycin for one week. Homogeneity of the derived cell pools was tested by addition of 100 ng/ml DOX for 48 hours and evaluation of GFP expression by fluorescence microscopy.

4.3.4 Cryo-Preservation of mammalian cells

Sub-confluent cells in the exponential growth phase were trypsinized, resuspended with medium and pelleted by centrifugation at 1200 rpm for five minutes. Resuspension of cells was done in 50% FCS, 40% growth medium and 10% (v/v) DMSO (Roth). Aliquots in cryo-vials were cooled down in a freezing device at -80°C and transferred into liquid nitrogen for long term storage.

For cell recovery, cryo-preserved cells were rapidly thawed in water bath at 37°C, resuspended in 10ml pre-warmed growth medium and pelleted by centrifugation at 1200 rpm for five minutes. After that, the cells were resuspended in respective growth medium and transferred into T25 cell culture flask for further cultivation.

4.3.5 Analysis of the transfection efficiency by flow cytometry

In order to detect the transfection efficiency of the pRTR vectors harboring an eGFP gene into mammalian cells, the percentage of eGFP-positive cells was determined after seventy two hours with or without addition of DOX (100 ng/ml). A BD AccuriTM C6 Flow Cytometer instrument (Accuri) and the corresponding Cflow® software were used to read out the proportion of fluorescent cells.

4.4 Isolation of genomic DNA from human diploid fibroblasts (HDFs)

Genomic DNA from HDFs was generated by seeding the cells on a 10 cm^2 dish at a confluence of 90% at the maximum. The DNA was isolated according to manufacturer's instructions using the Blood & Tissue Kit (Qiagen). The DNA concentration was measured using a Nanodrop spectrophotometer.

4.5 RNA analysis

4.5.1 Isolation of RNA and reverse transcription

Total RNA was isolated with the High Pure RNA Isolation Kit (Roche) according to the manufacturer's instructions. A Nanodrop spectrophotometer was used to determine the amount and quality of the RNA. For mRNA and primary miRNA analysis 1 µg of total RNA per sample was used to generate cDNA using the Verso cDNA synthesis kit (Thermo scientific).

For the detection of mature miRNAs, a High Pure miRNA Isolation Kit (Roche) was used to isolate small RNAs according to the manufacturer's instructions. After determining the amount and quality of the RNA by Nanodrop spectrophotometer, cDNA was synthesized from 500 ng of RNA per sample by applying the Exiqon Universal cDNA Synthesis Kit from the miRCURY LNA Universal RT microRNA PCR Kit (Exiqon, 203300) according to the manufacturer´s instructions. Primers specific for miR-34a (Exiqon: # 204486) and respective control primer SNORD48 (Exiqon: # 203903) were used for miRNA LNA PCR.

4.5.2 Quantitative Real-Time PCR (qPCR) and Exiqon qPCR

Quantitative real-time PCR (qPCR) was performed with the Fast SYBR Green Master Mix (Applied Biosystems) on a LightCycler 480 (Roche). For mature miRNA analyses, qPCR was performed using the Exiqon Universal cDNA Synthesis Kit, SYBR Green Master Mix Universal RT (Exiqon, # 203450), and commercially available primers (Exiqon). Expression of mRNA and primary miRNA was normalized to β-actin, mature miRNA expression were normalized to SNORD48. The qPCR results were calculated using the ΔΔCt method as described before [187]. Results are represented as fold induction of the treated/transfected condition compared with the control condition Experiments were performed in triplicates. Oligonucleotides used for qPCR are provided in **Table 3.6.1**.

4.6 Protein analysis

4.6.1 Protein Isolation, SDS-PAGE and Western blot

Protein isolation, SDS-PAGE and Western blot were performed as described previously [79]. Briefly, cells were washed with ice-cold PBS and harvested on ice using a plastic cell scraper and ice-cold RIPA lysis buffer (50 mM Tris/HCl, pH 8.0, 250 mM NaCl, 1% NP40, 0.5% (w/v) sodium deoxycholate, 0.1% sodium dodecylsulfate, complete mini protease inhibitor tablets (Roche) and Phosphatase Inhibitor tablets (Roche)). Lysates were sonicated using a HTU SONI130 (G. Heinemann Ultraschall- und Labortechnik) for three consecutive five-second pulses with 75% intensity. In order to separate the protein containing supernatant from any cell debris, the sonicated Lysates were centrifuged at 16.060 g for fifteen minutes at 4°C. After centrifugation, the supernatant containing protein lysate was transferred into a new tube. Protein concentration was measured with BCA Protein Assay Kit (Thermo Fisher Scientific) in Varioskan Flash Multimode Reader using the SkanIt RE for Varioskan 2.4.3 software (Thermo Scientific).

7.5 to 15% polyacrylamide protein gels were prepared depending on the size of analyzed proteins and overlaid with 4% stacking gel.

Subsequently, 30 to 60 µg of whole cell lysate per lane was supplemented with 4×Laemmlie buffer, denatured at 95°C for five minutes, and loaded on 7.5 to 15% SDS-acrylamide gels according to protein sizes. A pre-stained protein ladder (Fermentas) served as size control. Separation of the proteins by electrophoresis was performed at 60-130 V in a Mini-PROTEAN®-electrophoresis system (Bio-Rad) with Tris-glycine-SDS running buffer. The separated proteins were transferred onto Immobilon PVDF membranes (Millipore) with Towbin buffer using the PerfectBlue™ SEDEC blotting system (Peqlab) and a EPS 600 power supply (Pharmacia Biotech) constantly at a 125 mA per gel and a maximum voltage of 10 V.

To block unspecific protein binding, membranes were incubated for one hour in 5% skim milk/TBS-Tween20 (TBS-T). Then membranes were incubated with the primary antibodies (diluted in TBS-T) at 4°C overnight. The membranes were washed three times in TBS-T for ten-minute each. Then membranes were incubated with horseradish-peroxidase (HRP)-conjugated secondary antibodies for one hour at room temperature. Three times washing was conducted as describe above. Enhanced Chemiluminescence (ECL, Millipore) signals were recorded with 440CF imaging system (Eastman Kodak Co.). Antibodies used here are listed in **Table 3.5**.

4.6.2 Quantification of Western blot Signals

Intensities of protein band signals were quantified by densitometric analysis using KODAK MI SE software (Carestream Health). The resulting values were used for calculating the ratio of respective protein to loading control. The quotient of the respective experimental control was set equal to one.

4.6.3 Co-immunoprecipitation (Co-IP) analysis

For co-immunoprecipitation analysis, cell lysates were prepared in RIPA lysis buffer with Complete Mini Protease and Phosphatase Inhibitors (Roche) added, sonicated and centrifuged at 16.060 g for 15 min at 4°C. The immunoprecipitations were performed overnight at 4 °C with antibodies to VSV (V4888, Sigma-Aldrich) or INH3 (sc-376034, Santa Cruz) or corresponding IgG (as a control). Subsequently the immunoprecipitates were incubated at 4°C for 2 hours with Protein A-Sepharose beads (P9424, Sigma-Aldrich) for VSV antibody/Protein G-Sepharose beads (P3296, Sigma-Aldrich) for Inh3 antibody. Immunoprecipitates were collected by centrifugation and followed by 3 times washing with RIPA lysis buffer. Samples were resuspended in 4X sample buffer and subjected to Western blot analysis. Antibodies used here are listed in **Table 3.5**.

4.7 Chromatin immunoprecipitation (ChIP) assay

DLD-1 cells and their derivatives were cultured as described above. Cross-linking and harvesting of cells was performed as previously described [188]. Briefly, cross-linking was conducted with formaldehyde (Merck) at 1% final concentration and terminated after 5 minutes by addition of glycine at a final concentration of 0.125 M. Cells were harvested in SDS buffer (50 mM Tris pH 8.1, 0.5% SDS, 100 mM NaCl, 5 mM EDTA), pelleted and resuspended in IP buffer (2 parts of SDS buffer and 1 part Triton dilution buffer (100 mM Tris-HCl pH 8.6, 100 mM NaCl, 5 mM EDTA, pH 8.0, 0.2% NaN_3, 5.0% Triton X-100)). Chromatin was sheered by 8 sonication cycles (HTU SONI 130, G. Heinemann) to generate DNA fragments with an average size of 700 bp for qChIP. Preclearing and incubation with monoclonal HIF1A antibody (H1alpha67) (NB100-105, Novus Biologicals) or mouse IgG antibody control (M-7023, Sigma) for 16 hours was performed as previously described [189]. Washing and reversal of crosslinking was performed as described [190]. ChIP-DNA was analyzed by qPCR and the enrichment was expressed as fold enrichment compared to IgG. Binding to a

region on chromosome 16q22 served as negative control in all ChIP assays performed. Antibodies used here are listed in **Table 3.5**. The sequences of oligonucleotides used as qChIP primers are listed in Supplemental **Table 3.6.3**.

4.8 Indirect immunofluorescence and confocal laser-scanning microscopy

Cells cultivated on glass cover-slides were fixed in 4% paraformaldehyde/PBS for 10 minutes, permeabelized in 0.2% Triton X 100 for 20 minutes and blocked in 100% FBS for 30 minutes. F-Actin was detected with Phalloidin conjugated with Alexa Flour 647 (Invitrogen). Chromatin was stained by DAPI (Roth). Slides were covered with ProLong Gold Antifade (Invitrogen). Antibodies used here are listed in **Table 3.5**. CLSM (confocal laser scanning microscopy) images were captured with a LSM700 microscope using a Plan Apochromat 20x/0.8 M27 objective and ZEN 2009 software (Zeiss) with the following settings: image size: 2048x2048 and 16 bit; pixel/dwell of 25.2 µs; pixel size 0.31 µm; laser power 2% and master gain 600-1000. After image capturing the original CLSM files were converted into TIFF files.

4.9 Modified Boyden-chamber assay for analysis of migration and invasion

Migration and invasion analyses were conducted as described previously [48]. In short, cells were serum-starved by cultivation in 0.1% serum for 24 hours. To analyze migration, $5x10^4$ cells were seeded in the upper chamber (8.0 µm pore size membrane; Corning) in serum-free medium. To analyze invasion, chamber membranes were first coated with Matrigel (BD Bioscience) at a dilution of 3.3 ng/ml in medium without serum. Then $8x10^4$ cells were seeded on the Matrigel in the upper chamber in serum free medium. 10% FBS was placed as a chemo-attractant in the lower chamber. After cells were cultured for 48 hours, non-motile cells at the top of the filter were removed and the cells in the bottom chamber were fixed with methanol, stained with DAPI and counted using immunofluorescence microscopy. Relative invasion/migration was normalized to the corresponding control.

4.10 Wound-healing assay

The wound healing assay was performed as described previously [31]. In brief, Mitomycin C [10 ng/ml] was added two hours before generating a scratch using a Culture-Insert (IBIDI, 80241). After washing twice with HBSS to remove Mitomycin C and detached cells, medium was added. Cells were allowed to close the wound for the indicated periods. Images were captured on an Axiovert Observer Z.1 microscope connected to an AxioCam MRm camera using the Axiovision software (Zeiss).

4.11 Luciferase reporter assay

H1299 cells were seeded in 12-well format dishes at 3×10^4 cells/well for 24 hours, transfected 100 ng of the respective firefly luciferase reporter plasmid, 20 ng of *Renilla* reporter plasmid as a normalization control and 25 nM of *pre-miR-34a* or *pre-miR-34c* (Ambion, PM11030, PM11039) or a negative control oligonucleotide (Ambion, neg. control #1) with HiPerFect Transfection Reagent (Qiagen). The analysis was performed with Dual Luciferase Reporter assay kit (Promega) according to manufacturer's instructions. Luminescence intensities were measured by an Orion II luminometer (Berthold) in 96-well format and analyzed with the SIMPLICITY software package (DLR).

4.12 Site directed mutagenesis

Putative seed matching sequences were mutated from CACTGCCA to CAGTCGGA in order to abolish the binding reaction. This was achieved with the QuikChange II XL Site-Directed Mutagenesis Kit (Agilent Technologies) using the respective mutagenic primers and performing the mutagenic reaction according to the manufacturer's instructions. Plasmid sequences were verified by sequencing. Oligonucleotides used for cloning and mutagenesis are provided in **Table 3.6.2**.

The HRE2 site was mutated from ACGTG to AAAGG with the the QuikChange II XL Site-Directed Mutagenesis Kit (Agilent Technologies) using the respective mutagenic

primers and performing the mutagenic reaction according to the manufacturer's instructions. Plasmid sequences were verified by sequencing. Oligonucleotides used for cloning and mutagenesis are provided in **Table 3.6.4**.

4.13 RNA interference

For RNA interference, siRNAs (Ambion silencer siRNA negative control #1: ID#4611; *STAT3*-specific siRNAs: ID#6880; *Inh3*-specific siRNAs: ID#s13943; *HIF1A*-specific siRNAs: ID#s6539) were transfected at a final concentration of 10 nM for the indicated time-points using HiPerfect transfection reagent (Qiagen).

4.14 Colony formation assay

For low-density, colony formation assays, 200-500 cells were seeded into a 6-well plate and cultivated for one day at 20% O_2 and subsequently exposed to 0.5% O_2 for two days, and subsequently treated with or without 5-FU for three days. Subsequently, cells were fixed and stained with crystal violet. Colonies were photographed and the staining was extracted by 33% Acetic acid and subsequently measured with a Varioskan Flash Multimode Reader using SkanIt RE for Varioskan 2.4.3 software (Thermo Scientific). The measured values of were normalized to the corresponding controls.

4.15 Analysis of TCGA-COAD data

The expression profiles of 425 colon adenocarcinomas were obtained from the TCGA data portal [106] (https://tcga-data.nci.nih.gov/tcga/tcgaDownload.jsp). Spearman correlation coefficient analysis was performed with the Prism5 program (Graph Pad Software Inc.).

4.16 Animal experiments

4.16.1 Animal experiments

NOD/SCID mice were purchased from the Jackson Laboratory. The generation of *miR-34a*$^{-/-}$ mice with a C57BL6/SV129 back-ground has been described previously [79]. *miR-34b/c*$^{-/-}$ mice were kindly provided by Dr. Alexander Nikitin (Cornell University) [191]. *miR-34a*$^{-/-}$; *b/c*$^{-/-}$ compound mice were generated by crossing *miR-34a*$^{-/-}$ and *miR-34b/c*$^{-/-}$. *Apc*$^{Min/+}$ mice were kindly provided by Dr. Marlon Schneider. *miR-34a*$^{-/-}$; *b/c*$^{-/-}$ and *miR-34a*$^{+/+}$; *miR-34bc*$^{+/+}$ mice were crossed with *Apc*$^{Min/+}$ mice to obtain *miR-34a/b/c*$^{-/-}$; *Apc*$^{Min/+}$, and *miR-34a/b/c*$^{+/+}$ *Apc*$^{Min/+}$ mice. Mice were housed in individually ventilated cages (IVC) cages using “Lingocel Select” bedding. All experiments involving mice were conducted with approval by the local Animal Experimentation Committee (Regierung of Oberbayern). All experiments were performed in accordance with the ARRIVE guidelines and regulations.

4.16.2 Metastasis formation in NOD/SCID mice

DLD-1 cells stably expressing Luc2 were generated as described previously [30]. 4x10^6/0.2 ml HBSS DLD-1-luc2 cells were injected into the lateral tail vein of NOD/SCID mice using 25-gauge needles. Cells transfected with *Inh3* and control siRNAs were injected into sibling littermates. Anesthetized mice were injected intraperitoneal with D-luciferin (150 mg/kg) and imaged half hour after injection using the IVIS Illumina System (Caliper Life Sciences). In weekly intervals anesthetized mice were injected intraperitoneal with D-luciferin (150 mg/kg) and imaged ten minutes after injection using the IVIS Illumina System (Caliper Life Sciences). The acquisition time was two minutes. Seven weeks after tail vein injection, mice were sacrificed and examined for lung metastases using H&E (hematoxylin and eosin) staining, lungs were fixed with 4% paraformaldehyde and 5 µm paraffin sections were stained with H&E. The number of metastases was determined microscopically. All

studies involving mice were conducted with approval by the local Animal Experimentation Committee (Regierung of Oberbayern).

4.16.3 Immunohistochemical analysis of murine adenomas

The samples were collected from 18 weeks old mice. *MiR-34a*$^{-/-}$; *miR-34bc*$^{-/-}$; *Apc*$^{Min/+}$ and *miR-34a*$^{+/+}$; *miR-34bc*$^{+/+}$; *Apc*$^{Min/+}$ samples were fixed in formalin, and paraffin embedded. 3 µm thick sections were de-paraffinized in xylene and rehydrated in serial dilution of ethanol and water prior to antigen retrieval in Target Retrieval Solution (pH6.0, Dako Cytomation) in a microwave oven and TBST washing. After neutralization of endogenous peroxidase with 3% H2O2 for ten minutes, the sections were incubated with 20% goat serum in TBST for 1 hour. Afterwards, primary antibodies were applied at 4°C overnight (HIF1A (LS-B12555, LSBio LifeSpan BioSciences), INH3 (SAB4502938, Sigma-Aldrich)). Anti-rabbit conjugated to HPR were applied at room temperature for 1 hour. DAB (3, 3'-diaminobenzidine, Dako) was used as a substrate-chromogen. After counterstaining with hematoxylin, the sections were analyzed using Zeiss LSM 700 confocal microscopy. Antibodies used here are listed in **Table 3.5**.

4.16.4 Western blot analysis of murine adenomas

The samples were collected from 18 weeks old mice. For protein lysates from *MiR-34a*$^{-/-}$; *miR-34bc*$^{-/-}$; *Apc*$^{Min/+}$ and *miR-34a*$^{+/+}$; *miR-34bc*$^{+/+}$; *Apc*$^{Min/+}$ samples were lysed in RIPA buffer. Lysates were sonicated using a HTU SONI130 (G. Heinemann Ultraschall- und Labortechnik) and centrifuged at 16.060 g for fifteen minutes at 4°C. Protein concentration was measured with BCA Protein Assay Kit (Thermo Fisher Scientific) according to manufacturer's instructions. The protein concentration was measured with a Varioskan Flash Multimode Reader using the SkanIt RE for Varioskan 2.4.3 software (Thermo Scientific). Subsequently, 30 to 60 µg of whole cell lysate per lane were loaded. The separation of the proteins by electrophoresis was

performed and were transferred onto Immobilon PVDF membranes (Millipore) using standard protocols (Bio-Rad laboratories). Enhanced Chemiluminescence (ECL, Millipore) signals were recorded with 440CF imaging system (Eastman Kodak Co.). Antibodies used here are listed in **Table 3.5**.

4.16.5 qPCR analysis of murine adenomas

The samples were collected from 18 weeks old mice. Total RNA was isolated from *MiR-34a*$^{-/-}$; *miR-34bc*$^{-/-}$; *Apc*$^{Min/+}$ and *miR-34a*$^{+/+}$; *miR-34bc*$^{+/+}$; *Apc*$^{Min/+}$ samples using the RNeasy Plus Mini Kit (Qiagen). Nanodrop spectrophotometer was used to determine the amount and quality of the RNA. cDNA was generated using anchored oligo(dT) primers (Verso cDNA synthesis Kit (Thermo scientific)) following the manufacturer's instructions. qPCR was performed by using Fast SYBR Green Master Mix (Applied Biosystems) and a LightCycler 480 II (Roche Diagnostics). The expression of mRNA and primary miRNA was normalized by detection of β-actin as previously described in [192]. The qPCR results are indicated the fold of change, which was analysed by the comparative Ct (ΔΔCt) method with the control set to 1 as described before [187]. Oligonucleotides used for qPCR are provided in **Table 3.6.1**.

4.17 Tumoroid analysis

4.17.1 Tumoroid culture

Intestinal adenoma cells from 18 weeks old *miR-34a*$^{-/-}$; *miR-34bc*$^{-/-}$; *Apc*$^{Min/+}$ and *miR-34a*$^{+/+}$; *miR-34bc*$^{+/+}$; *Apc*$^{Min/+}$ mice were isolated and counted using a hemocytometer. Single cells were embedded in Matrigel and seeded in 24-well plates (15,000 single cells per 50 µl Matrigel per well). The tumor organoid culture medium was formulated as described before [193].

4.17.2 Immunofluorescence staining of tumoroids

Tumoroids were fixed with 4% paraformaldehyde (PFA) for twenty minutes at room temperature, followed by permeabilization in 0.1% Triton X-100. Immunofluorescence was performed using antidodies specific for cleaved caspase-3 (9661, Cell Signaling Technology). The secondary antibody was Alexa Fluor 488 conjugated antibodies. DNA was stained with DAPI. The images of tumoroids were taken with a Zeiss LSM 700 confocal microscope. Antibodies used here are listed in **Table 3.5**.

4.18 Analysis of human CRC samples

INH3 expression was evaluated using formalin-fixed, paraffin-embedded (FFPE) colon cancer samples of 84 patients who underwent surgical tumor resection at the Ludwig-Maximilians University of Munich (LMU) between 1994 and 2005. Follow-up data were recorded by the tumor registry Munich. All tumors were located on the right side of the colon. Half of the patients had colon cancers with synchronous liver metastases diagnosed by clinical imaging or liver biopsy. Controls consisted of colon cancer patients without distant metastases at the time of diagnosis and with a disease-free survival of at least 5 years after primary surgical resection. The samples of cases and controls were matched by tumor grade (according to WHO 2000), T-classification (according to TNM Classification of Malignant Tumors 2009), and tumor localization, resulting in 42 matched pairs. Tissue microarrays (TMAs) were generated with 6 representative 1 mm cores of each case. 5 µm TMA sections were prepared, deparaffinized, and stained with INH3 antibody (sc-376034, Santa Cruz) or Laminin 5γ2 antibody (MAB19562, Merck Millipore) or GLUT1 antibody (sc-377228, Santa Cruz) on a Ventana Benchmark XT Autostainer with UltraView Universal DAB and alkaline phosphatase detection kits (Ventana Medical Systems). Frequencies were analyzed using the Chi-square test. Statistical procedures were performed using SPSS Statistics 23.0 (IBM). Samples and patient data were anonymized and the need

for consent was waived by the institutional ethics committee of the Medical Faculty of the LMU. Antibodies used here are listed in **Table 3.5**.

4.19 Statistical analysis

Calculations of significant differences between two groups of samples were analyzed by a Student's t-test (unpaired, two tailed) using Prism5 (Graph Pad Software Inc.). *P*-values ≤ 0.05 were considered as significant.

5. Results

5.1 Hypoxia induces EMT via activation of HIF1A in CRC cells

In order to study the molecular regulation of hypoxia-induced EMT in CRC, the CRC cell lines DLD-1, HT29, and HCT15, which show epithelial characteristics, were exposed to low oxygen concentrations (0.5% O_2) for 30 hours. DLD-1 and HCT15 cells represent micro-satellite instable (MSI), whereas HT29 cells represent microsatellite stable (MSS) CRC lines (see also **Table 5.1** for the main genetic features of the CRC lines used here).

Table 5.1 *TP53, APC, KRAS, BRAF, PIK3CA* and microsatellite status of CRC cell lines.

Origin	Cell lines	*TP53*	*APC*	*KRAS*	*BRAF*	*PIK3CA*	MSI status
human	DLD-1	MUT	MUT	MUT	MUT	MUT	MSI
	HT29	MUT	MUT	WT	MUT	MUT	MSS
	HCT15	MUT	MUT	MUT	WT	MUT	MSI
	LoVo	WT	MUT	MUT	?	WT	MSI
	SW480	MUT	MUT	MUT	WT	WT	MSS
	SW620	MUT	MUT	MUT	WT	WT	MSS
	HCT116 *TP53*$^{-/-}$	KO	WT	MUT	WT	MUT	MSI
	HCT116 *TP53*$^{+/+}$	WT	WT	MUT	WT	MUT	MSI
	RKO *TP53*$^{-/-}$	KO	WT	WT	MUT	MUT	MSI
	RKO *TP53*$^{+/+}$	WT	WT	WT	MUT	MUT	MSI
	SW48 *TP53*$^{-/-}$	KO	WT	WT	WT	WT	MSI
	SW48 *TP53*$^{+/+}$	WT	WT	WT	WT	WT	MSI
murine	CT26	WT	WT	MUT	WT	WT	MSS

All lines displayed changes in morphology consistent with EMT, such as an increase in scattering, adoption of a spindle-like shape and decreased cell–cell contacts (**Figure 5.1A**). As expected, expression of HIF1A protein was induced by hypoxia (**Figure 5.1B**). In addition, hypoxia caused down-regulation of the epithelial marker *E-Cadherin* and up-regulation of mesenchymal markers, such as *Vimentin*

(VIM), SNAIL, FN and *ZEB1* in DLD-1 cells (**Figure 5.1B-C**). As reported previously [163, 194], STAT3 was activated by hypoxia, as evidenced by increased phosphorylation at residue S727.

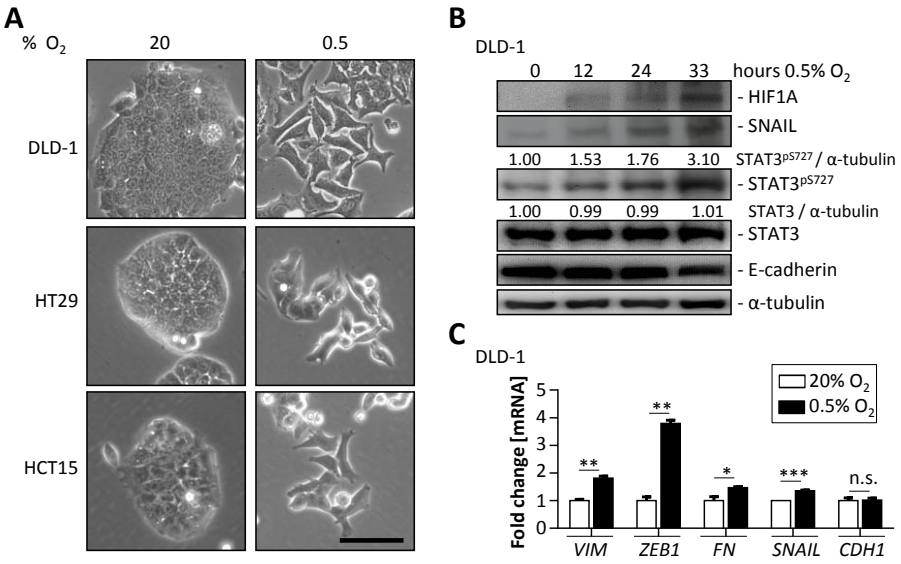

Figure 5.1 Hypoxia induces EMT. (**A**) Representative phase-contrast pictures, (**B**) Western blot and (**C**) qPCR analysis of DLD-1 cells exposed to 20% O_2 or 0.5% O_2 for 24 hours as indicated. Scale bar represents 25 µm. In panels **C** mean values ± SD (n = 3) are provided. (*) $P < 0.05$, (**) $P < 0.01$ and (***) $P < 0.001$.

Later, DLD-1 cells were treated with cobalt chloride ($CoCl_2$), a chemical inducer of HIF1A. Similar results were obtained after addition of $CoCl_2$ (**Figure 5.2**). $CoCl_2$ treatment caused down-regulation of the epithelial marker *E-Cadherin* and up-regulation of mesenchymal markers, such as *Vimentin (VIM), SNAIL, FN* and *ZEB1* in DLD-1 cells (**Figure 5.2A-B**). STAT3 was also activated by $CoCl_2$ treatment, as evidenced by increased phosphorylation at residue S727 (**Figure 5.2C**).

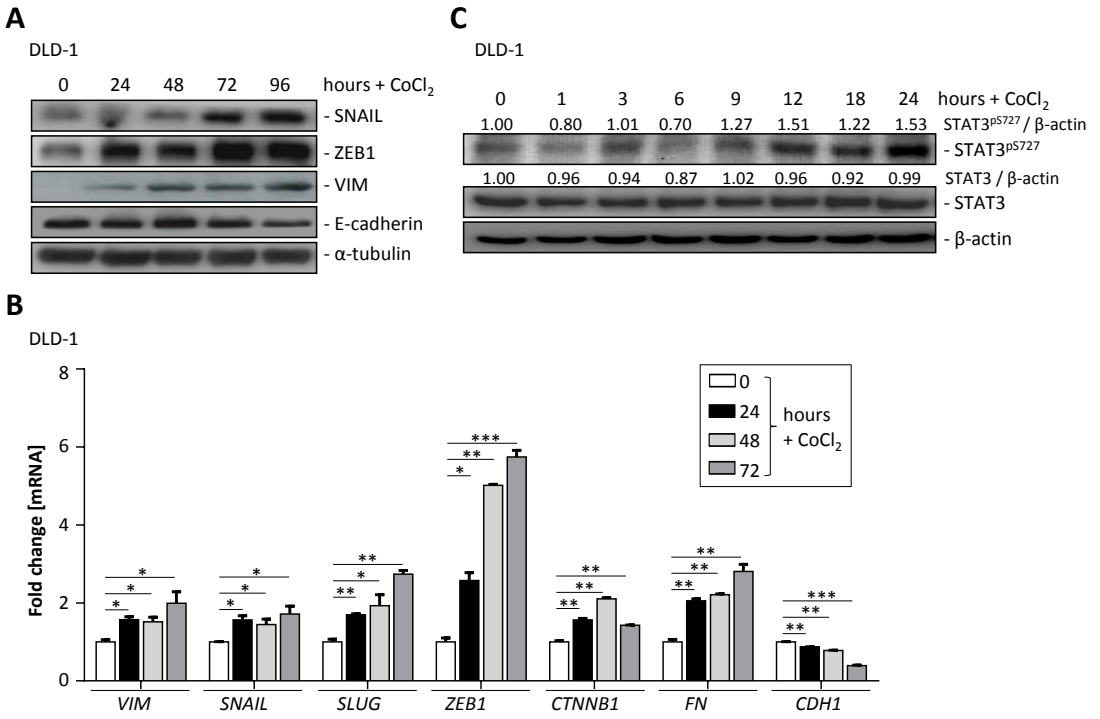

Figure 5.2 Cobalt Chloride induces EMT. (**A**) Western blot, (**B**) qPCR and (**C**) Western blot analysis of the indicated proteins in DLD-1 cells treated with $CoCl_2$ for the indicated periods. In panels **B** mean values ± SD (n = 3) are provided. (*) $P < 0.05$, (**) $P < 0.01$ and (***) $P < 0.001$.

Hypoxia also resulted in the loss of E-cadherin from the outer membrane and the formation of F-actin stress-fibers in the cytoplasm (**Figure 5.3**). Both events represent hallmarks of EMT [195].

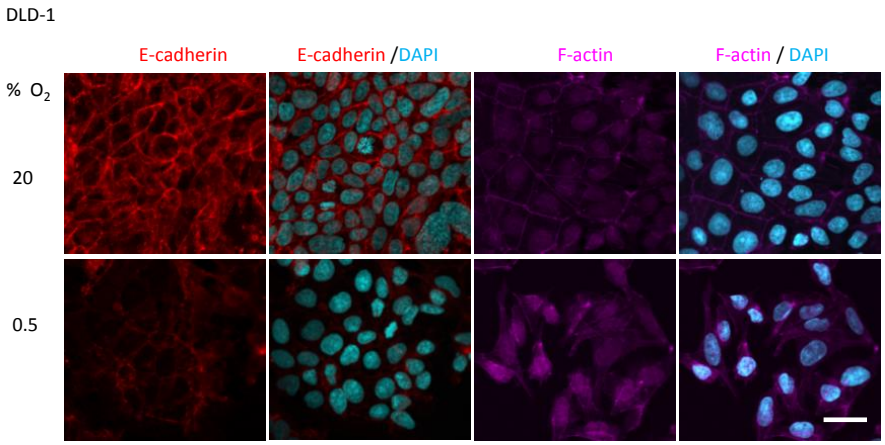

Figure 5.3 Hypoxia induces EMT. Indirect immunofluorescence detections of the indicated proteins in DLD-1 cells exposed to 20% O_2 or 0.5% O_2 for 24 hours. Scale bar represents 25 µm.

Hypoxia and $CoCl_2$ treatment also enhanced invasion and migration of DLD-1 cells in a modified Boyden-chamber assay (**Figure 5.4**).

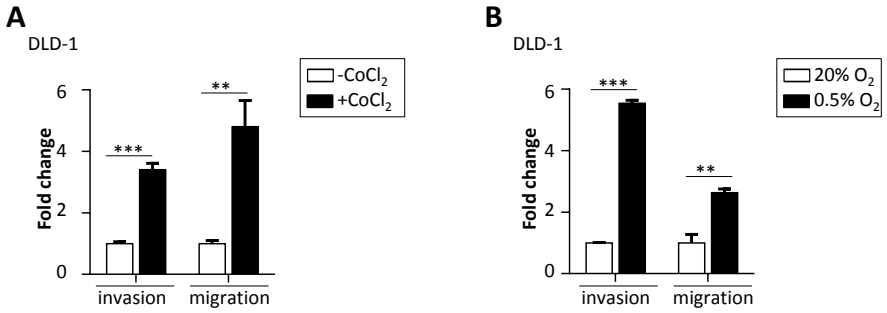

Figure 5.4 Hypoxia enhances invasion and migration. Relative invasion and migration of DLD-1 cells treated with cobalt chloride (40 ng/ml) (**A**) and hypoxia (**B**). mean values ± SD (n = 3) are provided. (*) $P < 0.05$, (**) $P < 0.01$ and (***) $P < 0.001$.

Hypoxia-induced EMT, as well as invasion and migration, were mediated by activation of HIF1A in CRC cells, since treatment with *HIF1A*-specific siRNAs suppressed these processes (**Figure 5.5**). Therefore, the subsequent analyses on HIF1A mediated effects were focused.

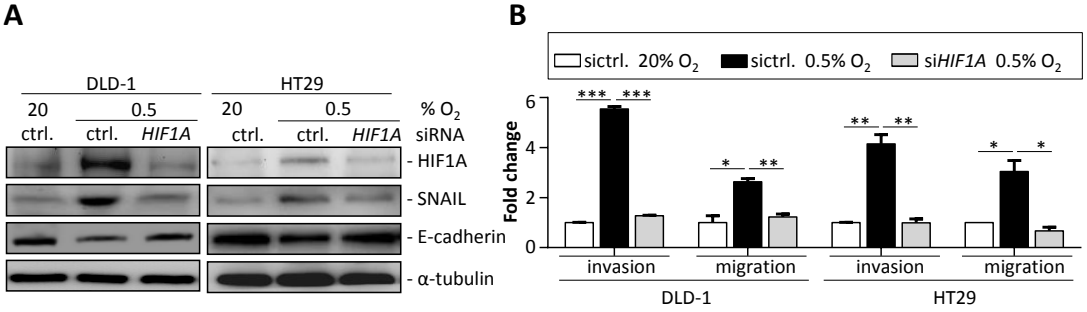

Figure 5.5 Hypoxia induces HIF1A-dependent EMT. (**A**) Western blot and (**B**) relative invasion and migration analyses in DLD-1 and HT29 cells transfected with indicated siRNA for 24 hours and then cultured at 20% O_2 or 0.5% O_2 for 30 hours. In panels **B** mean values ± SD (n = 3) are provided. (*) $P < 0.05$, (**) $P < 0.01$ and (***) $P < 0.001$.

5.2 HIF1A directly represses *miR-34a* expression

I also noted that the expression of primary and mature miR-34a and primary *miR-34b/c* was repressed in a number of *TP53*-deficient, whereas they were induced in *TP53*-proficient CRC cell lines (**Figure 5.6**) indicating a role of p53 in this context which will be addressed later.

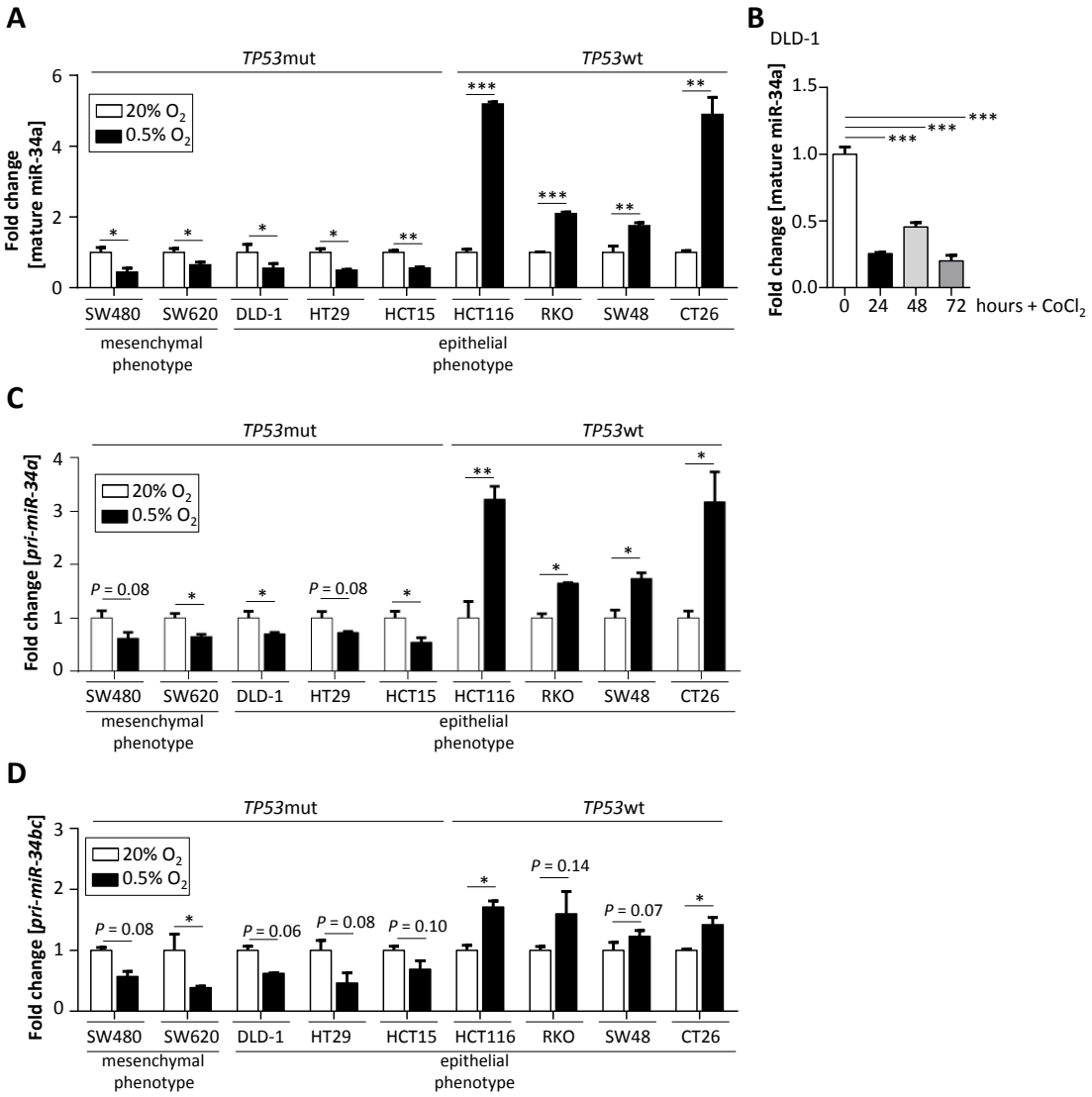

Figure 5.6 Differential expression of miR-34a and miR-34c in CRC cell lines in the response to hypoxia. (**A**) qPCR analysis of mature miR-34a expression in the indicated CRC cell lines at 0.5% O_2 for 48 hours. (**B**) qPCR analysis of indicated mRNAs in DLD-1 cells treated with $CoCl_2$ for the indicated periods. (**C**, **D**) qPCR analysis of indicated mRNAs and miRNAs in different cell lines kept at 20% O_2 or 0.5% O_2 for 48 hours. mean values ± SD (n = 3) are provided. (*) $P < 0.05$, (**) $P < 0.01$ and (***) $P < 0.001$.

Notably, inactivation of *HIF1A* by RNA interference prevented the down-regulation of *pri-miR-34a* (**Figure 5.7**), suggesting that HIF1A is directly represses *miR-34a,* which encodes a p53-inducible microRNA with tumor suppressive features [79, 156].

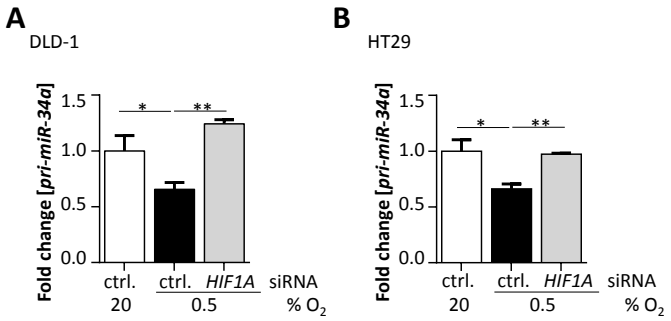

Figure 5.7 Hypoxia represses miR-34a via HIF1A. qPCR analysis of DLD-1 (**A**) and HT29 (**B**) cells transfected with indicated siRNAs for 24 hours and then cultured at 20% O_2 or 0.5% O_2 for 30 hours. mean values ± SD (n = 3) are provided. (*) $P < 0.05$, (**) $P < 0.01$ and (***) $P < 0.001$.

Indeed, three conserved HIF1A binding sites with the sequence 5'-[A/G]CGTG-3') 700 bp upstream of the *miR-34a* TSS (transcriptional start site) indicated as HRE (hypoxia-response element) 1-3 in **Figure 5.8A** were identified.

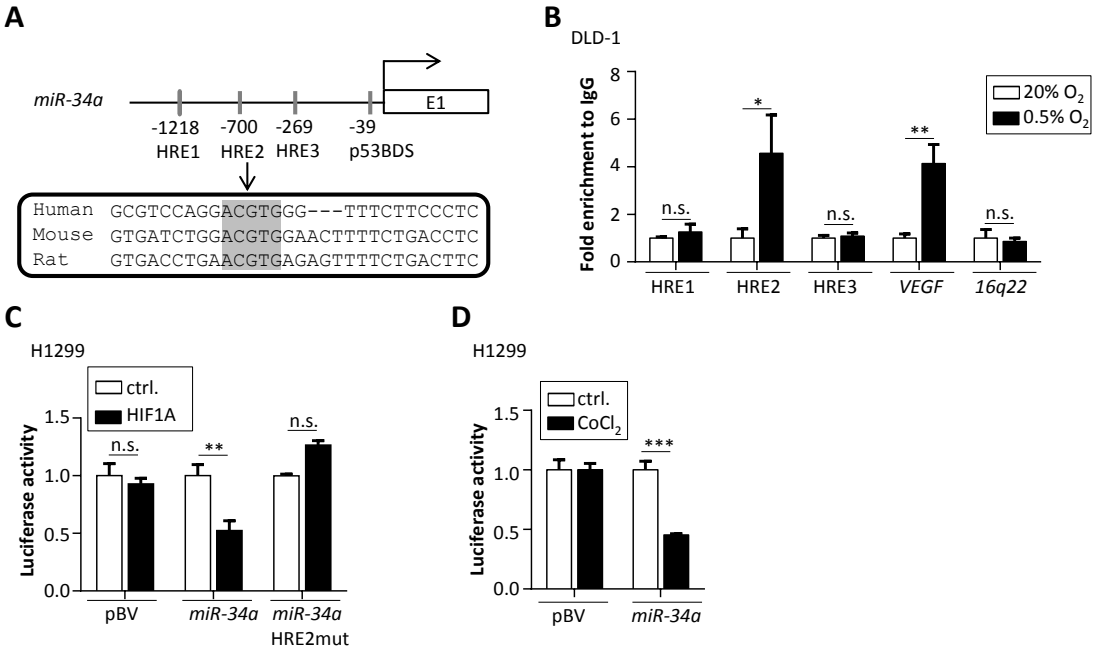

Figure 5.8 Direct repression of *miR-34a* by HIF1A. (**A**) Map of the human *miR-34a* genomic region indicating conserved HIF1A binding sites. (**B**) ChIP analysis of HIF1A occupancy at human *miR-34a* and *VEGF* (positive control) promoters. *16q22* locus served as neg. control. (**C**) Dual-reporter assay after transfection of H1299 cells with the indicated reporters and constitutively active HIF1A encoding plasmids. (**E**) Dual reporter assay after transfection of H1299 cells with the indicated reporter constructs and treatment with cobalt chloride (40 ng/ml) for 48 hours. In panels **B**, **C** and **D** mean values ± SD (n = 3) are provided. (*) $P < 0.05$, (**) $P < 0.01$ and (***) $P < 0.001$.

By chromatin immuno-precipitation (ChIP) HIF1A occupancy was detected at HRE2, but not at HRE1 and HRE3 in hypoxic DLD-1 cells (**Figure 5.8B**). HIF1A occupancy at the *VEGF* promoter served as a positive control. Furthermore, a reporter containing the *miR-34a* promoter region was repressed by ectopic expression of a constitutively active version of HIF1A and after treatment of cells with $CoCl_2$ (**Figure 5.8B-C**). The repression by HIF1A was abolished by introduction of mutations into HRE2 (**Figure 5.8B**).

As expected, the *miR-34a* reporter was induced by ectopic p53 expression (**Figure 5.9**). Interestingly, increasing amounts of HIF1A encoding plasmids were sufficient to suppress activation of the reporter by p53. However, in the presence of equimolar amounts of p53 and HIF1A plasmids activation of *miR-34a* by p53 was dominant over its repression by HIF1A.

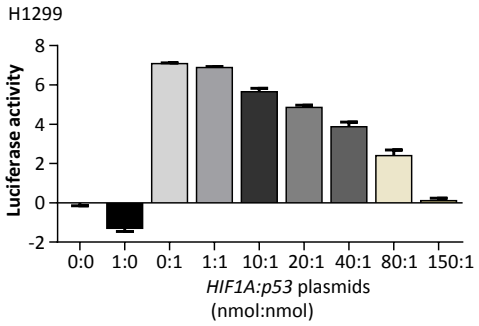

Figure 5.9 Analysis of HIF1A/p53 antagonism. Dual reporter assay after transfection of H1299 cells with the indicated reporter constructs for 48 hours.

Interestingly, the induction of *miR-34a* in *TP53*-proficient CRC cell lines under hypoxia was not reversed by long-term exposure to low oxygen concentrations (**Figure 5.10**), indicating that increasing or sustained levels of hypoxia in *TP53*-proficient CRC cells are not sufficient to overcome the induction of *miR-34a* by p53. Taken together, these results show that *miR-34a* is directly repressed by HIF1A under hypoxic conditions in the absence of wild-type *TP53*.

Also *miR-34b/c* expression was down-regulated under hypoxic conditions in *TP53*-deficient and induced in *TP53*-proficient CRC cell lines (**Figure 5.6D**). Since the *miR-34b/c* promoter does not harbor a HRE (data not shown), *miR-34b/c* might be repressed by hypoxia via an indirect mechanism. As miR-34a is expressed at least hundred times higher than miR-34b/c in CRC lines and tumors [31], miR-34b/c was not analyzed further.

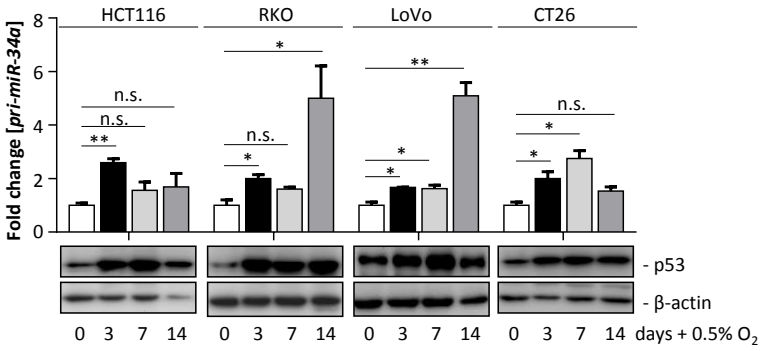

Figure 5.10 Effects of long-term hypoxia on *pri-miR-34a* expression. qPCR (upper panel) and Western blot (lower panel) analysis of human *TP53*-proficient CRC cell lines HCT116, RKO, LoVo and murine *TP53*-proficient CRC cell line CT26 exposed to 0.5% O_2 for indicated time points. mean values ± SD (n = 3) are provided. (*) $P < 0.05$, (**) $P < 0.01$ and (***) $P < 0.001$.

Ectopic miR-34a expression suppressed the hypoxia-mediated induction of *VIM*, *SNAIL*, *SLUG*, and *ZEB1*, as well as the down-regulation of *E-Cadherin* in DLD-1 cells (**Figure 5.11A-B**, upper panel). Moreover, ectopic miR-34a prevented hypoxia-induced invasion and migration of DLD-1 cells (**Figure 5.11B**, lower panel).

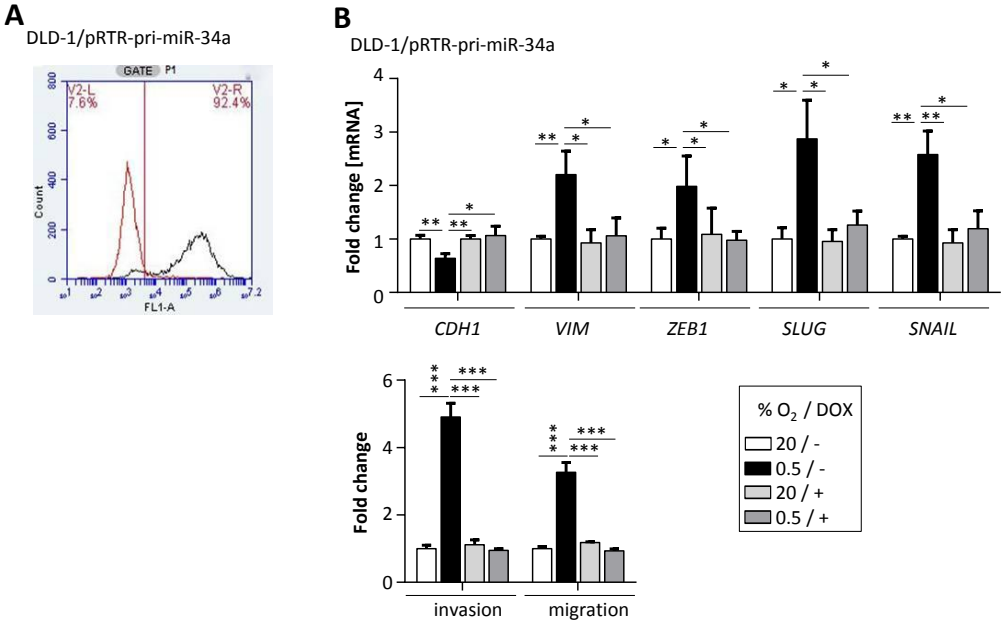

Figure 5.11 Requirement of miR-34a down-regulation for EMT induced by hypoxia. (**A**) Flow cytometric determination of the frequency of DLD-1 cells by detection of eGFP expression. pRTR-pri-miR-34a expression was induced by addition of DOX for 48 hours. (**B**) qPCR (upper panel) and relative invasion and migration (lower panel) in DLD-1/pRTR-pri-miR-34a cells exposed to DOX for 2 days and/or then to 0.5% O_2 for 30 hours. In panels **B** mean values ± SD (n = 3) are provided. (*) $P < 0.05$, (**) $P < 0.01$ and (***) $P < 0.001$.

Similar results were obtained after treatment of DLD-1 cells with $CoCl_2$ (**Figure 5.12**). Therefore, down-regulation of *miR-34a* by HIF1A is required for hypoxia-induced EMT and invasion.

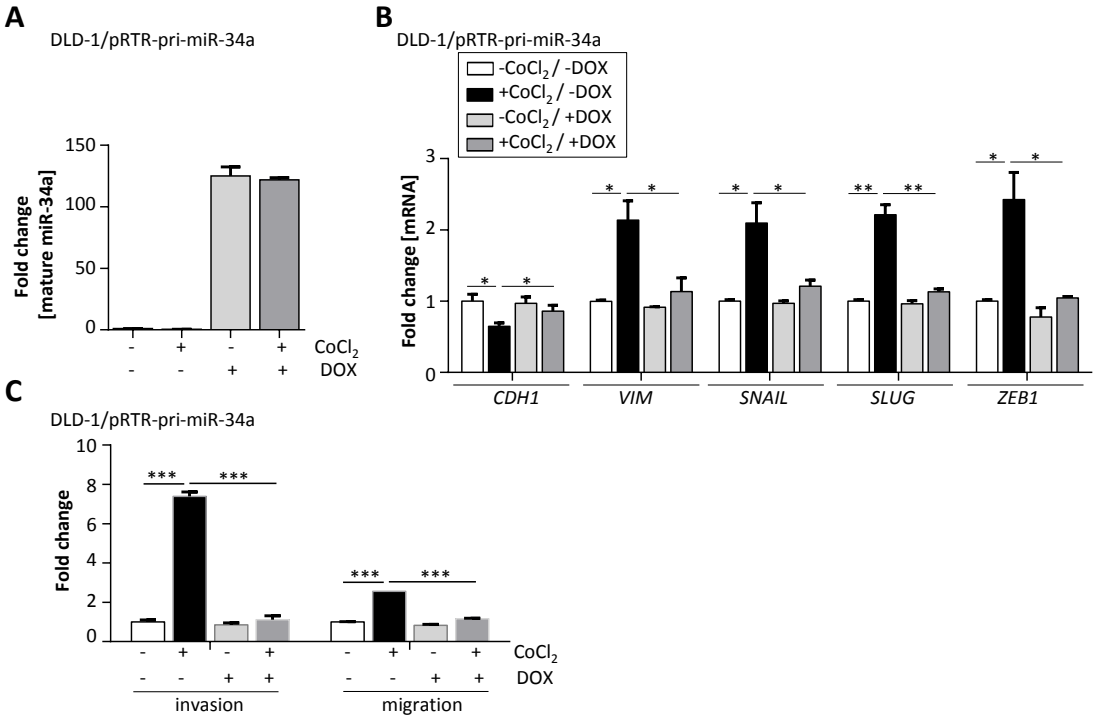

Figure 5.12 Requirement of miR-34a down-regulation for EMT induced by $CoCl_2$. qPCR analysis of the indicated mRNAs (**A**-**B**) and relative invasion and migration (**C**) in DLD-1/pRTR-pri-miR-34a cells after addition of DOX for 48 hours and subsequent treatment with $CoCl_2$ for 24 hours. In panels **B** and **C** mean values ± SD (n = 3) are provided. (*) $P < 0.05$, (**) $P < 0.01$ and (***) $P < 0.001$.

5.3 *Inh3* is a direct miR-34a target

The hypoxia-mediated phosphorylation of STAT3 at S727 was blocked by *HIF1A*-specific siRNAs in DLD-1 and HT29 cells (**Figure 5.13A**). Moreover, down-regulation of STAT3 by siRNAs reversed the hypoxia-mediated repression of *E-Cadherin* and the up-regulation of *SNAIL*, as well as invasion and migration in DLD-1 and HT29 cells (**Figure 5.13B-C**). Therefore, HIF1A-mediated STAT3 activation is required for the induction of EMT by hypoxia.

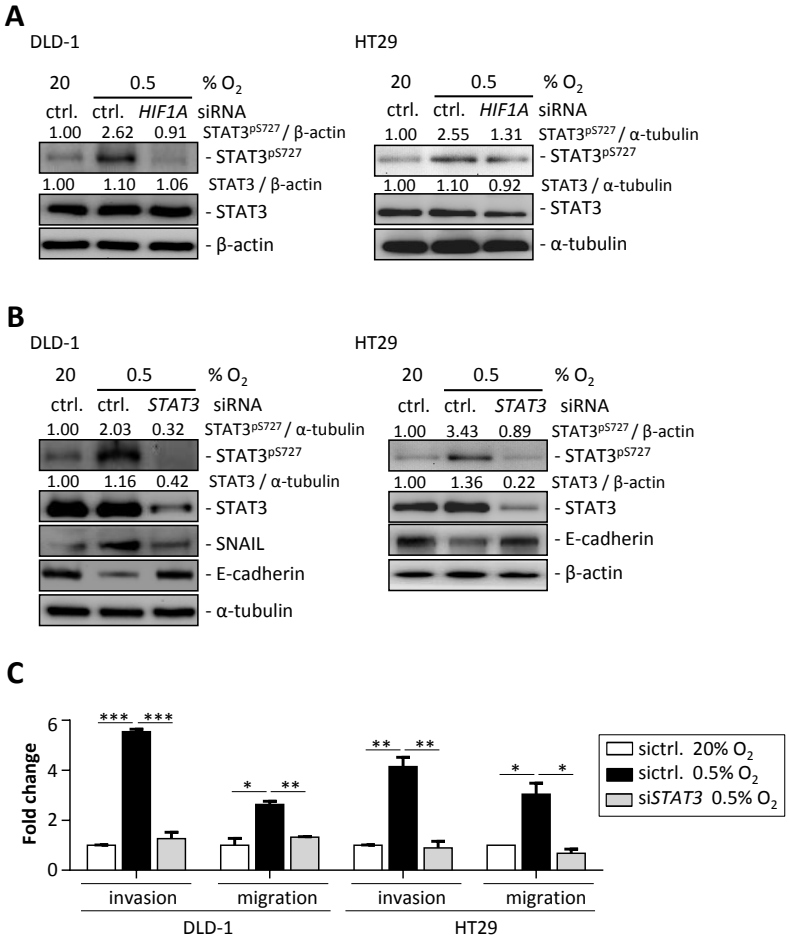

Figure 5.13 STAT3 mediates hypoxia-induced EMT. (**A**-**B**) Western blot and **(C)** relative invasion and migration analysis of DLD-1 and HT29 cells transfected with indicated siRNA for 24 hours and then cultured at 20% O_2 or 0.5% O_2 for 30 hours. In panels **C** mean values ± SD (n = 3) are provided. (*) $P < 0.05$, (**) $P < 0.01$ and (***) $P < 0.001$.

Since increased phosphorylation of STAT3 at S727 and down-regulation of miR-34a in DLD-1 cells exposed to hypoxia were observed (**Figure 5.2.1B**, and **Figure 5.6A**), whether these events may be causally related was asked. Indeed, $STAT3^{pS727}$ was decreased after ectopic expression of miR-34a in SW480 cells, which is known to induce MET in these cells [48], whereas total levels of STAT3 protein remained unchanged (**Figure 5.14**). Therefore, I hypothesized that the induction of an uncharacterized miR-34a target is presumably involved in the activation of STAT3 by hypoxia.

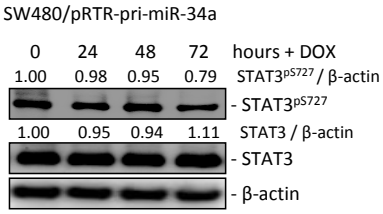

Figure 5.14 miR-34a decreases the level of STAT3^{pS727}. Western blot analysis in SW480/pRTR-pri-miR-34a cells after addition of DOX for the indicated periods.

To identify direct or indirect activators of STAT3 that are directly regulated by miR-34a I used the miRNA target prediction software miRWalk, which combines the results of 10 different algorithms (**Table 5.2**). Thereby, I found that the *Inh3/PPP1R11*, *PPP1R8*, *PPP1R9A* and *PPP1R9B* mRNAs, which encode protein phosphatase 1/PP1 inhibitors, contain miR-34a seed-matching sites and therefore represent putative miR-34a targets (data not shown).

Table 5.2 Predicted miR-34a seed-matching sites in human and murine *Inh3* 3'-UTRs.

miRNA SMS	miRNA target prediction software										SUM
	miR-Walk	Micr-ot4	miR-anda	miR-DB	miR-Map	Pic-tar2	PITA	RNA 22	RNA-hybrid	Target scan	
human *Inh3*:											
miR-34a-5p	1	1	1	1	1	1	0	1	1	1	9
miR-34a-3p	1	0	0	0	0	0	0	0	1	0	2
miR-34b-5p	1	1	1	0	1	0	0	1	1	1	7
miR-34c-5p	1	1	1	1	1	1	0	1	1	1	9
murine *Inh3*:											
miR-34a-5p	1	1	1	1	1	0	1	1	1	1	9
miR-34a-3p	1	0	0	0	0	0	0	0	1	0	2
miR-34b-5p	1	1	1	0	1	0	1	0	1	1	7
miR-34b-3p	1	0	0	0	1	0	1	0	1	1	5
miR-34c-5p	1	1	1	1	1	0	1	1	1	1	9
miR-34c-3p	0	0	0	0	1	0	0	0	1	1	3

Up-regulation of these PP1 inhibitors may lead to activation of STAT3 in cells that display *miR-34a* repression by hypoxia, since STAT3 is negatively regulated by PP1 [196, 197]. Since ectopic expression of miR-34a resulted in the repression of *Inh3* mRNA, but not of *PPP1R8*, *PPP1R9A* or *PPP1R9B* in SW480 cells (**Figure 5.15A-B**), the regulation and role of INH3 in this context was further analyzed. *Inh3* was also repressed by ectopic miR-34a in DLD-1 and SW620 cells (**Figure 5.15D-E**). In addition, INH3 protein expression was repressed by ectopic miR-34a in SW480 and

SW620 cells (**Figure 5.15C and F**). Also in the murine CRC cell line CT26 ectopic *pre-miR-34a* decreased *Inh3* mRNA and INH3 protein expression (**Figure 5.15G-H**).

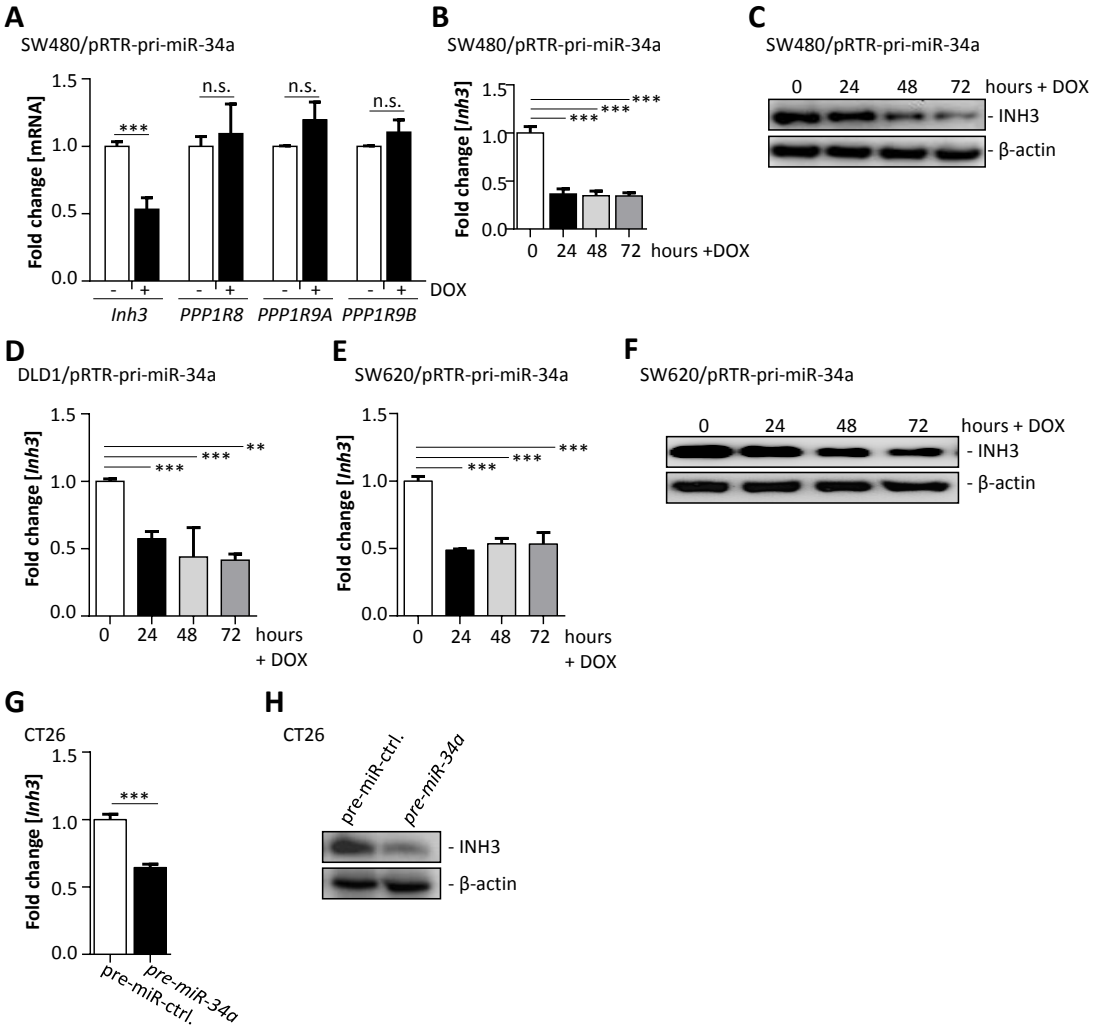

Figure 5.15 Regulation of *Inh3* expression by miR-34a. (**A**-**B**) qPCR and **(C)** Western blot analysis of indicated mRNAs in SW480 harboring pRTR-pri-miR-34a vectors after addition of DOX for the indicated periods. In (A) DOX was added for 48 hours. (**D**-**E**) qPCR and **(F)** Western blot analysis of indicated mRNAs in DLD-1 (**D**) and SW620 (**E**, **F**) harboring pRTR-pri-miR-34a vectors after addition of DOX for the indicated periods. In (A) DOX was added for 48 hours. (**G**) qPCR and **(H)** Western blot analysis of the indicated mRNAs in CT26 cells transfected with *pre-miR-34a* for 48 hours. In panels **A**, **B**, **D**, **E** and **G** mean values ± SD (n = 3) are provided. (*) $P < 0.05$, (**) $P < 0.01$ and (***) $P < 0.001$.

The 3'-UTR of the human and murine *Inh3* mRNA contains two conserved miR-34a seed-matching sites (SMS) (**Figure 5.16A** and **Figure 5.17A**). The human *Inh3* 3'-UTR reporters were both repressed after ectopic expression of miR-34a (**Figure 5.16**). Mutation of the human SMS-1 only partially abrogated this repression, whereas mutation of the human SMS-2 largely blocked repression by miR-34a. In

addition, the combined mutation of both SMS completely alleviated the repression by miR-34a.

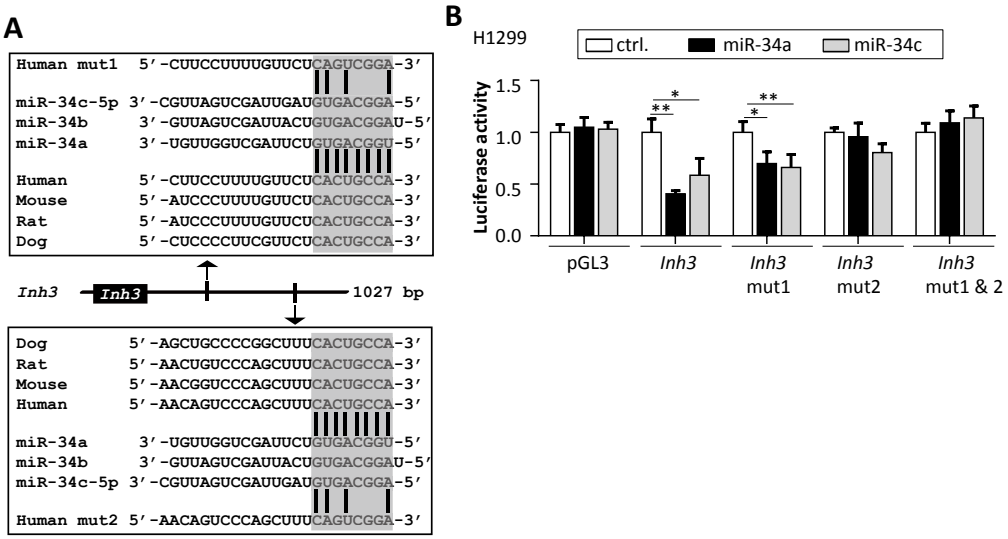

Figure 5.16 Human *Inh3* is a direct target of miR-34a. (**A**) Schematic representation of *Inh3* 3'-UTR indicating the miR-34 seed-matching sequences, phylogenetic conservation and mutagenesis. (**B**) Dual reporter assay after transfection of H1299 cells with the indicated miRNA oligonucleotides and human *Inh3* 3'-UTR reporter constructs. In panels **B** mean values ± SD (n = 3) are provided. (*) $P < 0.05$; (**) $P < 0.01$ and (***) $P < 0.001$.

Similar results were obtained with murine *Inh3* 3'-UTR reporters (**Figure 5.17**). In detail, the murine *Inh3* 3'-UTR reporters were both repressed after ectopic expression of miR-34a (**Figure 5.17**). Mutation of the human SMS-1 only partially abrogated this repression, whereas mutation of the human SMS-2 largely blocked repression by miR-34a. In addition, the combined mutation of both SMS completely alleviated the repression by miR-34a.

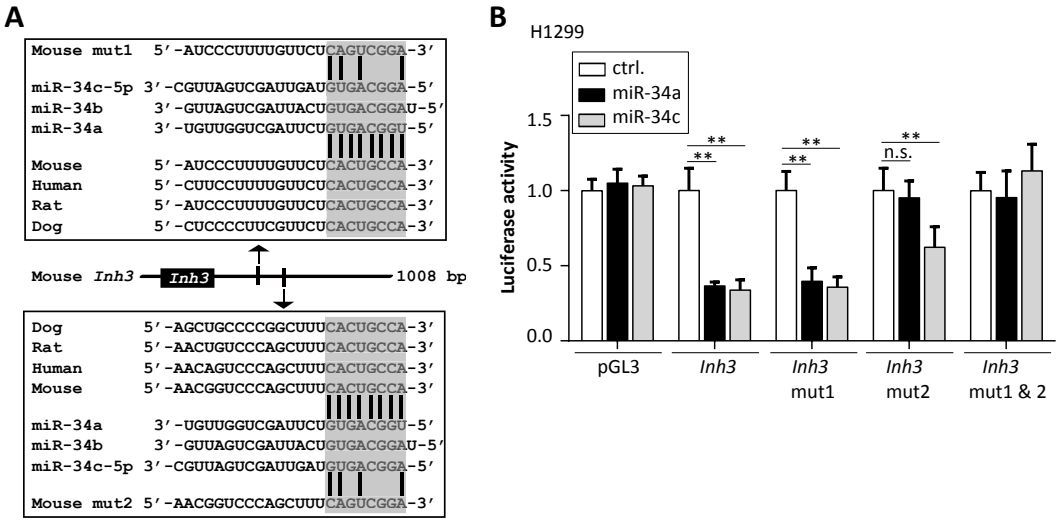

Figure 5.17 Murine *Inh3* is a direct target of miR-34a. (**A**) Schematic representation of the *Inh3* 3'-UTR indicating the miR-34 seed-matching sequences, their phylogenetic conservation and mutagenesis. (**B**) Dual reporter assay after co-transfection of H1299 cells with the indicated miRNA oligonucleotides and murine *Inh3* 3'-UTR reporter constructs. In panels **B** mean values ± SD (n = 3) are provided. (*) $P < 0.05$, (**) $P < 0.01$ and (***) $P < 0.001$.

Taken together, these results show that *Inh3* is a direct and conserved target of miR-34.

5.4 Direct induction of *Inh3* by HIF1A

The degree of INH3 induction by hypoxia in different CRC cell lines (**Figure 5.18**) suggested that HIF1A might also directly induce *Inh3* expression besides repressing its inhibitor miR-34a.

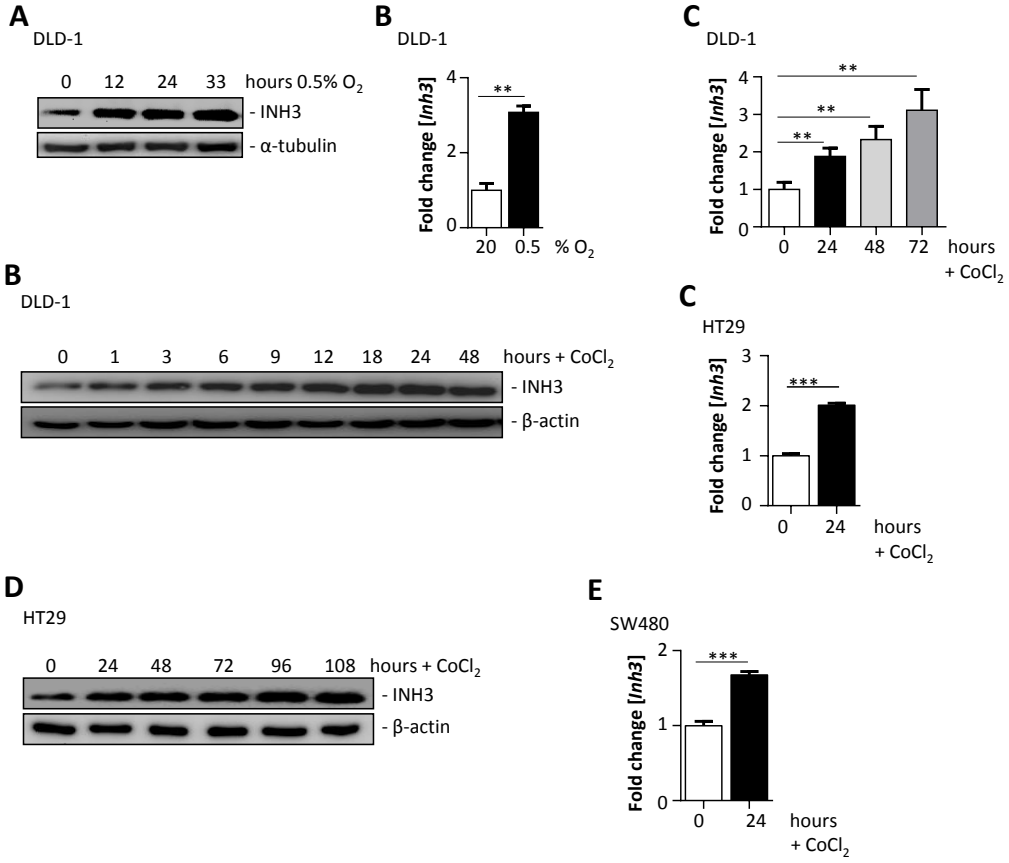

Figure 5.18 Hypoxia induces Inh3 expression. (**A**) Western blot analysis of the indicated proteins in DLD-1 cells cultured at 20% O_2 or 0.5% O_2 for the indicated periods. (**B**) qPCR analysis in DLD-1 cells cultured at 20% O_2 or 0.5% O_2 for 24 hours. (**C, E, G**) qPCR and Western blot (**D** and **F**) analysis in DLD-1 (**C** and **D**), HT29 (**E** and **F**) and SW480 (**G**) cells treated with $CoCl_2$ for the indicated periods. In panels **C**, **E** and **G** mean values ± SD (n = 3) are provided. (*) $P < 0.05$, (**) $P < 0.01$ and (***) $P < 0.001$.

Furthermore, the induction of INH3 by hypoxia was prevented by treatment with *HIF1A*-specific siRNAs (**Figure 5.19**).

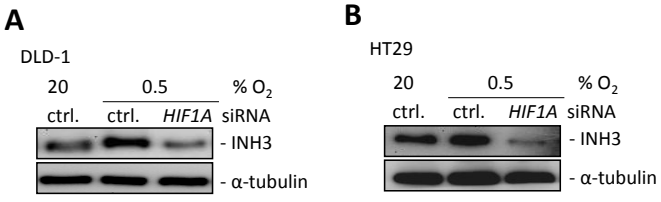

Figure 5.19 Hypoxia induces INH3 via HIF1A. Western blot analysis of the indicated proteins in DLD-1 (**A**) and HT29 (**B**) cells transfected with indicated siRNA for 24 hours and then cultured at 20% O_2 or 0.5% O_2 for 30 hours.

Indeed, inspection of the *Inh3* promoter revealed five HIF1A binding sites (**Figure 5.20A**). HIF1A occupancy was detected by qChIP at HRE4 and HRE5, but not at HRE1-3 in hypoxic DLD-1 cells (**Figure 5.20B**).

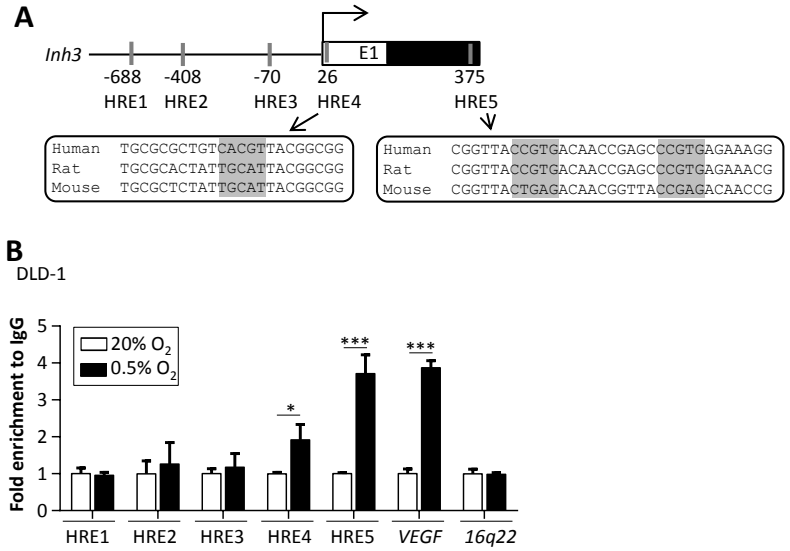

Figure 5.20 *Inh3* is a direct target of HIF1A. (**A**) Map of the human *Inh3* genomic region with conserved HIF1A binding sites. (**B**) ChIP analysis of HIF1A occupancy at the human *miR-34a* promoter in DLD-1 cells at 20% O_2 or 0.5% O_2. In panels **B** mean values ± SD (n = 3) are provided. (*) $P < 0.05$, (**) $P < 0.01$ and (***) $P < 0.001$.

In line with these results, *Inh3* expression showed a signficant, inverse correlation with miR-34a expression in 628 primary CRC tumors represented within the TCGA database (**Figure 5.21**).

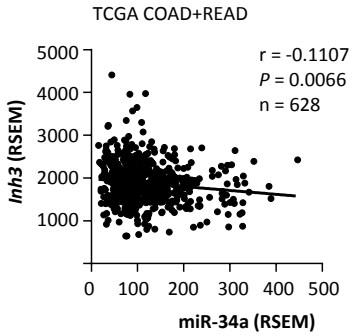

Figure 5.21 Correlative analysis of *Inh3* and miR-34a expression. Correlative analysis of *Inh3* and miR-34a expression in the samples of the TCGA collection of colon (COAD; n = 462) and rectal adenocarcinomas (READ; n = 166). Correlations were calculated using the Spearman coefficient. Matjaz Rokavec performed the analysis and generated the figure.

Moreover, PP1 interacts with INH3 in CRC cells was confirmed by co-immuno-precipitation (**Figure 5.22**), indicating that PP1 could indeed mediate the activating effect of INH3 on STAT3.

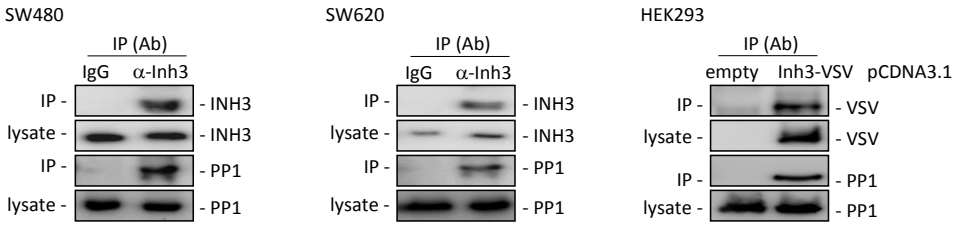

Figure 5.22 Co-immuno-precipitation (IP) analysis of INH3 and PP1. Co-immuno-precipitation (IP) analysis of endogenous INH3 and PP1 in SW480 (**A**) and SW620 (**B**) cells. (**C**) Co-immuno-precipitation (IP) analysis with the indicated antibodies (AB) of ectopic INH3 and PP1 in HEK293 cells.

Taken together, these results show that a coherent feed-forward regulation of *Inh3* by HIF1A and miR-34a mediates induction of INH3 by hypoxia leading to increased activity of STAT3 (**Figure 5.23**).

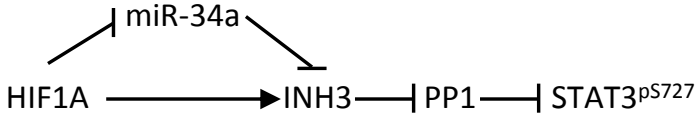

Figure 5.23 Model of the coherent feed-forward regulation of INH3 and downstream effects.

5.5 Induction of INH3 is required for hypoxia-induced EMT

In line with the results described above, the induction of Inh3 mRNA and protein by hypoxia was prevented by ectopic miR-34a expression (**Figure 5.24**).

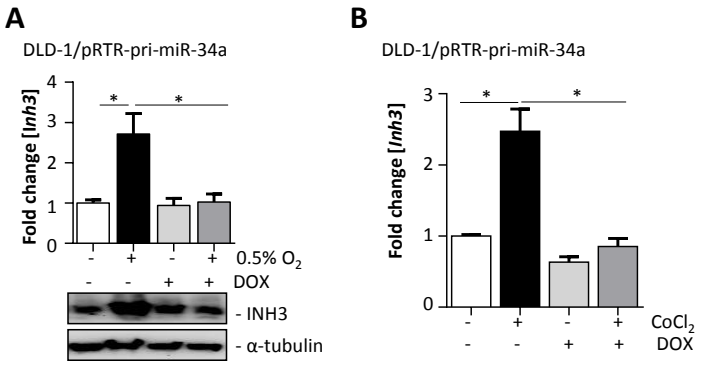

Figure 5.24 Repression of miR-34a is required for induction of *Inh3* by hypoxia. (**A**) qPCR (upper panel) and Western blot (lower panel) analysis of DLD-1 cells harboring a pRTR-pri-miR-34a vector exposed to DOX for 2 days and/or then at 0.5% O_2 for 30 hours. (**B**) qPCR analysis of *Inh3* mRNA expression in DLD-1/pRTR-pri-miR-34a cells treated with DOX for 2 days and then with $CoCl_2$ for 1 day. mean values ± SD (n = 3) are provided. (*) $P < 0.05$, (**) $P < 0.01$ and (***) $P < 0.001$.

Furthermore, ectopic expression of *Inh3* mRNA lacking miR-34a seed-matching sequences largely prevented inhibition of invasion and migration by ectopic miR-34a (**Figure 5.25**). Therefore, down-regulation of INH3 is required for inhibition of invasion and migration by miR-34a.

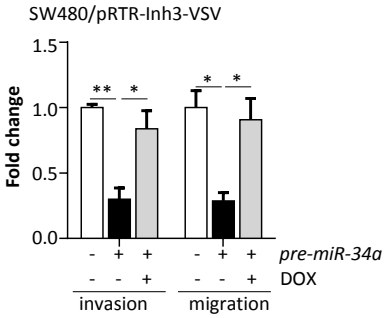

Figure 5.25 Down-regulation of INH3 is required for inhibition of invasion and migration by miR-34a. Relative invasion and migration of SW480/pRTR-Inh3-VSV cells transfected with *pre-miR-34a* oligonucleotides for 5-6 hours and then treated with for 2 days. mean values ± SD (n = 3) are provided. (*) $P < 0.05$, (**) $P < 0.01$ and (***) $P < 0.001$.

In addition, down-regulation of INH3 by siRNAs prevented the induction of SNAIL and repression of E-cadherin by hypoxia (**Figure 5.26A-C**), as well as hypoxia-induced invasion and migration (**Figure 5.26D-E**) in DLD-1 and HT-29 cells. Thus, INH3 is a required mediator of hypoxia-induced EMT, migration and invasion in CRC cells.

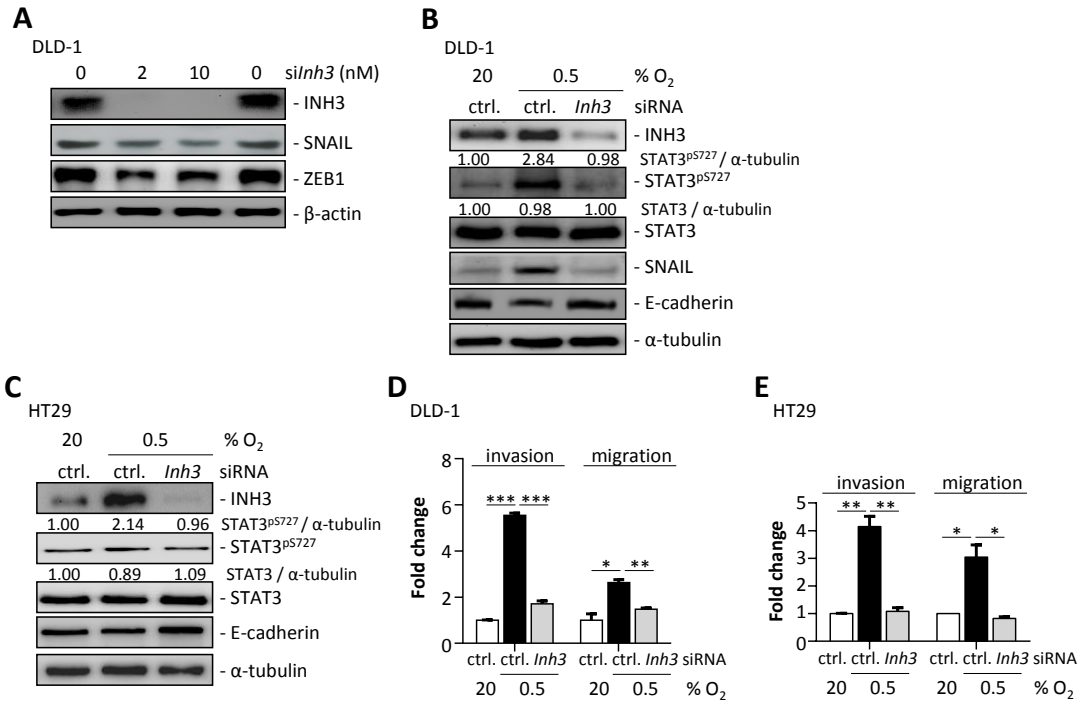

Figure 5.26 INH3 is a required mediator of hypoxia-induced EMT, migration and invasion in CRC cells. (**A-C**) Western blot analysis of the indicated proteins in DLD-1 (**A-B**) and HT29 (**C**) cells transfected with indicated siRNA for 48 hours. (**D-E**) relative invasion and migration analysis of DLD-1 (**D**) and HT29 (**E**) cells transfected with indicated siRNAs for 24 hours and then cultured at 20% O_2 or 0.5% O_2 for 30 hours. In panels **D** and **E** mean values ± SD (n = 3) are provided. (*) $P < 0.05$, (**) $P < 0.01$ and (***) $P < 0.001$.

In the mesenchymal-like SW480 cells down-regulation of INH3 by siRNAs at standard cell culture conditions (20% O_2) resulted in a decrease of VIM, SNAIL, STAT3^{pS727}, and induction of E-cadherin (**Figure 5.27A-B**). Moreover, knockdown of *Inh3* in SW480 cells decreased wound closure and attenuated cellular invasion and migration (**Figure 5.27C-D**). Similar results were obtained with mesenchymal-like SW620 (**Figure 5.27A**, **B and D**) and murine CT26 cells (**Figure 5.27E-F**). Therefore, elevated INH3 expression is also required for maintaining a mesenchymal-like state in human and murine CRC cell lines in the absence of hypoxia.

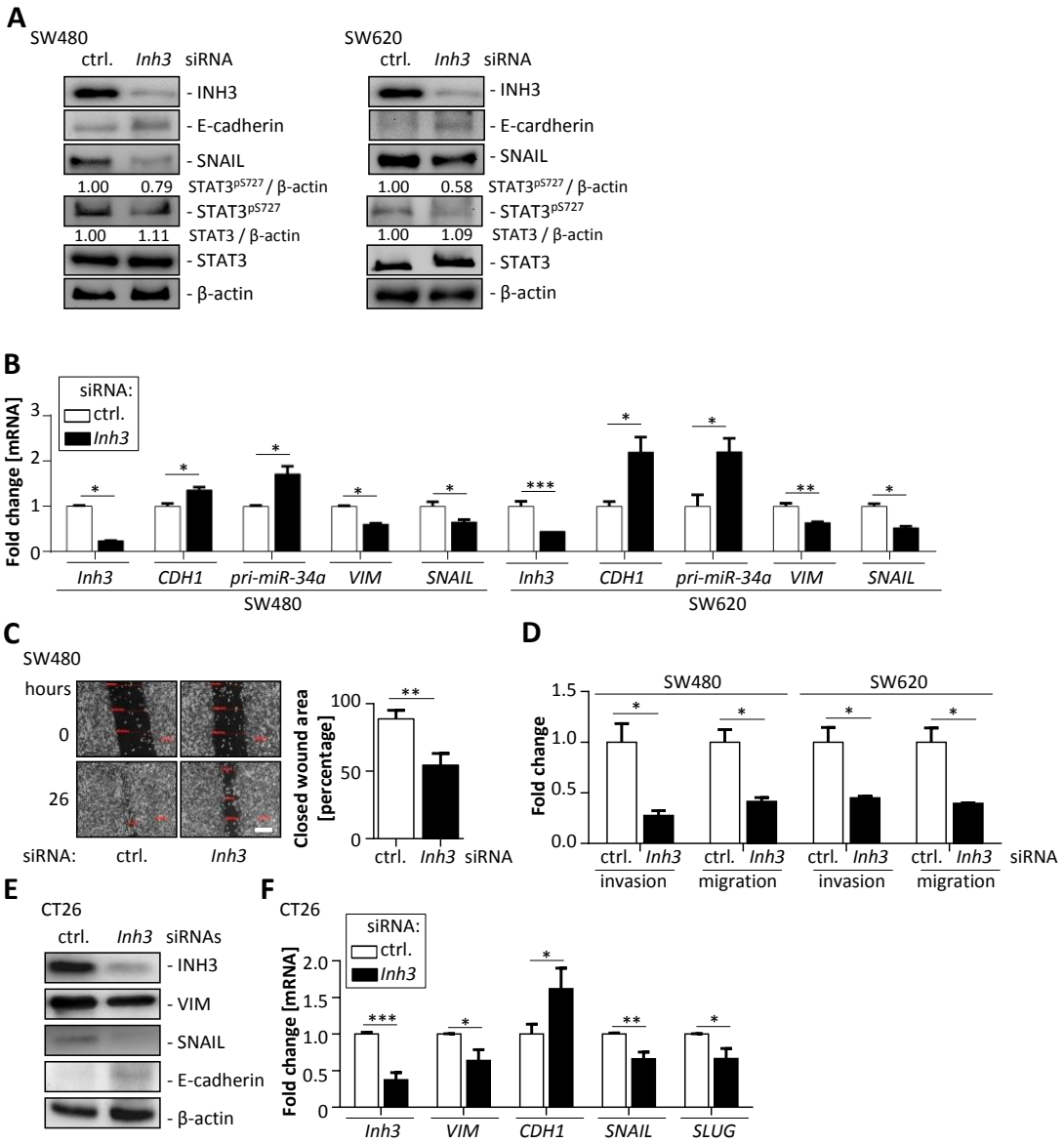

Figure 5.27 Elevated INH3 expression is required for maintaining a mesenchymal-like state. (**A**) Western blot, (**B**) qPCR and (**D**) relative invasion and migration analysis of SW480 and SW620 cells transfected with indicated siRNA for 48 hours. (**C**) Wound healing assay of SW480 cells transfected with indicated siRNA for 48 hours. (**E**) Western blot and (**F**) qPCR analysis of CT26 cells transfected with indicated siRNA for 48 hours. In panels **B**, **D** and **F** mean values ± SD (n = 3) are provided. (*) $P < 0.05$, (**) $P < 0.01$ and (***) $P < 0.001$.

5.6 Ectopic expression of INH3 induces EMT, migration and invasion

After ectopic INH3 expression epithelial DLD-1 cells adopted a mesenchymal morphology, while no changes were observed after ectopic eGFP expression (**Figure 5.28**).

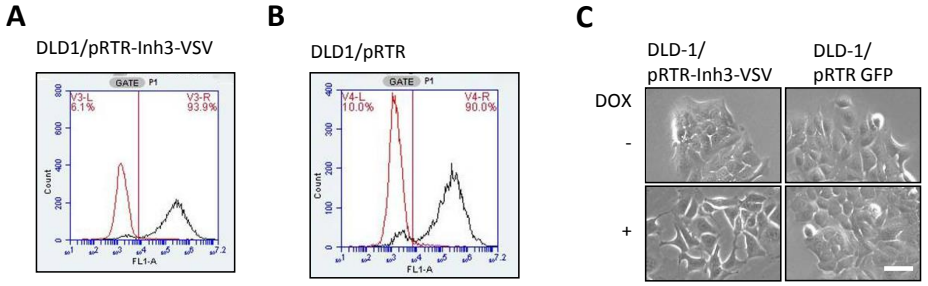

Figure 5.28 Effects of ectopic INH3 and eGFP expression on DLD-1 cells. (**A**, **B**) Flow cytometric determination of the frequency of cells with inducible expression of eGFP in DLD-1 cell pools harboring a (**A**) pRTR-Inh3-VSV or (**B**) a control pRTR vector after addition of DOX for 72 hours. (**E**) Representative phase-contrast pictures of DLD-1/pRTR-Inh3-VSV cells treated with or without DOX. Scale bars represents 25 µm.

Moreover, ectopic INH3 induced changes in protein expression consistent with EMT (**Figure 5.29A**). Furthermore, phosphorylation of STAT3 at S727 was induced by INH3 expression, while the total amount of STAT3 and phosphorylation of STAT3 at Y705 were not affected (**Figure 5.29A**). Notably, ectopic INH3 promoted wound closure (**Figure 5.29B**), and enhanced cellular invasion and migration (**Figure 5.29C**).

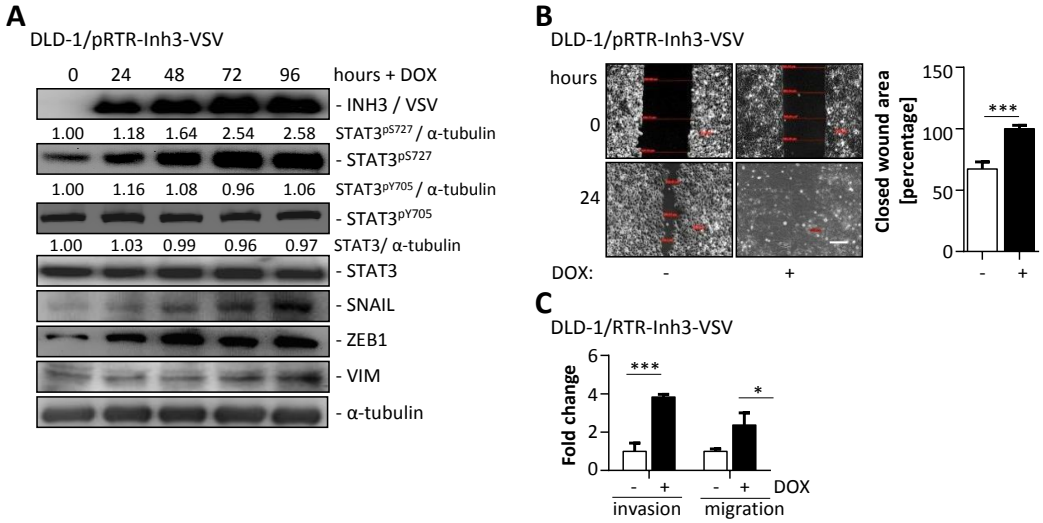

Figure 5.29 Ectopic expression of INH3 is sufficient for induction EMT in DLD1 cells. (**A**) Western blot analysis of indicated mRNAs in DLD-1/pRTR-Inh3-VSV cells treated with DOX for the indicated periods. (**B**) Wound healing assay and (**C**) relative invasion and migration of DLD-1/pRTR-Inh3-VSV cells treated with DOX. Scale bar represents 200 µm (**G**). In panels **B** and **C**, mean values ± SD (n = 3) are provided. (*) $P < 0.05$; (**) $P < 0.01$ and (***) $P < 0.001$.

DLD-1 cells ectopically expressing GFP displayed none of these effects (**Figure 5.30**).

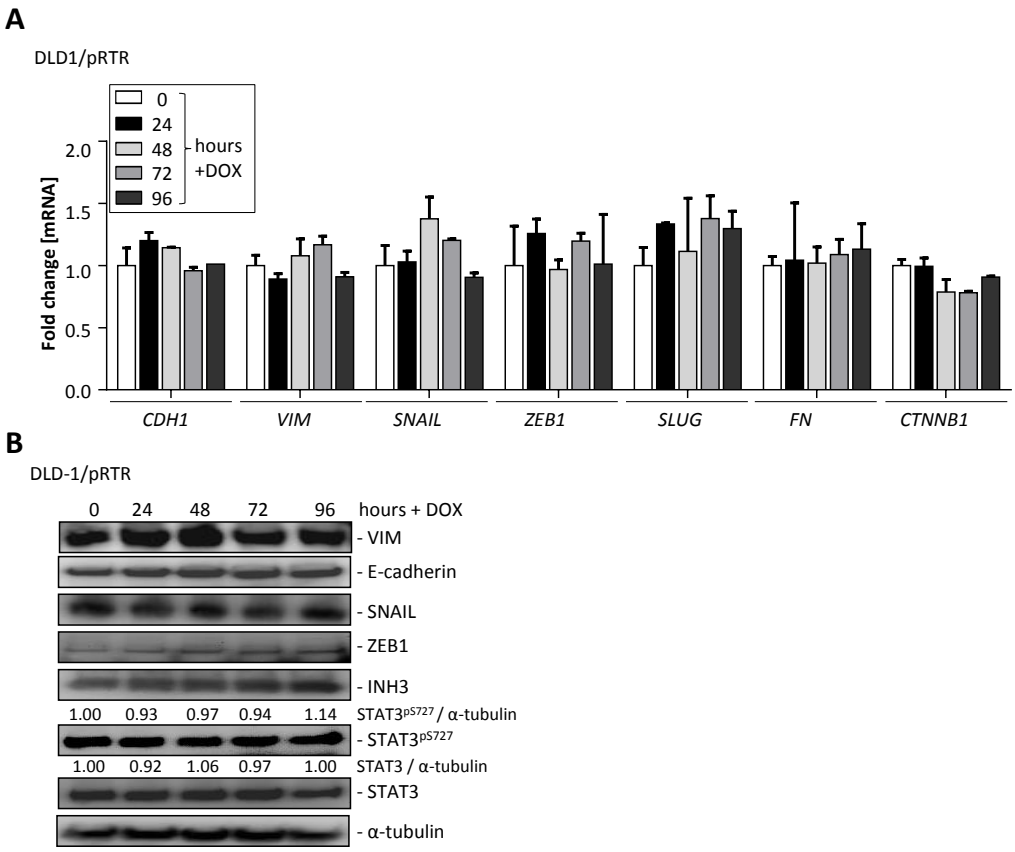

Figure 5.30 Effects of ectopic eGFP expression on DLD-1 cells. (**A**) qPCR and (**B**) Western blot analysis of the indicated mRNAs in DLD-1 cells harboring a pRTR vector treated with DOX for the indicated periods.

Similar results were obtained in HT29 cells (**Figure 5.31**). After ectopic INH3 expression epithelial HT29 cells adopted a mesenchymal morphology (**Figure 5.31A**). Moreover, ectopic INH3 induced changes in protein expression consistent with EMT (**Figure 5.31B**). Furthermore, phosphorylation of STAT3 at S727 was induced by INH3 expression, while the total amount of STAT3 was not affected (**Figure 5.31B**). Notably, ectopic INH3 enhanced cellular invasion and migration (**Figure 5.31C**).

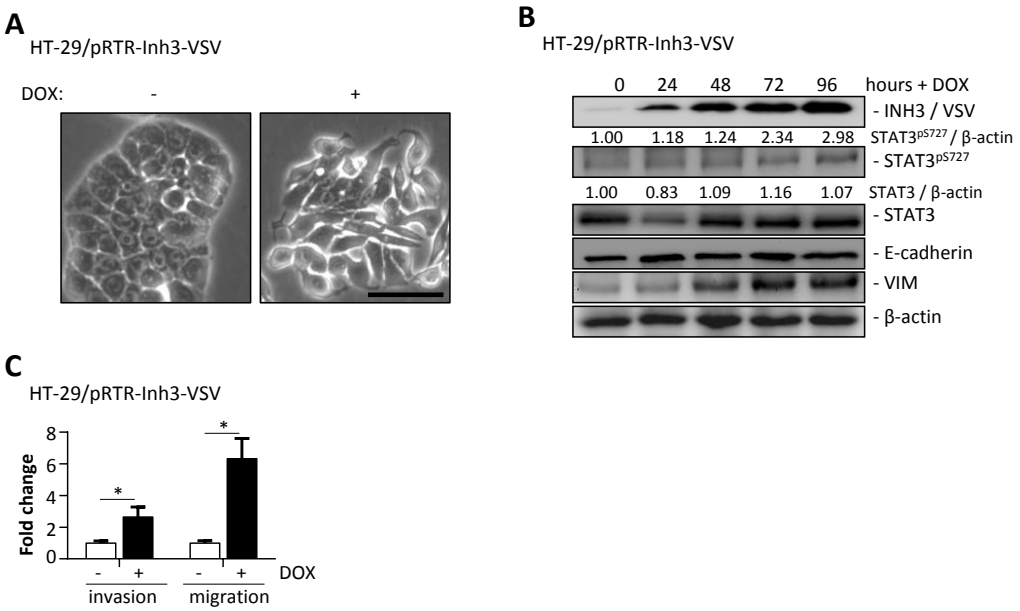

Figure 5.31 Ectopic expression of INH3 is sufficient for induction of EMT HT-29 cells. (**A**) Representative phase-contrast pictures of HT29/pRTR-Inh3-VSV cells treated with or without DOX. Scale bar represents 25 µm. (**B**) Western blot analysis of indicated mRNAs in HT29/pRTR-Inh3-VSV cells treated with DOX for the indicated periods. (**C**) Relative invasion and migration of HT29/pRTR-Inh3-VSV cells treated with DOX. In panel **C** mean values ± SD (n = 3) are provided, (*) $P < 0.05$, (**) $P < 0.01$ and (***) $P < 0.001$.

Notably, siRNA-mediated down-regulation of STAT3 prevented the up-regulation of *VIM* and *SNAIL* and the down-regulation of *E-cadherin* (**Figure 5.32A-B**), as well as the enhancement of invasion and migration by ectopic INH3 in DLD-1 cells (**Figure 5.32C**).

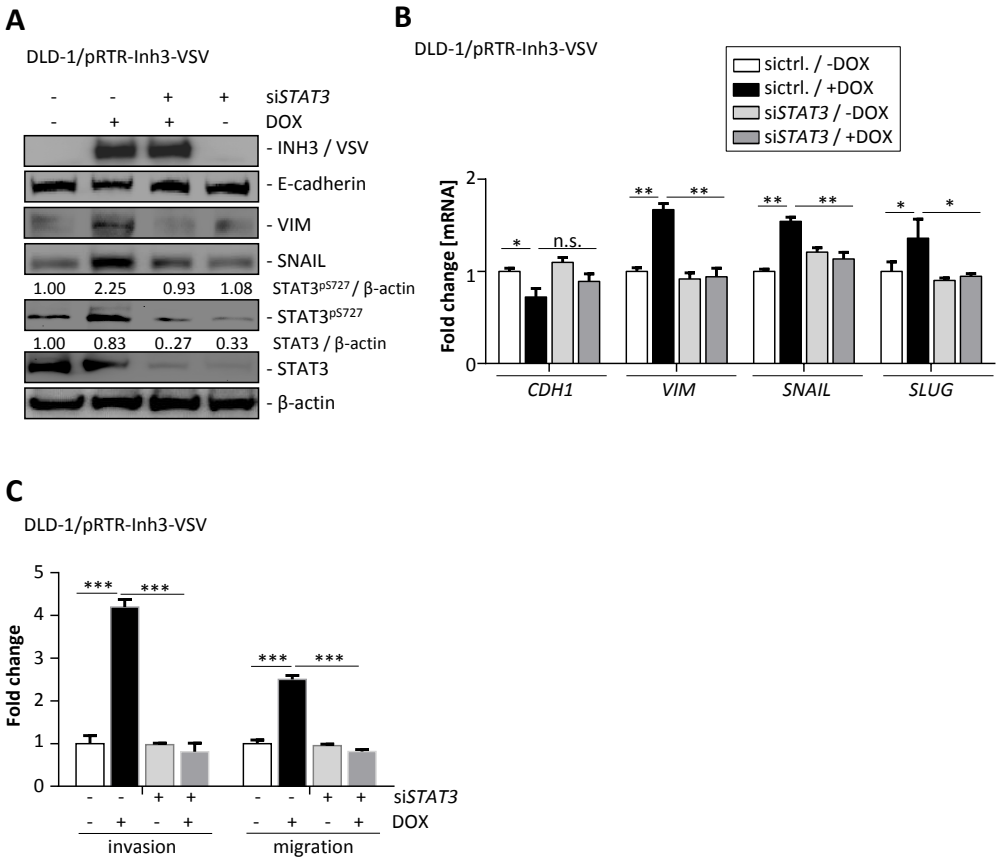

Figure 5.32 STAT3 is a mediator of INH3 function. (**A**) Western blot, (**B**) qPCR and (**C**) relative invasion and migration analysis of DLD-1/pRTR-Inh3-VSV cells transfected with indicated siRNAs for 24 hours. Subsequently DOX was added for 30 hours. In panels **B** and **C** mean values ± SD (n = 3) are provided. (*) $P < 0.05$, (**) $P < 0.01$ and (***) $P < 0.001$.

Taken together, these results show that INH3 activation is sufficient to induce EMT, invasion and migration in a STAT3-dependent manner.

5.7 INH3 mediates hypoxia-induced metastasis formation

We had previously observed that DLD-1 cells are unable to form lung metastases after tail-vein injection in NOD/SCID mice [31] . However, pretreatment of Luc-expressing DLD-1 cells with 0.5% O_2 for 48 hours allowed lung metastasis formation as documented by non-invasive imaging of luciferase activity over a period of 7 weeks (**Figure 5.33A-C**). Moreover, siRNAs directed against *Inh3* largely inhibited lung metastasis formation. Histological analysis of resected lungs confirmed that knockdown of INH3 resulted in a decreased number of metastatic tumor nodules (**Figure 5.33D-F**). Taken together, these results show that INH3 mediates hypoxia-induced metastases formation.

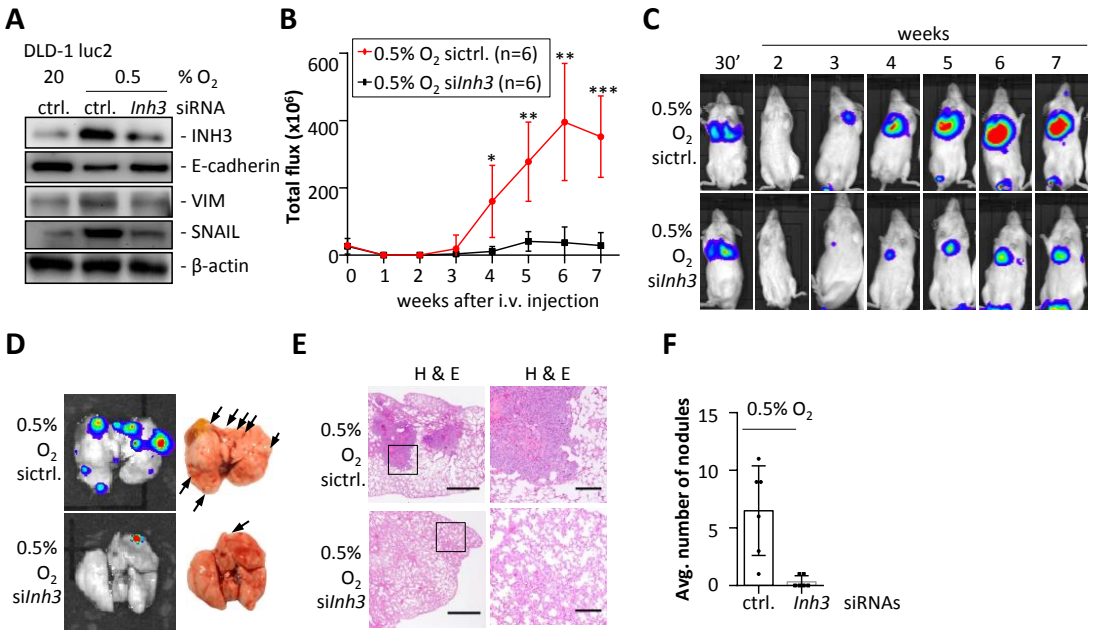

Figure 5.33 Analysis of INH3 function in a xenograft lung-metastasis assay. (**A**) Western blot analysis of DLD-1 cells kept at 0.5% O_2 for 24 hours and then transfected with control and *Inh3*-specific siRNAs for 24 hours. (**B**-**F**) DLD-1 cells were kept at 0.5% O_2 for 24 hours and then transfected with control and *Inh3*-specific siRNAs for 24 hours, subsequently injected into the tail veins of immune-compromised NOD/SCID mice (n = 6), and followed by noninvasive bioluminescence imaging for 7 weeks. (**B**) Quantification of non-invasive imaging at the indicated time points. Bioluminescence signals are presented as 'total flux'. (**C**) representative examples of bioluminescence imaging at the indicated time points, (**D**, left panels) representative examples of bioluminescence imaging of lungs 7 weeks after tail vein injection; (**D**, right panels) representative images of lungs, arrows indicate metastatic nodules; (**E**) representative examples of H & E stained lung sections. Scale bars represent 1mm (left panels), and 200 µm (right panels). (**F**) Quantification of metastatic tumor nodules in the lung per mouse 7 weeks after tail-vein injection**.** In panels **B** and **F** mean values ± SD (n = 6), in **H** mean values ± SD (n = 3) are provided. (*) $P < 0.05$; (**) $P < 0.01$ and (***) $P < 0.001$. Huihui Li performed the analysis and generated the figure (**A**, **F**). Matjaz Rokavec performed the analysis and generated the figure (**B-C**). Longchang Jiang performed the analysis and generated the figure (**D-E**).

5.8 *miR-34*-deficiency increases INH3 expression in adenomas of *Apc*$^{Min/+}$ mice

In order to obtain evidence for a conservation of the identified regulations at the organismal level, the expression of INH3 and HIF1A in intestinal tumors of *miR-34a/b/c*-deficient *Apc*$^{Min/+}$ mice [80] were determined. The expression of INH3 and HIF1A largely co-localized in the epithelial tumor cells of adenomas in *Apc*$^{Min/+}$ mice

proficient and deficient *miR-34a/b/c*, consistent with the direct regulation of *Inh3* expression by HIF1A described above (**Figure 5.34A**). INH3, HIF1A, *VIM* and also STAT3^{pS727} levels were elevated in most of the 6 *miR-34a/b/c*-deficient adenomas analyzed here (**Figure 5.34B**).

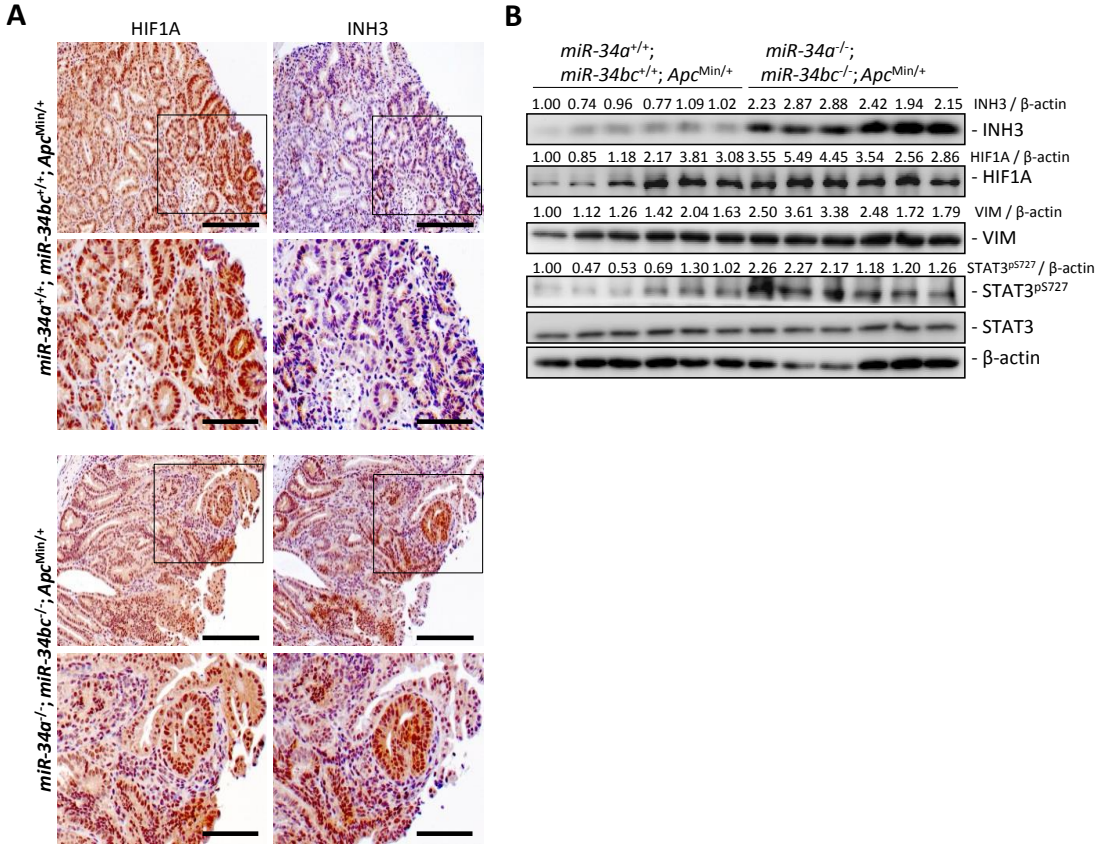

Figure 5.34 Analysis of INH3 expression in adenomas of *miR-34*-deficient *Apc*$^{Min/+}$ mice. (**A**) Representative examples of immunohistochemical detections of INH3 and HIF1A protein expression in serial sections of adenomas from *miR-34ab/c*$^{+/+}$; *Apc*$^{Min/+}$ and *miR-34a/b/c*$^{-/-}$; *Apc*$^{Min/+}$ mice. Scale bars represent 200 µm (1. and 3. row) and 100 µm (2. and 4. row). (n = 6 per genotype). (**B**) Western blot analysis of indicated proteins in lysates prepared from tumors of *miR-34a/b/c*$^{+/+}$; *Apc*$^{Min/+}$ and *miR-34ab/c*$^{-/-}$; *Apc*$^{Min/+}$ mice (1 tumor/mice, n = 6 per genotype). Relative densitometric quantifications of the indicated proteins normalized to β-actin are indicated. Longchang Jiang provided *Apc*$^{Min/+}$ tumor samples and Huihui Li performed the analysis and generated the figure.

Next the response of tumoroids derived from adenomas of *Apc*$^{Min/+}$ mice to hypoxia were compared. Notably, *Inh3* and *VIM* was up- and *CDH1* mRNA down-regulated in *miR-34a/b/c*-deficient tumoroids, whereas miR-34a/b/c-proficient tumoroids showed the opposite regulations (**Figure 5.35A**). In addition, elevated INH3 protein

expression and induction of STAT3^{pS727} was consistently observed in *miR-34a/b/c-deficient* tumoroids exposed to hypoxia (**Figure 5.35B**).

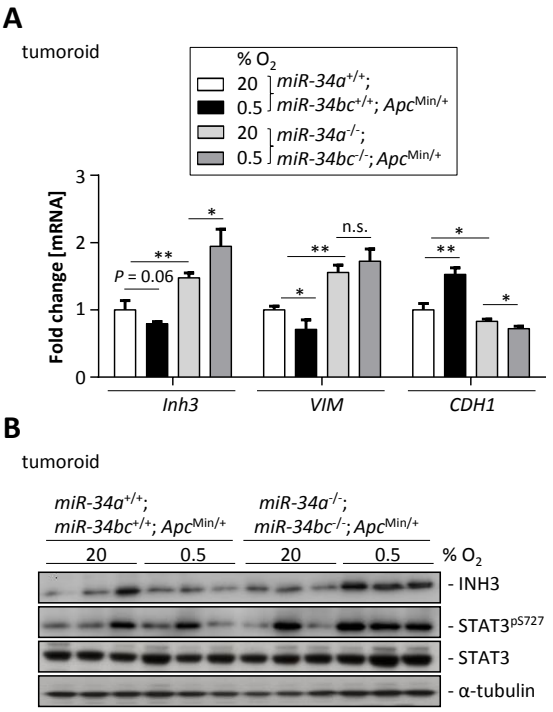

Figure 5.35 Analysis of INH3 expression in *miR-34*-deficient *Apc*$^{Min/+}$ tumoroids. (**A**) qPCR and (**B**) Western blot analyses of tumoroids derived from adenomas of mice with the indicated genotypes exposed to 20% or 0.5% O_2 for 48 hours as indicated. In panels **A** mean values ± SD (n = 6), in **H** mean values ± SD (n = 3) are provided. (*) $P < 0.05$; (**) $P < 0.01$ and (***) $P < 0.001$. Longchang Jiang provided *Apc*$^{Min/+}$ tumor samples and Huihui Li performed the analysis and generated the figure.

Taken together, these results show that the regulations identified in human CRC lines also occur *in vivo* in a genetic mouse model of intestinal tumor formation and *ex vivo* in tumoroids derived from these adenomas.

5.9 *miR-34a* mediates the repression of *Inh3* by p53

Since the induction of MET is considered to be an important aspect of the tumor suppressive activity of p53 which is mediated, at least in part, by miR-34a, whether hypoxia-induced EMT is suppressed by p53 was determined. Indeed, the enhancement of invasion and migration observed after exposure to $CoCl_2$ was abolished by ectopic expression of p53 (**Figure 5.36A**). Similarly, ectopic expression of p53 also inhibited cellular migration induced by $CoCl_2$ as determined in a scratch-wound assay (**Figure 5.36B**).

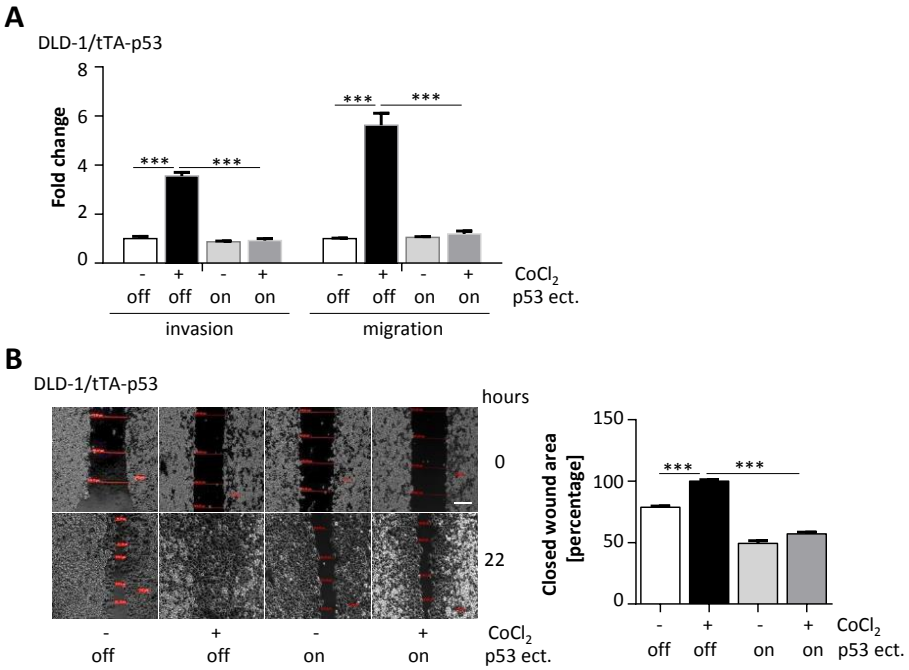

Figure 5.36 p53 suppresses invasion and migration induced by $CoCl_2$. (**A**) Relative invasion and migration and (**B**) wound healing assay of DLD-1/tTA-p53 cells treated with DOX for 2 days and/or subsequently with $CoCl_2$ for 1 day. Scale bar represents 200 µm. mean values ± SD (n = 3) are provided. (*) $P < 0.05$, (**) $P < 0.01$ and (***) $P < 0.001$.

Ectopic expression of p53 in SW480 cells resulted in repression of Inh3 mRNA and protein expression (**Figure 5.37A-B**) and decreased phosphorylation of $STAT3^{pS727}$ (**Figure 5.37B**). Ectopic expression of INH3 largely prevented the suppression of invasion and migration by p53 (**Figure 5.37C**), indicating that *Inh3* repression by p53 is required for these effects of p53. The repression of INH3 by p53 was alleviated by transfection of miR-34a-specific antagomirs (**Figure 5.37D-E**). Therefore, miR-34a mediates the repression of *Inh3* by p53.

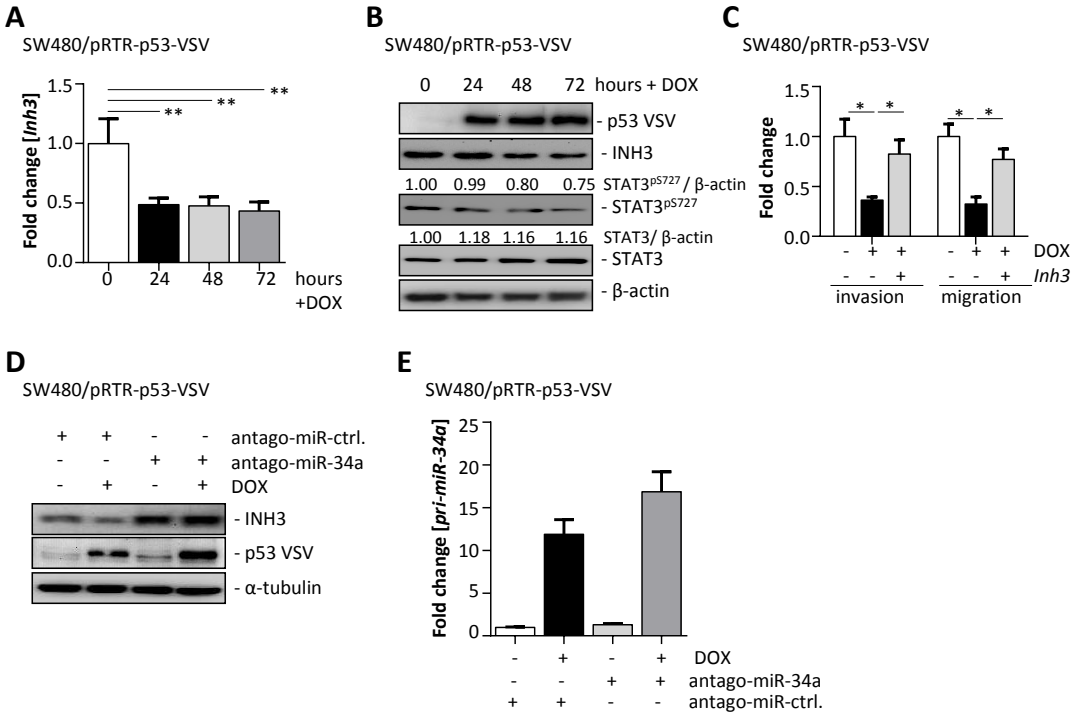

Figure 5.37 *MiR-34a* mediates the repression of *Inh3* by p53. (**A**) qPCR and (**B**) Western blot analysis of *INH3* expression in SW480/pRTR-p53-VSV cells after addition of DOX for the indicated periods. (**C**) Relative invasion and migration of SW480/pRTR-p53-VSV cells transfected with pCDNA3.1-Inh3-VSV for 5-6 hours and then treated with DOX for 48 hours. (**D**) Western blot analysis of SW480/pRTR-p53-VSV cells transfected with antago-miR-34a or antago-miR-negative control oligonucleotide for 24 hours and/or subsequently treated with DOX for 48 hours. (**C**) qPCR analysis of the indicated mRNAs in SW480/pRTR-p53-VSV cells transfected with antago-miR-34a or antago-miR-negative control oligonucleotide for 24 hours and/or treated with DOX for 48 hours. Antago-miR does not influence *pri-miR-34a* expression level but inhibits the function of the mature miR-34a [198-200]. In panels **A**, **C** and **E** mean values ± SD (n = 3) are provided. (*) $P < 0.05$, (**) $P < 0.01$ and (***) $P < 0.001$.

Furthermore, treatment with the DNA damaging agent etoposide caused the down-regulation of INH3 protein expression in $TP53^{+/+}$, but not in $TP53^{-/-}$ RKO cells (**Figure 5.38A**). Therefore, INH3 is also repressed after activation of endogenous p53 by DNA damage. Furthermore, the repression of INH3 and also the decrease in $STAT3^{pS727}$ mediated by p53 activation after DNA damage was prevented by miR-34a-specific antagomirs (**Figure 5.38B**).

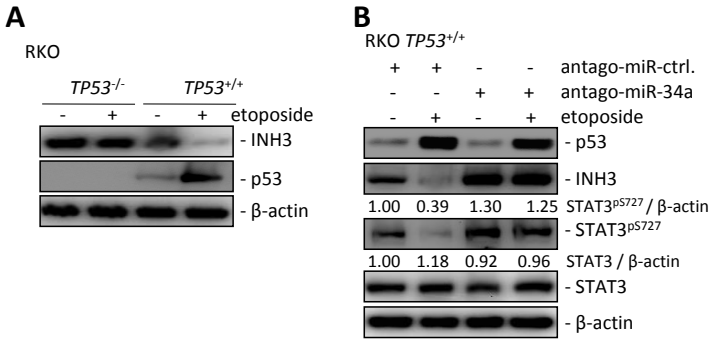

Figure 5.38 *MiR-34a* mediates the repression of *Inh3* by p53. (**A**) Western blot analysis of the indicated proteins in RKO *TP53*$^{+/+}$ and RKO *TP53*$^{-/-}$ cells after addition of etoposide (20 µM) for 48 hours. (**B**) Western blot analysis of the indicated proteins in RKO *TP53*$^{+/+}$ cells transfected with antago-miR-34a or antago-miR-negative control oligonucleotide for 24 hours and/or subsequently treated with etoposide for 48 hours.

Moreover, the HIF1A-mediated induction of INH3 was prevented by ectopic p53 expression (**Figure 5.39**).

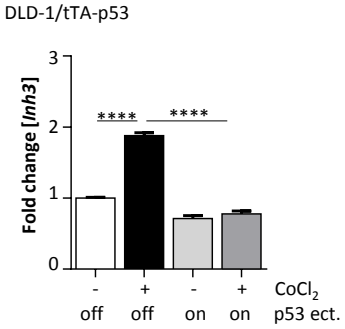

Figure 5.39 p53 suppresses *Inh3* induced by $CoCl_2$. qPCR analysis of the indicated mRNAs in DLD-1/tTA-p53 cells treated with DOX for 2 days and subsequently with $CoCl_2$ for 1 day. mean values ± SD (n = 3) are provided. (*) $P < 0.05$, (**) $P < 0.01$ and (***) $P < 0.001$.

Taken together, these results show that activation of p53 suppresses hypoxia-induced EMT and associated processes, such as enhanced invasion and migration, via miR-34a-mediated suppression of INH3.

5.10 The p53/miR-34a/INH3/Stat3 pathway as a determinant of the hypoxic response

Next, the hypothesis that the differential regulation of *miR-34a* and Inh3 may determine the distinct cellular responses to hypoxia observed in *TP53*-positive and *TP53*-negative cells was made. Therefore, the response of three isogenic CRC cell lines differing in their *TP53* status to hypoxia was analyzed.

Under hypoxia, HCT116 *TP53*$^{-/-}$ cells adopted a mesenchymal morphology, while HCT116 *TP53*$^{+/+}$ cells remained unchanged (**Figure 5.40A**). Furthermore, expression of miR-34a and *pri-miR-34a* was up-regulated and *Inh3* was down-regulated under hypoxia in *TP53*$^{+/+}$ cells, whereas *TP53*$^{-/-}$ cells showed the opposite regulations (**Figure 5.40B**). Moreover, SNAIL was repressed in *TP53*$^{+/+}$ cells and induced in *TP53*$^{-/-}$ cells upon exposure to hypoxia (**Figure 5.40C**).

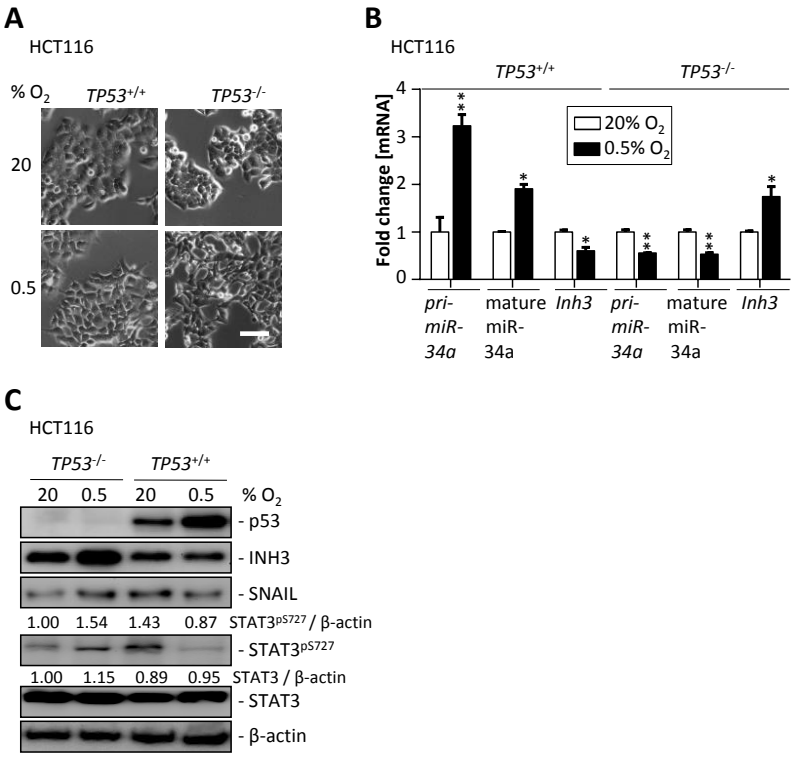

Figure 5.40 *TP53* status influences the differential expression of miR-34a/b/c and INH3 after hypoxia in HCT116 cells. Representative phase-contrast pictures (**A**), qPCR (**B**) and Western blot (**C**) analysis of HCT116 *TP53*$^{-/-}$ and *TP53*$^{+/+}$ cells at 0.5% O_2 for 48 hours. Scale bar represents 25 µm. In panels **B** mean values ± SD (n = 3) are provided. (*) $P < 0.05$, (**) $P < 0.01$ and (***) $P < 0.001$.

Similar results were obtained in *TP53*$^{+/+}$ and *TP53*$^{-/-}$ RKO (**Figure 5.41**). Under hypoxia, RKO *TP53*$^{-/-}$ cells adopted a mesenchymal morphology, while HCT116 *TP53*$^{+/+}$ cells remained unchanged (**Figure 5.41A**). Furthermore, expression of miR-34a and *pri-miR-34a* was up-regulated and *Inh3* was down-regulated under hypoxia in *TP53*$^{+/+}$ cells, whereas *TP53*$^{-/-}$ cells showed the opposite regulations (**Figure 5.41B**).

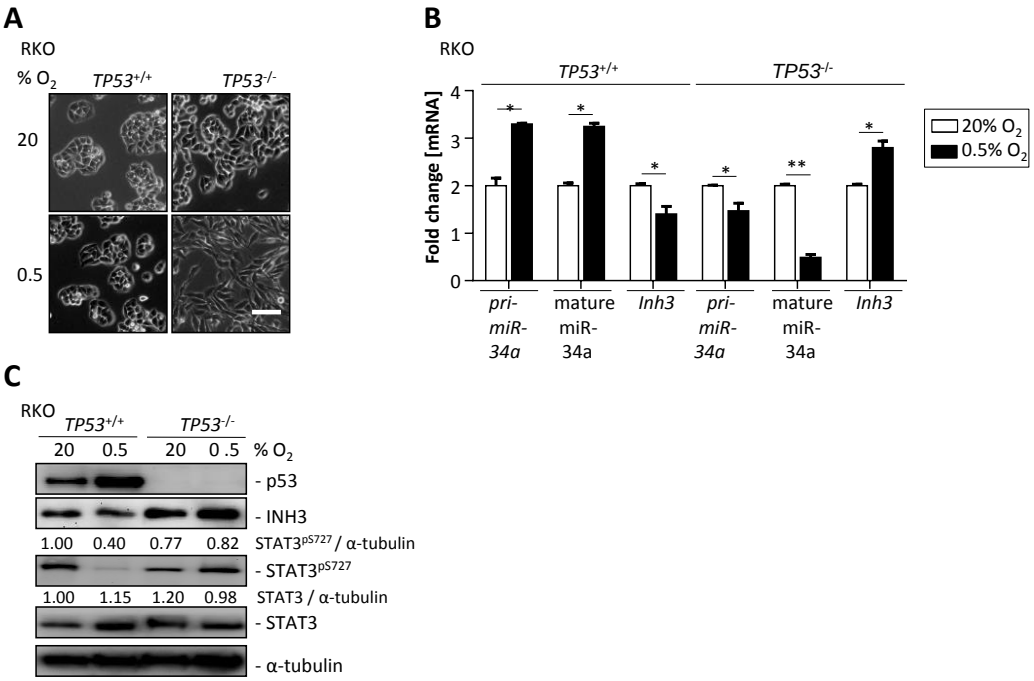

Figure 5.40 *TP53* status influences the differential expression of miR-34a/b/c and INH3 after hypoxia in RKO cells. (**A**) Representative phase-contrast pictures, (**B**) qPCR and (**C**) Western blot analysis of HCT116 *TP53*$^{-/-}$ and *TP53*$^{+/+}$ cells kept at 0.5% O_2 for 48 hours. Scale bar represents 25 µm. In panels **B** mean values ± SD (n = 3) are provided. (*) $P < 0.05$, (**) $P < 0.01$ and (***) $P < 0.001$.

Similar results were also obtained in SW48 CRC cell lines (**Figure 5.42**). The expression of miR-34a and *pri-miR-34a* was up-regulated and *Inh3* was down-regulated under hypoxia in *TP53*$^{+/+}$ cells, whereas *TP53*$^{-/-}$ cells showed the opposite regulations (**Figure 5.42**). Moreover, *SNAIL* and *VIM* was repressed in *TP53*$^{+/+}$ cells and induced in *TP53*$^{-/-}$ cells upon exposure to hypoxia (**Figure 5.42**). Therefore, these p53-dependent regulations are not restricted to a specific CRC cell line.

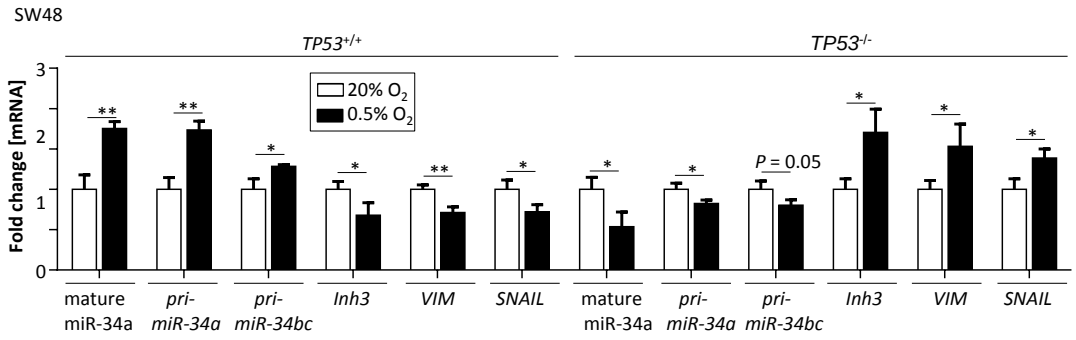

Figure 5.40 *TP53* status influences the differential expression of miR-34a/b/c and INH3 after hypoxia in SW48 cells. qPCR analysis of SW48 *TP53*$^{-/-}$ and *TP53*$^{+/+}$ cells kept at 0.5% O_2 for 48 hours. mean values ± SD (n = 3) are provided. (*) $P < 0.05$, (**) $P < 0.01$ and (***) $P < 0.001$.

In addition, the analysis of the *TP53*-proficient murine CRC cell line CT26 showed that the regulations mediated by wild-type *TP53* are conserved between species (**Figure 5.43**).

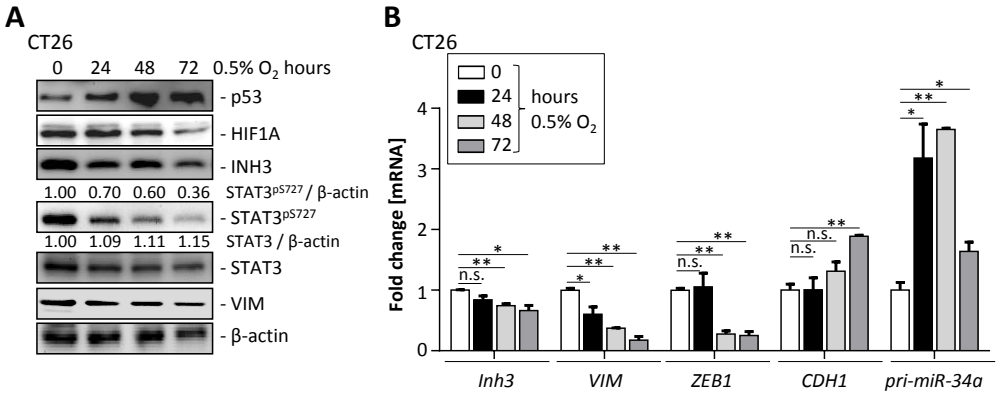

Figure 5.43 Hypoxia represses mesenchymal markers in the *TP53*-proficient murine CRC cell line CT26. (**A**) Western blot and (**B**) qPCR analysis of the indicated mRNAs in CT26 cultured at 0.5% O_2 for the indicated periods. In panels **B** mean values ± SD (n = 3) are provided. (*) $P < 0.05$, (**) $P < 0.01$ and (***) $P < 0.001$.

The repression of INH3 and STAT3^{pS727} by hypoxia in HCT116 *TP53*$^{+/+}$ cells was prevented by a miR-34a-specific antagomir (**Figure 5.44A-B**, left panel), demonstrating that miR-34a mediates the repression of INH3 and STAT3^{pS727} by hypoxia. Notably, hypoxia suppressed invasion and migration of *TP53*-proficient HCT116 cells (**Figure 5.44B**, right panel), which was prevented by miR-34a-specific antagomirs.

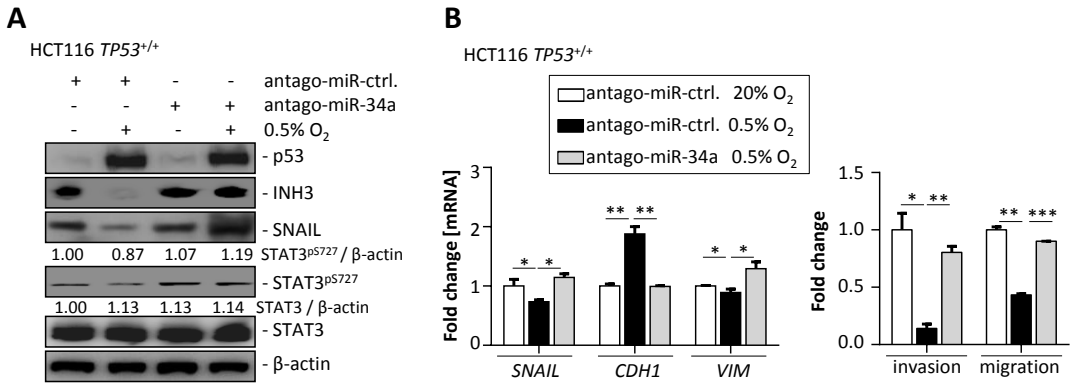

Figure 5.44 Inhibition of miR-34a prevents MET by hypoxia in *TP53*-proficient CRC HCT116 cell line. Western blot (**A**), qPCR (**B**, left panel) and relative invasion and migration (**B**, right panel) analysis of HCT116 *TP53*$^{+/+}$ transfected with antago-miR-34a or antago-miR-negative control oligonucleotide for 48 hours and/or subsequently cultured at 20% O_2 or 0.5% O_2 for 30 hours. In panels **B**, **C** and **E** mean values ± SD (n = 3) are provided. (*) $P < 0.05$, (**) $P < 0.01$ and (***) $P < 0.001$.

Similar results were obtained in RKO *TP53*$^{+/+}$ cells (**Figure 5.45**). Hypoxia repressed invasion and migration of *TP53*-proficient RKO cells, which was prevented by miR-34a-specific antagomirs.

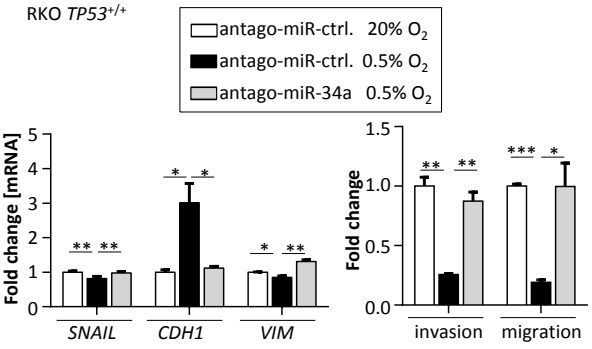

Figure 5.45 Inhibition of miR-34a prevents hypoxia-induced MET in the *TP53*-proficient RKO cells. qPCR (left panel) and relative invasion and migration (right panel) analysis RKO *TP53*$^{+/+}$ transfected with antago-miR-34a or antago-miR-negative control oligonucleotides for 48 hours and subsequently cultured at 20% O_2 or 0.5% O_2 for 30 hours. mean values ± SD (n = 3) are provided. (*) $P < 0.05$, (**) $P < 0.01$ and (***) $P < 0.001$.

Similar results were also obtained in murine CRC cell line CT26 (**Figure 5.46**).

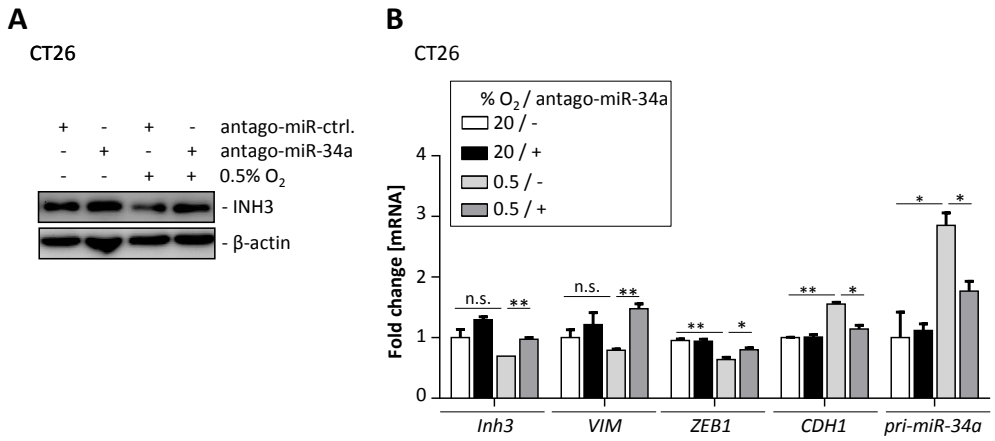

Figure 5.46 Inhibition of miR-34a prevents hypoxia-induced MET in the *TP53*-proficient murine CT26 cells. (**A**) Western blot and (**B**) qPCR analysis of CT26 transfected with antago-miR-34a or antago-miR-negative control oligonucleotide for 6 hours and subsequently cultured at 20% O_2 or 0.5% O_2 for 48 hours. In panels **B** mean values ± SD (n = 3) are provided. (*) $P < 0.05$, (**) $P < 0.01$ and (***) $P < 0.001$.

In contrast, exposure of *TP53*-deficient HCT116 cells to hypoxia resulted in an increase in invasion and migration and signs of EMT (**Figure 5.47**). The repression of *CDH1* on the mRNA and protein levels by hypoxia was abolished by treatment with *pre-miR-34a* oligonucleotide in HCT116 *TP53*$^{-/-}$ cells (**Figure 5.47**, left panel and middle panel). Also the induction of *VIM* (**Figure 5.47**, middle panel) and invasion and migration by hypoxia was abrogated by ectopic miR-34a (**Figure 5.47**, right panel).

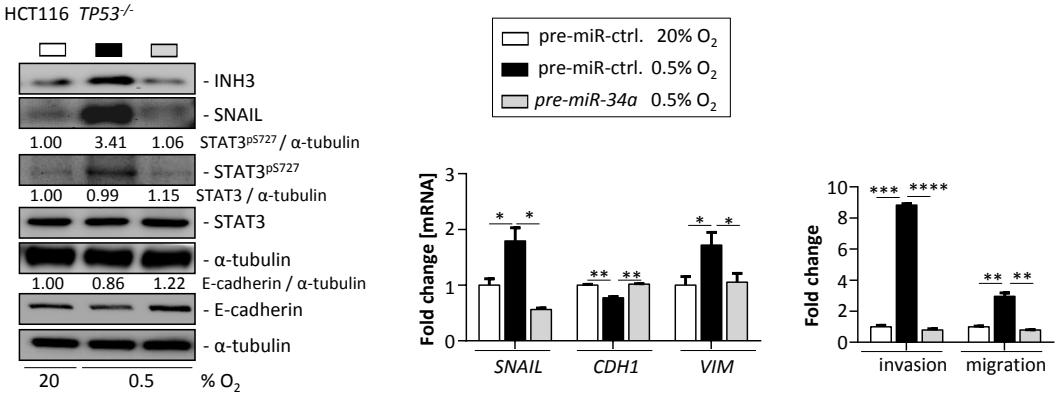

Figure 5.47 Ectopic miR-34a prevents EMT induced by hypoxia in *TP53*-deficient HCT116 cells. Western blot (left panel), qPCR (middle panel) and relative invasion and migration (right panel) analysis of HCT116 *TP53*$^{-/-}$ transfected with *pre-miR-34a* for 48 hours and/or subsequently cultured under 20% O_2 or 0.5% O_2 for 30 hours. mean values ± SD (n = 3) are provided. (*) $P < 0.05$, (**) $P < 0.01$ and (***) $P < 0.001$.

Similar results were also obtained with RKO *TP53*$^{-/-}$ cells (**Figure 5.48**). The repression of *CDH1* on the mRNA level by hypoxia was abolished by treatment with *pre-miR-34a* oligonucleotide in RKO *TP53*$^{-/-}$ cells (**Figure 5.48**, middle panel). Also the induction of *VIM* or SNAIL (**Figure 5.48**, left panel and middle panel) and invasion and migration by hypoxia was abrogated by ectopic miR-34a (**Figure 5.48**, right panel). Therefore, the repression of miR-34a by HIF1A is necessary for hypoxia-induced EMT and associated invasion and migration.

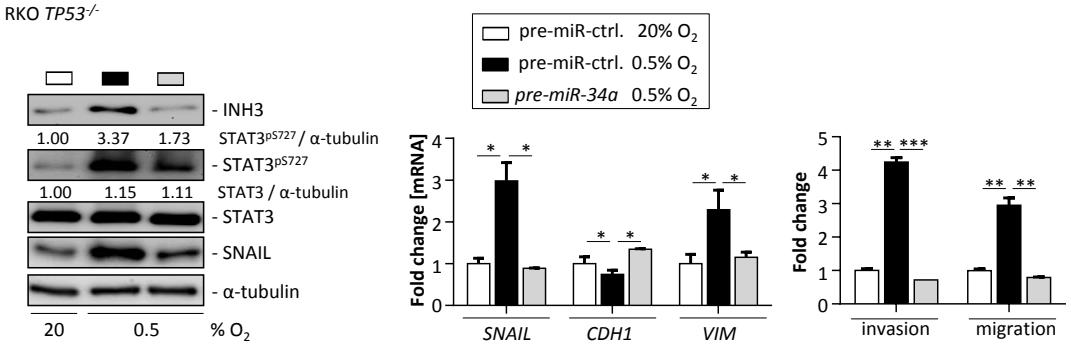

Figure 5.48 Ectopic miR-34a prevents EMT induced by hypoxia in *TP53*-deficient RKO cells. Western blot (left panel) and qPCR (middle panel) and (right panel) relative invasion and migration analysis of RKO *TP53*$^{-/-}$ cells transfected with *pre-miR-34a* for 48 hours and subsequently cultured at 20% O_2 or 0.5% O_2 for 30 hours. mean values ± SD (n = 3) are provided. (*) $P < 0.05$, (**) $P < 0.01$ and (***) $P < 0.001$.

Taken together, the results show that the *TP53* status and the resulting differential expression of miR-34a and INH3 control the response of CRC cells to hypoxia.

5.11 Modulation of chemo-resistance by the p53/HIF1A/miR-34a/INH3/Stat3 pathway

It has been reported that EMT confers chemo-resistance during tumor progression [174]. Therefore, whether the regulations identified here modulate the cellular response to 5-Fluoro-Uracil (5-FU), a chemotherapeutic agent commonly used for treating CRC [201] was determined. For this *TP53*$^{+/+}$ and *TP53*$^{-/-}$ HCT116 cells were compared in a colony-formation assay. Cells were cultured at 20% or 0.5% O_2 for 48 hours and subsequently treated with either 5-FU or, as a control, DMSO for 3 days.

As previously shown [202], HCT116 *TP53*$^{-/-}$ cells were more resistant to 5-FU and therefore formed more colonies than *TP53*$^{+/+}$ cells at 20% O_2 (**Figure 5.49A**). In line with a protective effect of hypoxia-induced EMT, treatment with 5-FU at 0.5% O_2 was

less inhibitory to the colony-formation of *TP53*-negative cells than treatment with 5-FU at 20% O_2 (**Figure 5.49A**). Moreover, the relative resistance of HCT116 *TP53*$^{-/-}$ cells to 5-FU at 0.5% O_2 was abolished by knockdown of INH3 (**Figure 5.49B**).

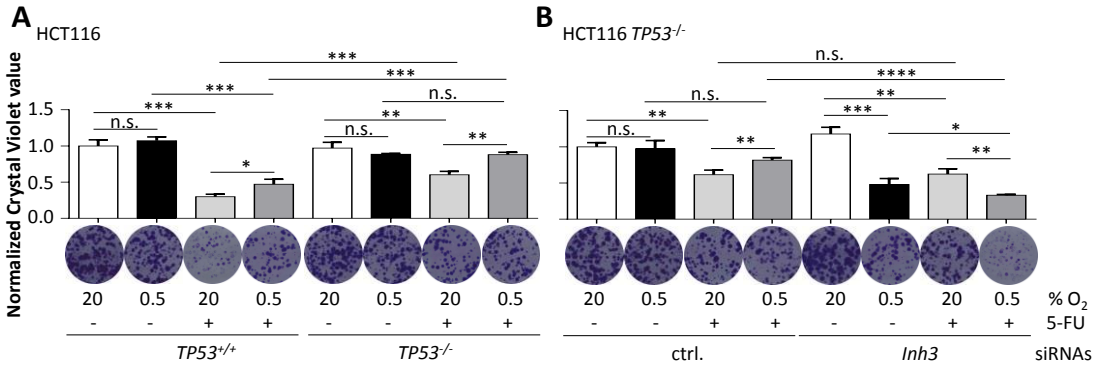

Figure 5.49 Analysis of hypoxia-mediated resistance to 5-FU and apoptosis in HCT116 cells. (**A-B**) 500 cells were seeded per well into a six well plate and cultivated for 24 hours at 20% O_2, then exposed to 0.5% O_2 for 48 hours, and subsequently treated with or without 5-FU for 72 hours. Subsequently cells were fixed and stained with crystal violet. Quantification of crystal violet staining (G, H, upper panel) and representative examples of crystal violet staining (G, H, lower panel). mean values ± SD (n = 3) are provided. (*) $P < 0.05$, (**) $P < 0.01$ and (***) $P < 0.001$.

Similar results were obtained with the *TP53*$^{+/+}$ and *TP53*$^{-/-}$ pair of RKO CRC cells (**Figure 5.50**).

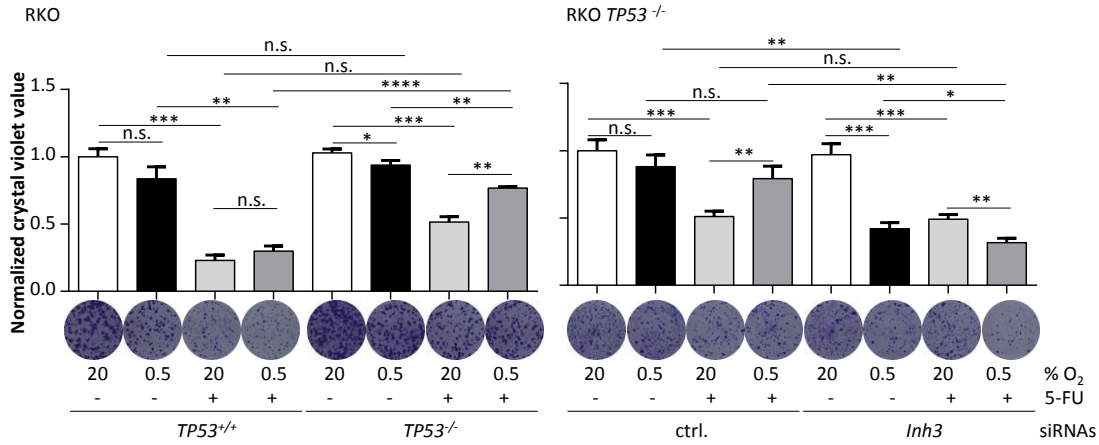

Figure 5.50 Analysis of hypoxia-mediated resistance to 5-FU and apoptosis in RKO cells. 500 indicated cells were seeded per well into a six well plate and cultivated for 24 hours at 20% O_2 and subsequently exposed to 0.5% O_2 for 48 hours, and subsequently treated with or without 5-FU for 72 hours. Subsequently cells were fixed and stained with crystal violet. (upper panel) Quantification of crystal violet staining and (lower panel) representative examples of crystal violet staining. mean values ± SD (n = 3) are provided. (*) $P < 0.05$, (**) $P < 0.01$ and (***) $P < 0.001$.

In line with results obtained in CRC lines in cell culture, *miR-34a*$^{-/-}$*; miR-34bc*$^{-/-}$ tumoriods derived from adenomas of *Apc*$^{Min/+}$ mice showed less apoptosis in response to 5-FU at 0.5% O_2 than *miR-34a*$^{+/+}$*; miR-34bc*$^{+/+}$ tumoroids (**Figure 5.51**).

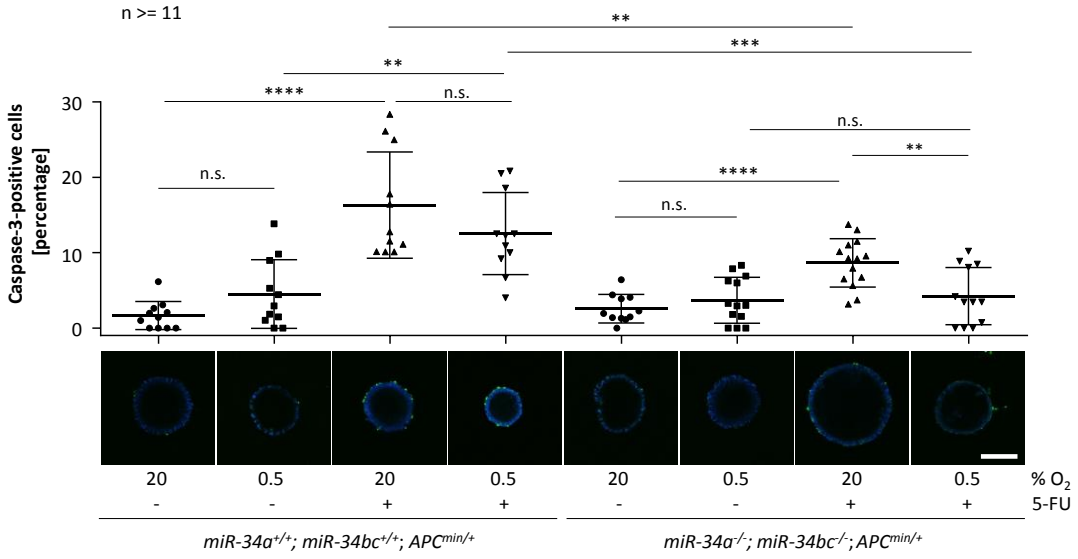

Figure 5.51 Analysis of hypoxia-mediated resistance to 5-FU and apoptosis in tumoriods derived from adenomas of *Apc*$^{Min/+}$ mice. Quantification of cleaved-Caspase-3 staining of tumoroids derived from adenomas of *Apc*$^{Min/+}$ mice proficient or deficient for *miR-34a/b/c* exposed to 20% O_2 or 0.5% O_2 for 48 hours and subsequently treated with or without 5-FU for 48 hours. For each condition n >= 11 tumoroids derived from 3 mice were analyzed per genotype. (*) $P < 0.05$, (**) $P < 0.01$ and (***) $P < 0.001$. Longchang Jiang performed the analysis and generated the figure.

Taken together, these results show that the p53/HIF1A/miR-34a/INH3/STAT3 regulatory pathway mediates the differential response towards 5-FU and its modulation by hypoxia.

5.12 INH3 expression in primary CRC samples

Next whether *Inh3* expression is affected by the *TP53* status in primary CRCs represented in the Cancer Genome Atlas (TCGA) database [106] was determined.

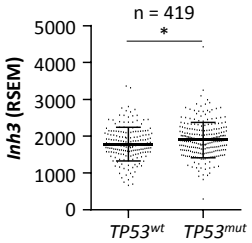

Figure 5.52 *TP53* status influences *Inh3* expression in primary CRCs. Associations of *Inh3* expression with (**A**) the *TP53* status in TCGA-COAD and TCGA-READ samples with known TP53 status (n = 419). Significance was calculated using Student's *t* test. (*) $P < 0.05$, (**) $P < 0.01$ and (***) $P < 0.001$. Matjaz Rokavec performed the analysis and generated the figure.

The 238 CRC samples with mutant *TP53* displayed significantly elevated expression of *Inh3* compared to 181 CRC samples expressing wild-type *TP53* (**Figure 5.52** and Table **5.3**). These findings were in line with the observations described above.

Table 5.3 *TP53* status of samples in the TCGA collection of human colon adenocarcinomas (n = 628).

	Number of cases	Percentage
TP53^{wt}	181	43.19%
TP53^{mut}	238	56.81%
TP53 status known	419	100.00%
TP53 status unknown	209	N.A.
Total	628	N.A.

Matjaz Rokavec performed the analysis and generated the table.

In addition, primary CRCs with local metastasis to the lymph-nodes, showed significantly elevated expression of *Inh3* compared to CRCs without local metastasis (**Figure 5.53A**). Moreover, primary tumors exhibiting distant metastases (M1) showed a trend towards increased expression of *Inh3* (**Figure 5.53B**).

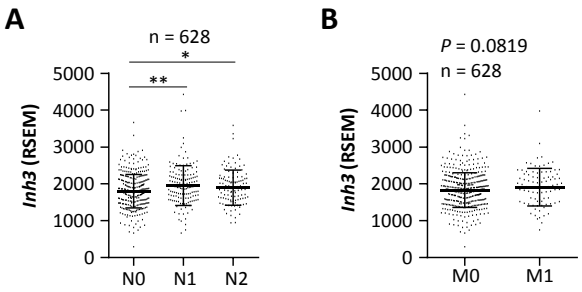

Figure 5.53 Association of *Inh3* expression with local and distant metastases. Associations of *Inh3* expression with (**B**) nodal and (**C**) distant metastasis in the combined TCGA-COAD and TCGA-READ database (n = 628). Significance was calculated using Student's *t* test. (*) $P < 0.05$, (**) $P < 0.01$ and (***) $P < 0.001$. Matjaz Rokavec performed the analysis and generated the figure.

In a matched case control cohort of primary colon cancers with (n = 42) and without (n =42) synchronous liver metastasis up-regulation of INH3 protein expression at the infiltrative tumor edge was significantly associated with liver metastasis (**Figure 5.54A** and **Table 5.4**).

Table 5.4 INH3 expression and clinical variables.

Characteristics	Total	Inh3 invasion front up		*P*
		No	Yes	
All patients	84 (100)	32 (38.1)	52 (61.9)	
Age (y, Median 68)				
< 68	40 (47.6)	15 (17.9)	25 (29.8)	0.91
≥ 68	44 (52.4)	17 (20.2)	27 (32.1)	
Gender				
Male	40 (47.6)	16 (19.0)	24 (28.6)	0.73
Female	44 (52.4)	16 (19.0)	28 (33.3)	
Tumor size (UICC)				
T2	8 (9.5)	5 (6.0)	3 (3.6)	0.27
T3	62 (73.8)	21 (25.0)	41 (48.8)	
T4	14 (16.7)	6 (7.1)	8 (9.5)	
Nodal status				
N0	37 (44.0)	18 (21.4)	19 (22.6)	0.08
N+	47 (56.0)	14 (16.7)	33 (39.3)	
Metastasis (Liver)				
M0	42 (50.0)	23 (27.4)	19 (22.6)	**0.002**
M1	42 (50.0)	9 (10.7)	33 (39.3)	
Tumor grade (WHO)				
Low	28 (33.3)	8 (9.5)	20 (23.8)	0.2
High	56 (66.7)	24 (28.6)	32 (38.1)	

Percent values are given in parentheses
Human patient sample collection was stained by the diagnostics laboratory, Pathology Institute, LMU, Munich. David Horst performed the microscope evaluation and generated the table.

Interestingly, HIF1A was shown to be up-regulated at the invasion front of CRCs indicating that these regions are hypoxic [203]. Accordingly, elevated INH3 expression in infiltrative CRC cells that had undergone EMT, as evidenced by Laminin 5γ2 positivity, was associated with increased expression the hypoxia marker GLUT1 (**Figure 5.54B**).

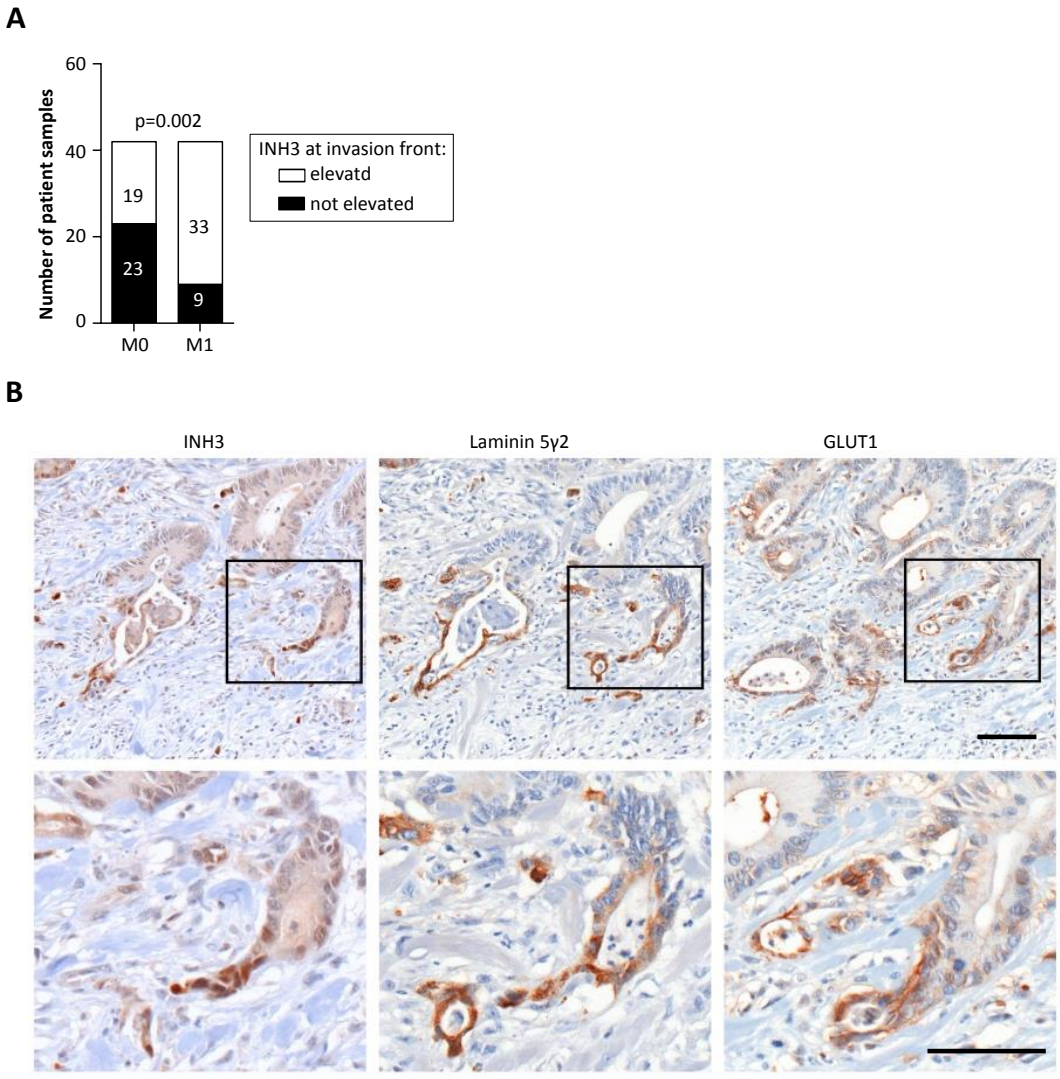

Figure 5.54 INH3 expression at the invasion front of primary CRCs. (**A**) INH3 expression in primary colon cancer samples of 84 patients who underwent surgical tumor resection at the Ludwig-Maximilians-University, Munich between 1994 and 2005. Percentage values are given in parentheses. Data were analyzed using the χ^2 test. (**B**) Examples of representative immunohistochemical detections. Scale bar represents 100 µm. Human patient sample collection was stained by the diagnostics laboratory, Pathology Institute, LMU, Munich (**A-B**). David Horst performed the microscope evaluation (**A**). Huihui Li generated the figure (**A**). David Horst took pictures and generated the figure (**B**).

Moreover, the expression of INH3 protein at the infiltrative tumor edge showed a significantly negative correlation with the expression of miR-34a (**Figure 5.55**) which is consistent with the above mentioned analysis of the TCGA database (**Figure 5.21**).

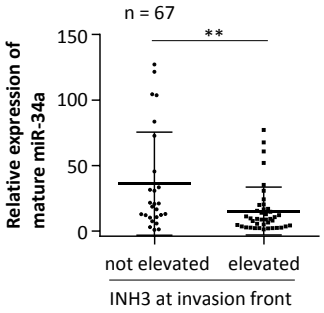

Figure 5.55 Correlative analysis of miR-34a and INH3 in primary CRCs. Correlative analysis of Inh3 and *pri-miR-34a* expression in primary colon cancer samples of 67 patients as in D. *pri-miR-34a* expression was determined previously [204]. Significance was calculated using Student's *t* test. (*) $P < 0.05$, (**) $P < 0.01$ and (***) $P < 0.001$. Human patient sample collection was stained by the diagnostics laboratory, Pathology Institute, LMU, Munich. David Horst performed the microscope evaluation. Huihui Li generated the figure.

The negative correlation between miR-34a and *Inh3* was more pronounced in ascending colon, hepatic flexure, and rectum than in other regions of the large intestine (**Figure 5.56**).

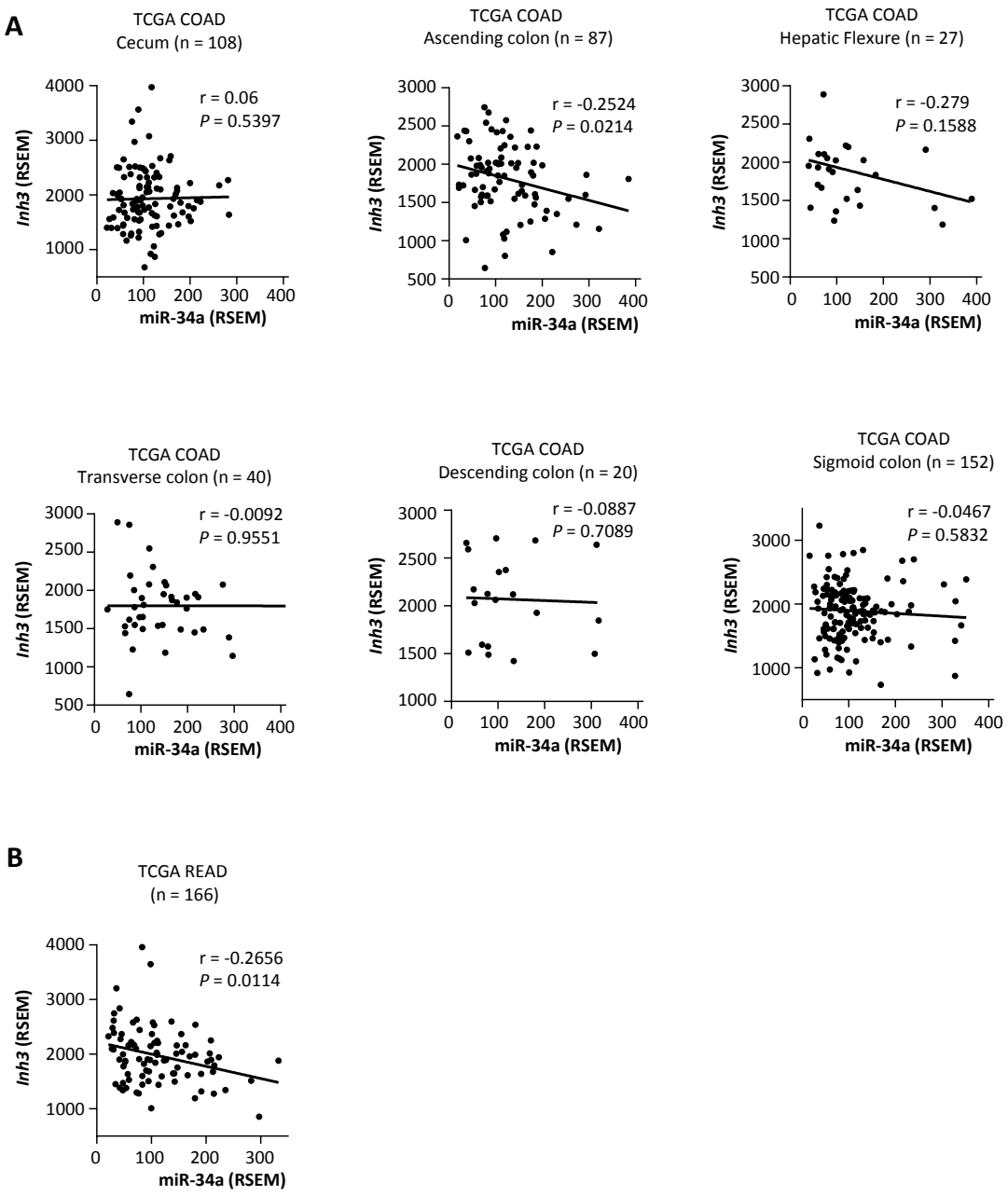

Figure 5.56 Analysis of *Inh3* and miR-34a expression in CRC samples within the TCGA collection. Analysis of Inh3 and miR-34a expression in (**A**) colon adenocarcinomas (COAD) of the indicated location and (**B**) rectal adenocarcinomas (READ) from the TCGA database. Correlations were calculated using the Spearman coefficient. Matjaz Rokavec performed the analysis and generated the figure.

Next, the levels of INH3, Laminin 5γ2, and Glut1 in paired primary and metastatic lesions from 17 patients was determined (**Figure 5.57A**). The elevated expression of INH3, Glut1, and Laminin 5γ2 at the infiltrative tumor edge of primary tumors was also found at the edge of matched metastases in the majority of patient samples (**Figure 5.57B**).

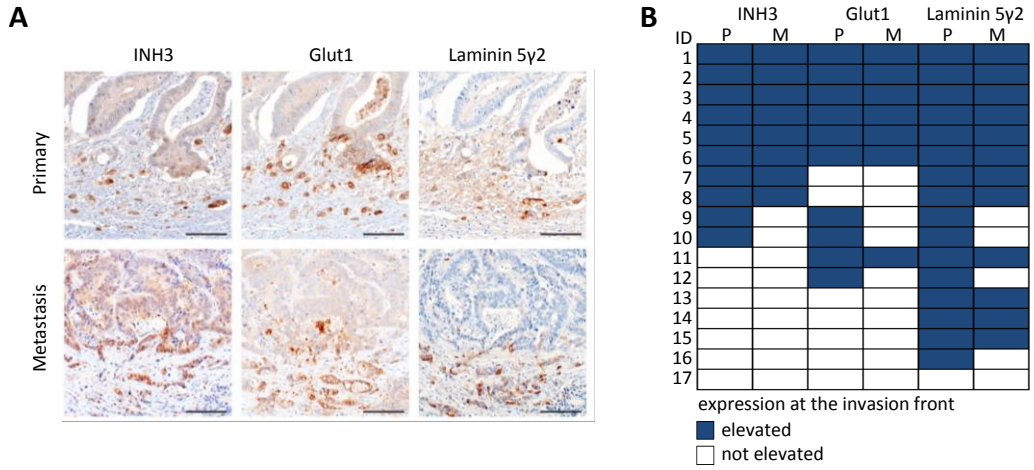

Figure 5.57 INH3, Glut1 and Laminin 5γ2 protein expression in primary CRCs and metastases. (**A**) Examples of representative immunohistochemical detections of INH3, Glut1, and Laminin 5γ2 expression at the invasion front of primary colon tumors and matched metastases. Scale bar represents 100 µm. (**B**) Summary of INH3, Glut1, and Laminin 5γ2 expression at the invasion front of primary colon tumors (P) and matched metastases (M) in individual patients. Human patient sample collection was stained by the diagnostics laboratory, Pathology Institute, LMU, Munich (**A**-**B**). David Horst performed the microscope evaluation (**A**-**B**). Huihui Li took the pictures (**A**), and Matjaz Rokavec performed the calculation and generated the figure (**B**).

Moreover, elevated expression of INH3 was significantly associated with elevated expression of Glut1 and Laminin 5γ2 at the edge of primary tumors and metastases (**Figure 5.58**).

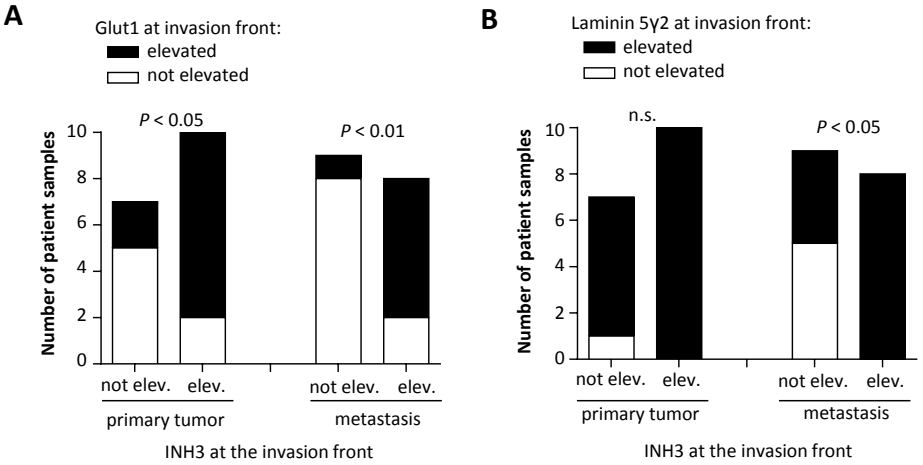

Figure 5.58 Correlative analysis of INH3 and Glut1 or Laminin 5γ2 protein expression in primary CRCs and metastases. (**A**) Association between expression of Inh3 and Glut1 at the invasion front of primary tumors and metastases. (**B**) Association between expression of INH3 and Laminin 5γ2 at the invasion front of primary tumors and metastases. significance was calculated using the χ^2 test. Not elev., not elevated; elev., elevated. Human patient sample collection was stained by the diagnostics laboratory, Pathology Institute, LMU, Munich. David Horst performed the microscope evaluation, and Matjaz Rokavec performed the calculation and generated the figure.

In addition, expression of INH3, Glut1 and Laminin 5γ2 was similar in the bulk areas of primary tumors and matched metastases (**Figure 5.59**).

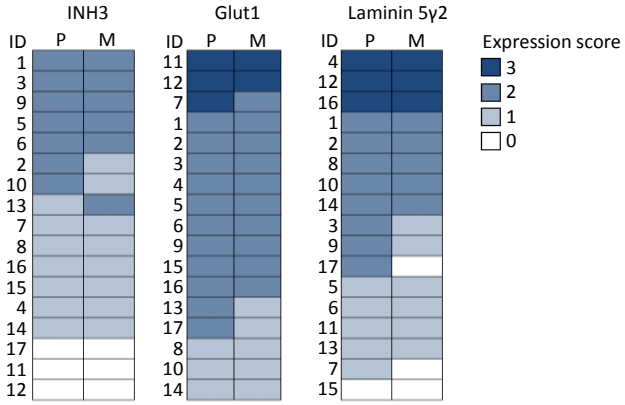

Figure 5.59 Analysis of INH3, Glut1 and Laminin 5γ2 protein expression in the bulk areas of primary CRCs and metastases. Summary of INH3, Glut1, and Laminin 5γ2 expression in the bulk of primary colon tumors (P) and matched metastases (M) in individual patients. Human patient sample collection was stained by the diagnostics laboratory, Pathology Institute, LMU, Munich. David Horst performed the microscope evaluation, and Matjaz Rokavec performed the calculation and generated the figure.

Taken together, the expression pattern of INH3 detected in patient derived tumor samples indicates that the regulatory circuit characterized in this study is also manifest at the invasion front of primary CRCs and metastases.

6. Discussion

The results presented in this thesis demonstrate that the decision between EMT or MET in response to hypoxia is mediated by a regulatory network involving HIF1A, p53, miR-34a, INH3, PP1 and STAT3 (**Figure 6.1**). Since we could detect these regulations in both MSS and MSI CRC cell lines and also found an inverse correlation between Inh3 and miR-34a in tumors derived from different sites of the large intestine, the identified pathway seems to apply to CRCs in general. In the absence of functional p53, HIF1A mediates repression of *miR-34a*, whereas in the presence of wild-type *TP53* expression of *miR-34a* is induced under hypoxia. HIF1A, miR-34a and *Inh3* form a coherent, feed-forward regulatory loop, wherein HIF1A represses *miR-34a*, which encodes a repressor of INH3 and also directly activates *Inh3* transcription. This type of dual regulation has been described for other transcription factor and miRNA pairs, and confers increased robustness to regulatory systems [205]. The resulting induction of INH3 was necessary for hypoxia-induced EMT, invasion and migration, as well as hypoxia-mediated resistance towards 5-FU. Since inactivation of INH3 prevented hypoxia-induced formation of lung-metastases of xenografted CRC lines in mice, these regulations may ultimately affect metastases formation in human patients. In line with these results, INH3 was not only required for hypoxia-induced EMT but also sufficient for the induction of EMT. However, in *TP53*-proficient cells, hypoxia resulted in p53 activation, miR-34a induction and a miR-34a-mediated induction of MET and down-regulation of INH3. This response may contribute to the strong selection for loss of *TP53* and *miR-34a* during tumor progression. In support of this conjecture, we determined a significant association between *TP53* mutation and INH3 up-regulation in primary CRC. Furthermore, increased INH3 expression at the invasion front of primary CRCs was associated with metastasis. Interestingly, also the invasion fronts of metastasis showed elevated expression of INH3 suggesting that it may contribute to secondary metastasis formation.

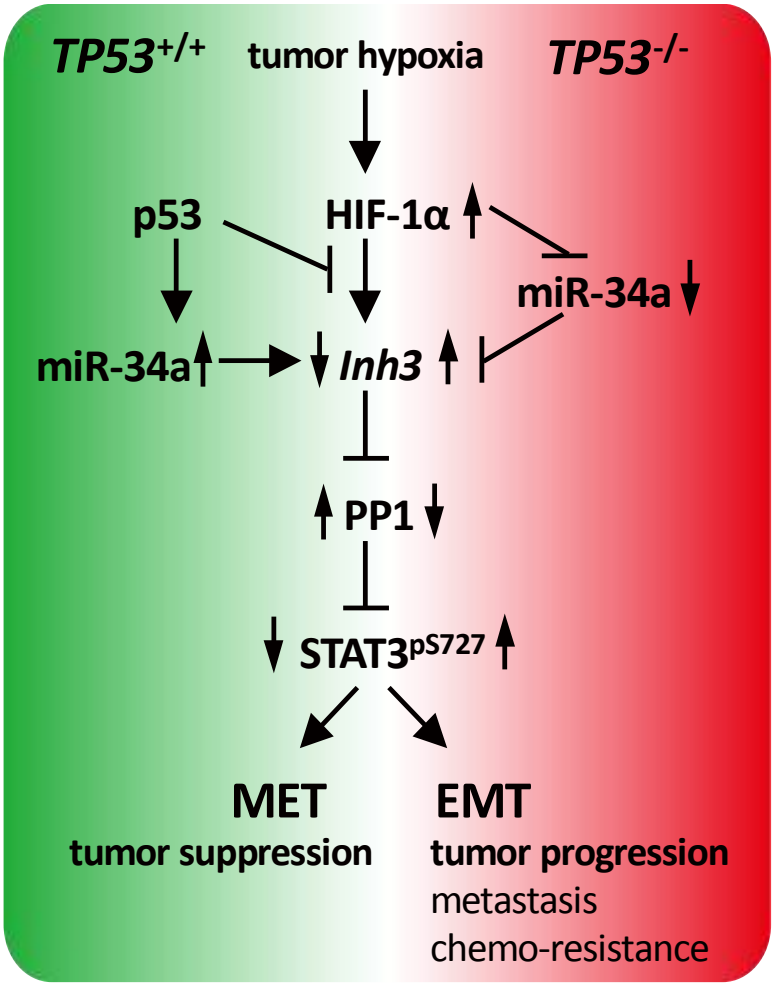

Figure 6.1 Model of the antagonistic regulation of the miR-34a/INH3/STAT3 pathway by p53 and HIF1A.

Previously, Graeber et al. showed that hypoxia induces apoptosis in murine tumors with wild-type *TP53* expression, whereas *TP53*-deficient tumors progress under hypoxic conditions [121]. Our findings imply that the differential regulation of miR-34a in these two scenarios may explain, at least in part, the different cellular responses under these conditions: in p53-proficient cells the hypoxia-mediated activation of p53 and subsequent induction of miR-34a was dominant over the repression of *miR-34a* by HIF1A, causing inhibition of EMT which is generally associated decreased cell survival. In p53-deficient cells, miR-34a was repressed by HIF1A promoting EMT,

which confers resistance to apoptosis and enhances migration and invasion. Certain factors provided by the tumor micro-environment are able to induce EMT in cells expressing wild-type *TP53* (e.g. e.g. IL-6 and TGF-B [206-210]). This is, at least in part, facilitated by the down-regulation of genes encoding MET-mediating miRNAs, which are inducible by p53 (such as the miR-34 and miR-200 family members). Here we show that hypoxia leads to repression of *miR-34a* by HIF1A selectively in *TP53*-negative cells. However, it is conceivable that also CRCs expressing wild-type *TP53* may undergo EMT when exposed to hypoxia in combination with EMT-inducing ligands.

Here we studied the effect of 5-FU on CRC cell lines and murine, intestinal tumoroids. We observed a desensitization upon loss of *TP53* or *miR-34a/b/c* that was enhanced under hypoxic conditions. In addition, the increased resistance was dependent on the up-regulation of INH3. Since 5-FU is commonly used to treat CRC these results may be clinically relevant. Others have shown that isogenic CRC cell lines with either wild-type or deleted *TP53* do not respond uniformly to different chemotherapeutic drugs [202]: e.g. in the case of etoposide CRC cells with wild-type *TP53* were less sensitive than *TP53*-deficient CRC cells. Therefore, further analyses are necessary to evaluate the role of the mechanisms identified here in the cellular response to other chemotherapeutic agents.

Besides, we also analyzed the expression pattern of INH3, the hypoxia marker Glut1 and the EMT-marker Laminin 5γ2 from 17 paired primary and metastatic lesions. However, no significant increase or decrease of these three proteins in the main areas of the metastases was observed when compared with matched primary CRCs. Furthermore, at the invasion front of both primary and metastatic cases, we did again observe a consistent increase in the expression of these proteins when compared to the bulk areas of the tumors or metastases in approximately half of cases. This may because tumor cells are heterogeneous with mixed epithelial and mesenchymal traits in the primary and metastatic lesions. The online data, which analyzed the expression

profiles of 18 matched primary colorectal cancers and associated liver metastases [211], also showed no significant difference in the expression of Laminin 5y2, Inh3, GLUT1, and HIF1A mRNAs in the bulk tumor mass when compared to the matched metastasis as well. Moreover, there was also no difference in expression of EMT-associated mRNAs *VIM*, *CDH1*, *SNAI*, and *SLUG* between primary tumors and metastases [211].

Interestingly, elevated expression of INH3 was significantly associated with elevated expression of Glut1 and Laminin 5γ2 at the edge of primary tumors and metastases, indicating INH3 is associated with hypoxia-induced EMT in primary CRC and metastases. Moreover, the similar expression was observed in 17 paired primary and metastatic lesions, suggesting that INH3 may contribute to secondary metastasis formation. Therefore, the regulations, we initially detected in CRC cell lines, are also manifest at the invasion front of primary colorectal cancers and derived metastatic lesions. Elevated expression of EMT-TFs SNAIL, SLUG, ZEB1, ZEB2, and TWIST was found at the invasion front in different cancers [203, 212-216]. Moreover, the expression of the EMT marker Vimentin at invasion front was also upregulated [217]. Also downregulation of E-cadherin at invasion front was reported previously [218]. Thus, the upregulation of INH3 at the invasion front indicates that INH3 may also be an important EMT regulator in vivo. Interestingly, it was previously shown that HIF1A is significantly up-regulated at the invasion front of CRCs indicating that these regions are hypoxic [203]. Moreover, endogenous marker of hypoxia carbonic anhydrase 9 (CA9) was also found with high abundance at the invasion front of gastric cancers [219]. We found that expression of another hypoxia marker GLTU1 was also elevated at invasion front. Altogether, elevated expression of INH3 at the invasion front was associated with markers of EMT and hypoxia, indicating that INH3 may be a new marker for hypoxia-induced EMT.

Here, we showed that p53/miR-34a regulates hypoxia-induced EMT via INH3. Indeed, the TCGA data showed that Inh3 expression was increased in mutant *TP53*

CRC samples and significantly inversely correlated with miR-34a expression in primary CRCs. Besides, In 67 of the cases analyzed by TMA for INH3 expression, we had previously determined the expression of mature miR-34a [204]. The results showed that increased expression of INH3 protein at the infiltrative tumor edge with a significantly decreased expression of miR-34a and vice versa. Thus, the expression of INH3 protein and miR-34a negatively correlate in clinical samples.

We have shown that epigenetic silencing of *miR-34a* in primary tumors is associated with increased lymph node infiltration and metastasis in colon cancer patients [204]. It is conceivable that the transient repression of *miR-34a* by hypoxia observed here is fixated over time by DNA hyper-methylation in its promoter region. The loss of miR-34a expression by epigenetic silencing subsequent to hypoxia-mediated repression might facilitate cancer cell survival and local invasion or migration. In addition, the silencing of *miR-34a* may itself contribute to the adaptation of tumor cells to the hypoxic tumor microenvironment, since miR-34a has many targets that would favor a survival under such circumstances, such as LDH-A and Survivin [182].

Tumor suppressor miRNAs represent an essential direction for new therapeutic investigation for their function during cancer progression. The repression of INH3 by miR-34 may be an essential component in the regulation of EMT under hypoxia. Our results suggest that inhibiting HIF1A, INH3 and/or STAT3 in combination with restoring miR-34a function may have therapeutic potential for the treatment of invasive colorectal cancers that display hypoxia. Targeting hypoxic tumor cells is one of the most attractive therapies for cancer treatment. Several approaches, including hypoxia-activated prodrugs, gene therapy, recombinant anaerobic bacteria, specific targeting of HIF, or targeting pathways important for hypoxic cells, such as the mTOR and UPR pathways have been designed [220]. Moreover, many pharmacological inhibitors that target STAT3 were reported [221]. Re-expression of miR-34a caused to 20% to 83% repression of tumor growth [82] without severe toxicity or unwanted

immune response [81-83]. Intriguingly, in April 2013, MRX34, a liposome-based miR-34 mimic, became the first cancer-targeted miRNA-based drug in phase I clinical trial in patients with advanced hepatocellular carcinoma [82, 84]. Interestingly, a miR-34a restoration may also harness the patients' immune system against tumors, since the T lymphocyte inhibitory molecule PD-L1, which is expressed at elevated levels on certain tumors, represents a miR-34a target [222, 223]. As suggested by our results this may be especially relevant in tumors that are driven by hypoxia. Since the HIF1A pathway has been targeted by multiple approaches [110], a combination of HIF1A inactivation and miR-34a restoration may be feasible in order to prevent or inhibit hypoxia-driven formation of metastases.

7. Summary

In colorectal cancer (CRC), hypoxia causes resistance to therapy and promotes metastasis. Mutation of the tumor suppressor *TP53* provides a selective advantage to cancer cells under conditions of hypoxia, but little is known about the mediators of this effect.

In this thesis I could show that the hypoxia inducible factor 1 alpha subunit (HIF1A) directly represses the *MIR34A* gene in *TP53*-defective CRC cells, whereas expression of MIR34A was induced in *TP53*-proficient CRC cells exposed to hypoxia. Down-regulation of MIR34A was required for hypoxia-induced epithelial to mesenchymal transition (EMT), invasion and migration, and activation of STAT3 in CRC cells. In this study the *PPP1R11 (protein phosphatase 1 regulatory inhibitor subunit 11; INH3; HCGV; IPP3; HCG-V; TCTE5; TCTEX5; CFAP255)*, was identified and characterized as a target of MIR34A. PPP1R11 mediates phosphorylation (activation) of STAT3 by inhibiting protein phosphatase (PP1), so expression of MIR34A inhibited STAT3 activity in *TP53*-negative CRC cells. Ectopic expression of INH3 in CRC cells induced EMT, invasion, and migration, which all required STAT3. Increased expression of INH3 in *TP53*-negative CRC cells was required for hypoxia-induced EMT, invasion, migration, and chemo-resistance to 5-fluorouracil, as well as metastases of xenograft tumors to lungs of mice. Adenomas and derived tumoroids of $Apc^{Min/+}$ mice with disruption *miR34a*, *miR34b* and *miR34c* expressed increased levels of INH3. Colorectal tumors from patients dispalyed increased levels of INH3 at areas of invasion, compared with other areas of the tumor. Increased INH3 levels associated with *TP53* mutations and metastasis to liver.

HIF1A represses, whereas p53 increases, expression of MIR34A in CRC cells. MIR34A reduces expression of INH3 to prevent activation of STAT3 and inhibit the EMT and metastasis. In the future strategies to target this pathway might be developed to inhibit CRC metastasis and overcome resistance to therapy associated with hypoxia.

8. Zusammenfassung

Hypoxie verursacht Therapieresistenz und fördert die Metastasierung von kolorektalen Karzinomen (KRK). Unter hypoxischen Bedingungen verleiht die Mutation des Tumorsuppressorgens *TP53* den Krebszellen einen selektiven Vorteil. Die Mediatoren dieses Effektes sind jedoch weitgehend unbekannt.

In der vorliegenden Arbeit konnte ich zeigen, dass unter Hypoxie der Hypoxie-induzierbare Faktor-1α (HIF1A) das *MIR34A*-Gen in TP53-defekten KRK-Zellen unterdrückt, während in *TP53*-kompetenten KRK-Zellen die Expression von MIR34A induziert wird. Die Herabregulierung von MIR34A in KRK-Zellen war für die Hypoxie-induzierte Epithelial-Mesenchymale-Transition (EMT), Invasion und Migration, sowie Aktivierung von STAT3 verantwortlich. In dieser Arbeit wurde die *Protein Phosphatase 1 regulatorische Inhibitor Untereinheit 11* (*PPP1R11; INH3; HCGV; IPP3; HCG-V; TCTE5; TCTEX5; CFAP255)*, welche einen Inhibitor der Protein Phosphatase 1 (PP1) kodiert, als eine durch MIR34A-regulierte mRNA identifiziert und charakterisiert. INH3 vermittelt die Phosphorylierung und damit Aktivierung des STAT3 Proteins durch Inhibition von PP1. Die Expression von MIR34A in *TP53*-negativen KRK-Zellen reduzierte daher die Aktivität von STAT3. Die ektopische Expression von INH3 in KRK-Zellen induzierte STAT3-abhängige EMT, Invasion und Migration. Die erhöhte Expression der INH3 in TP53-negativen CRC-Zellen war erforderlich für Hypoxie-induzierte EMT, Invasion, Migration und Chemo-Resistenz gegenüber 5-Fluorouracil, sowie für die Metastasierung von Xeno-transplantierten KRK-Zellen in Lungen von Mäusen. Adenome und abgeleitete Tumoroide von *Apc*$^{Min/+}$ Mäusen mit Deletion von *miR34a, miR34b* und *miR34c* zeigten eine erhöhte INH3 Proteinexpression. Primäre KRKs von Patienten wiesen erhöhte INH3 Proteinexpression an der Invasionsfront im Vergleich zu anderen Bereichen des Tumors auf. Erhöhte INH3-Levels waren mit *TP53*-Mutationen und Lebermetastasen assoziiert.

Insgesamt konnte gezeigt werden, dass die Expression von MIR34A in KRK-Zellen durch HIF1A inhibiert und durch p53 hingegen erhöht wird. MIR34A unterdrückt die Expression von INH3 und verhindert so die Aktivierung von STAT3 und hemmt EMT und Metastasierung. In der Zukunft könnten Strategien zur gezielten Beeinflussung dieses Signalwegs genutzt werden, um die Metastasierung von KRKs zu hemmen und die Hypoxie-induzierte Therapieresistenz beim KRK zu überwinden.

9. Acknowledgements

First of all, I would like to thank my supervisor Prof. Dr. rer. nat. Heiko Hermeking for giving me the opportunity to work on several fascinating projects, for his knowledgeable experience, continuous help and support, visionary advice, constant fruitful discussions and ideas which are invaluable for the ongoing project, for his excellent arrangement to collaborate with other scientists, for his passion and perseverance on science, for his patience and always support when I met unexpected problems. He is not only an excellent supervisor, a knowledgeable, visionary scientist, but also an excellent advisor and a great friend.

I would like to acknowledge all the past and present members of the group for helpfulness and valuable scientific support and discussions. In particularly, I would like to thank Dr. Markus Kaller, Dr. Sabine Hünten, Dr. Helge Siemens, our “Mutti” Dr. Stefanie Hahn, Dr. Rene Jackstadt, Dr. Markus Winter and Dr. Shi Lei for their excellent scientific help and for constructive discussions. I want to thank my co-author Dr. Matjaz Rokavec, Wikipedia boy Longchang Jiang, Meryem Gülfem Öner, and Prof Dr. med. David Horst for their great collaboration and for their valuable samples. I am grateful to Dr. Antje Menssen for technical explanations and sharing her knowledge. I want to acknowledge our lab mama Ursula Götz for her reliable and valuable technical support. Besides, I also would like to thank my friends Marina Schmidt, Dr. Yina Zhang, Xiaolong Shi for their help, support and faith.

I would like to acknowledge to China Scholarship Council (CSC) for supporting me for 4 years to achieve my doctor degree. I would like to thank Consul Jiqiang Dai and Consul Prof. Dr. Chongling Huang for supporting us in Munich.

I am deeply grateful to my family, especially my mother Mrs. Yuhua Wei and my aunt Mrs Yuhong Wei for their endless support and love, for “being there”. I also would like to thank my husband Dr. Kefeng Lu and my son Leo (Yuxun Lu) for their eternal support, encouragement and love. I would like to thank all my friends for their yearly support, encouragement and motivation.

Thanks all of you for your company and being part of my life.

10. References

1. Ferlay J, Soerjomataram I, Dikshit R, et al. Cancer incidence and mortality worldwide: Sources, methods and major patterns in GLOBOCAN 2012. Int J Cancer 2014.
2. Urbach D, Lupien M, Karagas MR, et al. Cancer heterogeneity: origins and implications for genetic association studies. Trends Genet 2012;28:538-43.
3. Hanahan D, Weinberg RA. Hallmarks of cancer: the next generation. Cell 2011;144:646-74.
4. Hanahan D, Weinberg RA. The hallmarks of cancer. Cell 2000;100:57-70.
5. Grady WM, Markowitz SD. Genetic and epigenetic alterations in colon cancer. Annu Rev Genomics Hum Genet 2002;3:101-28.
6. Tariq K, Ghias K. Colorectal cancer carcinogenesis: a review of mechanisms. Cancer Biol Med 2016;13:120-35.
7. Sadanandam A, Lyssiotis CA, Homicsko K, et al. A colorectal cancer classification system that associates cellular phenotype and responses to therapy. Nat Med 2013;19:619-25.
8. De Sousa EMF, Wang X, Jansen M, et al. Poor-prognosis colon cancer is defined by a molecularly distinct subtype and develops from serrated precursor lesions. Nat Med 2013;19:614-8.
9. Fearon ER, Vogelstein B. A genetic model for colorectal tumorigenesis. Cell 1990;61:759-67.
10. Vogelstein B, Kinzler KW. The Path to Cancer --Three Strikes and You're Out. N Engl J Med 2015;373:1895-8.
11. Spano D, Heck C, De Antonellis P, et al. Molecular networks that regulate cancer metastasis. Semin Cancer Biol 2012;22:234-49.
12. Cartwright TH. Treatment decisions after diagnosis of metastatic colorectal cancer. Clinical colorectal cancer 2012;11:155-166.
13. Edwards MS, Chadda SD, Zhao Z, et al. A systematic review of treatment guidelines for metastatic colorectal cancer. Colorectal Dis 2012;14:e31-47.
14. Yang J, Weinberg RA. Epithelial-mesenchymal transition: at the crossroads of development and tumor metastasis. Dev Cell 2008;14:818-29.
15. Thiery JP, Acloque H, Huang RY, et al. Epithelial-mesenchymal transitions in development and disease. Cell 2009;139:871-90.
16. Tsai JH, Yang J. Epithelial-mesenchymal plasticity in carcinoma metastasis. Genes Dev 2013;27:2192-206.

17. Kalluri R, Weinberg RA. The basics of epithelial-mesenchymal transition. J Clin Invest 2009;119:1420-8.
18. Scheel C, Weinberg RA. Cancer stem cells and epithelial-mesenchymal transition: concepts and molecular links. Semin Cancer Biol 2012;22:396-403.
19. Zheng H, Kang Y. Multilayer control of the EMT master regulators. Oncogene 2013;33:1755-63.
20. Beauchemin N. The colorectal tumor microenvironment: the next decade. Cancer Microenviron 2011;4:181-5.
21. Joyce JA, Pollard JW. Microenvironmental regulation of metastasis. Nat Rev Cancer 2009;9:239-52.
22. Brabletz T, Jung A, Reu S, et al. Variable beta-catenin expression in colorectal cancers indicates tumor progression driven by the tumor environment. Proc Natl Acad Sci U S A 2001;98:10356-61.
23. Franci C, Takkunen M, Dave N, et al. Expression of Snail protein in tumor-stroma interface. Oncogene 2006;25:5134-44.
24. Thiery JP. Epithelial-mesenchymal transitions in tumour progression. Nat Rev Cancer 2002;2:442-54.
25. De Craene B, Berx G. Regulatory networks defining EMT during cancer initiation and progression. Nat Rev Cancer 2013;13:97-110.
26. Peinado H, Olmeda D, Cano A. Snail, Zeb and bHLH factors in tumour progression: an alliance against the epithelial phenotype? Nat Rev Cancer 2007;7:415-28.
27. Sanchez-Tillo E, Liu Y, de Barrios O, et al. EMT-activating transcription factors in cancer: beyond EMT and tumor invasiveness. Cell Mol Life Sci 2012;69:3429-56.
28. de Herreros AG, Peiro S, Nassour M, et al. Snail family regulation and epithelial mesenchymal transitions in breast cancer progression. J Mammary Gland Biol Neoplasia 2010;15:135-47.
29. Vandewalle C, Comijn J, De Craene B, et al. SIP1/ZEB2 induces EMT by repressing genes of different epithelial cell-cell junctions. Nucleic Acids Res 2005;33:6566-78.
30. Hahn S, Jackstadt R, Siemens H, et al. SNAIL and miR-34a feed-forward regulation of ZNF281/ZBP99 promotes epithelial-mesenchymal transition. EMBO J 2013;32:3079-95.

31. Rokavec M, Oner MG, Li H, et al. IL-6R/STAT3/miR-34a feedback loop promotes EMT-mediated colorectal cancer invasion and metastasis. J Clin Invest 2014;124:1853-67.
32. Tam WL, Weinberg RA. The epigenetics of epithelial-mesenchymal plasticity in cancer. Nat Med 2013;19:1438-49.
33. Graff JR, Gabrielson E, Fujii H, et al. Methylation patterns of the E-cadherin 5' CpG island are unstable and reflect the dynamic, heterogeneous loss of E-cadherin expression during metastatic progression. J Biol Chem 2000;275:2727-32.
34. Lombaerts M, van Wezel T, Philippo K, et al. E-cadherin transcriptional downregulation by promoter methylation but not mutation is related to epithelial-to-mesenchymal transition in breast cancer cell lines. Br J Cancer 2006;94:661-71.
35. Takeno S, Noguchi T, Fumoto S, et al. E-cadherin expression in patients with esophageal squamous cell carcinoma: promoter hypermethylation, Snail overexpression, and clinicopathologic implications. Am J Clin Pathol 2004;122:78-84.
36. Byles V, Zhu L, Lovaas JD, et al. SIRT1 induces EMT by cooperating with EMT transcription factors and enhances prostate cancer cell migration and metastasis. Oncogene 2012;31:4619-29.
37. Baker SJ, Preisinger AC, Jessup JM, et al. p53 gene mutations occur in combination with 17p allelic deletions as late events in colorectal tumorigenesis. Cancer Res 1990;50:7717-22.
38. Vogelstein B, Lane D, Levine AJ. Surfing the p53 network. Nature 2000;408:307-10.
39. Oren M. Decision making by p53: life, death and cancer. Cell Death Differ 2003;10:431-42.
40. Lane D, Levine A. p53 Research: the past thirty years and the next thirty years. Cold Spring Harb Perspect Biol 2010;2:a000893.
41. Goh AM, Coffill CR, Lane DP. The role of mutant p53 in human cancer. J Pathol 2011;223:116-26.
42. Hermeking H. p53 enters the microRNA world. Cancer cell 2007;12:414-8.
43. Rokavec M, Li H, Jiang L, et al. The p53/microRNA connection in gastrointestinal cancer. Clin Exp Gastroenterol 2014;7:395-413.
44. Powell E, Piwnica-Worms D, Piwnica-Worms H. Contribution of p53 to metastasis. Cancer Discov 2014;4:405-14.

45. Lambert AW, Pattabiraman DR, Weinberg RA. Emerging Biological Principles of Metastasis. Cell 2017;168:670-691.
46. Wei CL, Wu Q, Vega VB, et al. A global map of p53 transcription-factor binding sites in the human genome. Cell 2006;124:207-19.
47. Chang CJ, Chao CH, Xia W, et al. p53 regulates epithelial-mesenchymal transition and stem cell properties through modulating miRNAs. Nat Cell Biol 2011;13:317-23.
48. Siemens H, Jackstadt R, Hunten S, et al. miR-34 and SNAIL form a double-negative feedback loop to regulate epithelial-mesenchymal transitions. Cell Cycle 2011;10:4256-71.
49. Kim NH, Kim HS, Li X-Y, et al. A p53/miRNA-34 axis regulates Snail1-dependent cancer cell epithelial-mesenchymal transition. The Journal of cell biology 2011;195:417-33.
50. Muller PA, Vousden KH, Norman JC. p53 and its mutants in tumor cell migration and invasion. J Cell Biol 2011;192:209-18.
51. Attardi LD, Jacks T. The role of p53 in tumour suppression: lessons from mouse models. Cell Mol Life Sci 1999;55:48-63.
52. Esquela-Kerscher A, Slack FJ. Oncomirs - microRNAs with a role in cancer. Nat Rev Cancer 2006;6:259-69.
53. Wightman B, Ha I, Ruvkun G. Posttranscriptional regulation of the heterochronic gene lin-14 by lin-4 mediates temporal pattern formation in C. elegans. Cell 1993;75:855-62.
54. Lee RC, Feinbaum RL, Ambros V. The C. elegans heterochronic gene lin-4 encodes small RNAs with antisense complementarity to lin-14. Cell 1993;75:843-54.
55. Kozomara A, Griffiths-Jones S. miRBase: integrating microRNA annotation and deep-sequencing data. Nucleic Acids Res 2011;39:D152-7.
56. Sayed D, Abdellatif M. MicroRNAs in development and disease. Physiol Rev 2011;91:827-87.
57. Gangaraju VK, Lin H. MicroRNAs: key regulators of stem cells. Nat Rev Mol Cell Biol 2009;10:116-25.
58. Ji Q, Karnak D, Hao P, et al. No small matter: microRNAs - key regulators of cancer stem cells. Int J Clin Exp Med 2010;3:84-7.
59. Jansson MD, Lund AH. MicroRNA and cancer. Mol Oncol 2012;6:590-610.
60. Frankel LB, Lund AH. MicroRNA regulation of autophagy. Carcinogenesis 2012;33:2018-25.

61. Le Bot N. MicroRNAs in angiogenesis. Nature Cell Biology 2012;14:342-342.
62. Jackson A, Linsley PS. The therapeutic potential of microRNA modulation. Discov Med 2010;9:311-8.
63. Li Z, Rana TM. Therapeutic targeting of microRNAs: current status and future challenges. Nat Rev Drug Discov 2014;13:622-38.
64. Calin GA, Dumitru CD, Shimizu M, et al. Frequent deletions and down-regulation of micro- RNA genes miR15 and miR16 at 13q14 in chronic lymphocytic leukemia. Proc Natl Acad Sci U S A 2002;99:15524-9.
65. Mendell JT, Olson EN. MicroRNAs in stress signaling and human disease. Cell 2012;148:1172-87.
66. Lu J, Getz G, Miska EA, et al. MicroRNA expression profiles classify human cancers. Nature 2005;435:834-8.
67. Volinia S, Calin GA, Liu CG, et al. A microRNA expression signature of human solid tumors defines cancer gene targets. Proc Natl Acad Sci U S A 2006;103:2257-61.
68. Calin GA, Sevignani C, Dumitru CD, et al. Human microRNA genes are frequently located at fragile sites and genomic regions involved in cancers. Proc Natl Acad Sci U S A 2004;101:2999-3004.
69. Raver-Shapira N, Marciano E, Meiri E, et al. Transcriptional activation of miR-34a contributes to p53-mediated apoptosis. Molecular cell 2007;26:731-43.
70. Tarasov V, Jung P, Verdoodt B, et al. Differential Regulation of microRNAs by p53 ND ES SC RIB. 2007:1586-1593.
71. Welch C, Chen Y, Stallings RL. MicroRNA-34a functions as a potential tumor suppressor by inducing apoptosis in neuroblastoma cells. Oncogene 2007;26:5017-22.
72. Lize M, Klimke A, Dobbelstein M. MicroRNA-449 in cell fate determination. Cell Cycle 2011;10:2874-82.
73. Christoffersen NR, Shalgi R, Frankel LB, et al. p53-independent upregulation of miR-34a during oncogene-induced senescence represses MYC. Cell Death Differ 2010;17:236-45.
74. Kress TR, Cannell IG, Brenkman AB, et al. The MK5/PRAK kinase and Myc form a negative feedback loop that is disrupted during colorectal tumorigenesis. Mol Cell 2011;41:445-57.
75. Wang R, Ma J, Wu Q, et al. Functional Role of miR-34 Family in Human Cancer. Current drug targets 2013;14:1185-91.

76. Hermeking H. The miR-34 family in cancer and apoptosis. Cell Death Differ 2010;17:193-9.
77. Bommer GT, Gerin I, Feng Y, et al. p53-mediated activation of miRNA34 candidate tumor-suppressor genes. Current biology 2007;17:1298-307.
78. Bouhallier F, Allioli N, Lavial F, et al. Role of miR-34c microRNA in the late steps of spermatogenesis. RNA 2010;16:720-31.
79. Rokavec M, Li H, Jiang L, et al. The p53/miR-34 axis in development and disease. J Mol Cell Biol 2014;6:214-30.
80. Jiang L, Hermeking H. miR-34a and miR-34b/c Suppress Intestinal Tumorigenesis. Cancer Res 2017;77:2746-2758.
81. Pramanik D, Campbell NR, Karikari C, et al. Restitution of tumor suppressor microRNAs using a systemic nanovector inhibits pancreatic cancer growth in mice. Mol Cancer Ther 2011;10:1470-80.
82. Craig VJ, Tzankov A, Flori M, et al. Systemic microRNA-34a delivery induces apoptosis and abrogates growth of diffuse large B-cell lymphoma in vivo. Leukemia 2012;26:2421-4.
83. Wiggins JF, Ruffino L, Kelnar K, et al. Development of a lung cancer therapeutic based on the tumor suppressor microRNA-34. Cancer research 2010;70:5923-30.
84. Ling H, Fabbri M, Calin GA. MicroRNAs and other non-coding RNAs as targets for anticancer drug development. Nat Rev Drug Discov 2013;12:847-65.
85. Lodygin D, Tarasov V, Epanchintsev A, et al. Inactivation of miR-34a by aberrant CpG methylation in multiple types of cancer. Cell Cycle 2008;7:2591-600.
86. Lujambio A, Calin GA, Villanueva A, et al. A microRNA DNA methylation signature for human cancer metastasis. Proc Natl Acad Sci U S A 2008;105:13556-61.
87. Vogt M, Munding J, Gruner M, et al. Frequent concomitant inactivation of miR-34a and miR-34b/c by CpG methylation in colorectal, pancreatic, mammary, ovarian, urothelial, and renal cell carcinomas and soft tissue sarcomas. Virchows Arch 2011;458:313-22.
88. Kong D, Heath E, Chen W, et al. Epigenetic silencing of miR-34a in human prostate cancer cells and tumor tissue specimens can be reversed by BR-DIM treatment. American journal of translational research 2012;4:14-23.

89. Östling P, Leivonen S-K, Aakula A, et al. Systematic analysis of microRNAs targeting the androgen receptor in prostate cancer cells. Cancer research 2011;71:1956-67.
90. Mandke P, Wyatt N, Fraser J, et al. MicroRNA-34a modulates MDM4 expression via a target site in the open reading frame. PLoS One 2012;7:e42034.
91. Okada N, Lin CP, Ribeiro MC, et al. A positive feedback between p53 and miR-34 miRNAs mediates tumor suppression. Genes Dev 2014;28:438-50.
92. Sotillo E, Laver T, Mellert H, et al. Myc overexpression brings out unexpected antiapoptotic effects of miR-34a. Oncogene 2011;30:2587-94.
93. Yamakuchi M, Ferlito M, Lowenstein CJ. miR-34a repression of SIRT1 regulates apoptosis. Proc Natl Acad Sci U S A 2008;105:13421-6.
94. Choi SE, Fu T, Seok S, et al. Elevated microRNA-34a in obesity reduces NAD+ levels and SIRT1 activity by directly targeting NAMPT. Aging Cell 2013;12:1062-72.
95. Menssen A, Hydbring P, Kapelle K, et al. The c-MYC oncoprotein, the NAMPT enzyme, the SIRT1-inhibitor DBC1, and the SIRT1 deacetylase form a positive feedback loop. Proc Natl Acad Sci USA 2012;109:E187-96.
96. Marshall GM, Liu PY, Gherardi S, et al. SIRT1 promotes N-Myc oncogenesis through a positive feedback loop involving the effects of MKP3 and ERK on N-Myc protein stability. PLoS Genet 2011;7:e1002135.
97. Kim T, Veronese A, Pichiorri F, et al. p53 regulates epithelial-mesenchymal transition through microRNAs targeting ZEB1 and ZEB2. J Exp Med 2011;208:875-83.
98. Gregory PA, Bert AG, Paterson EL, et al. The miR-200 family and miR-205 regulate epithelial to mesenchymal transition by targeting ZEB1 and SIP1. Nat Cell Biol 2008;10:593-601.
99. Burk U, Schubert J, Wellner U, et al. A reciprocal repression between ZEB1 and members of the miR-200 family promotes EMT and invasion in cancer cells. EMBO Rep 2008;9:582-9.
100. Kim NH, Kim HS, Li XY, et al. A p53/miRNA-34 axis regulates Snail1-dependent cancer cell epithelial-mesenchymal transition. J Cell Biol 2011;195:417-33.
101. Siemens H, Jackstadt R, Kaller M, et al. Repression of c-Kit by p53 is mediated by miR-34 and is associated with reduced chemoresistance, migration and stemness. Oncotarget 2013;4:1399-415.

102. Kaller M, Liffers S-T, Oeljeklaus S, et al. Genome-wide characterization of miR-34a induced changes in protein and mRNA expression by a combined pulsed SILAC and microarray analysis. Molecular & cellular proteomics 2011;10:M111.010462-M111.010462.
103. Mudduluru G, Ceppi P, Kumarswamy R, et al. Regulation of Axl receptor tyrosine kinase expression by miR-34a and miR-199a/b in solid cancer. Oncogene 2011;30:2888-99.
104. Ahn YH, Gibbons DL, Chakravarti D, et al. ZEB1 drives prometastatic actin cytoskeletal remodeling by downregulating miR-34a expression. J Clin Invest 2012;122:3170-83.
105. Garofalo M, Jeon YJ, Nuovo GJ, et al. MiR-34a/c-Dependent PDGFR-alpha/beta Downregulation Inhibits Tumorigenesis and Enhances TRAIL-Induced Apoptosis in Lung Cancer. PLoS ONE 2013;8:e67581.
106. Muzny DM, Bainbridge MN, Chang K, et al. Comprehensive molecular characterization of human colon and rectal cancer. Nature 2012;487:330-7.
107. Yang S, Li Y, Gao J, et al. MicroRNA-34 suppresses breast cancer invasion and metastasis by directly targeting Fra-1. Oncogene 2013;32:4294-303.
108. Li N, Fu H, Tie Y, et al. miR-34a inhibits migration and invasion by down-regulation of c-Met expression in human hepatocellular carcinoma cells. Cancer Lett 2009;275:44-53.
109. Finger EC, Giaccia AJ. Hypoxia, inflammation, and the tumor microenvironment in metastatic disease. Cancer Metastasis Rev 2010;29:285-93.
110. Semenza GL. Hypoxia-inducible factors in physiology and medicine. Cell 2012;148:399-408.
111. Leith JT, Padfield G, Faulkner L, et al. Hypoxic fractions in xenografted human colon tumors. Cancer Res 1991;51:5139-43.
112. Rankin E, Giaccia A. The role of hypoxia-inducible factors in tumorigenesis. Cell Death & Differentiation 2008;15:678-685.
113. Schindl M, Schoppmann SF, Samonigg H, et al. Overexpression of hypoxia-inducible factor 1α is associated with an unfavorable prognosis in lymph node-positive breast cancer. Clinical Cancer Research 2002;8:1831-1837.
114. Brown JM, Giaccia AJ. The unique physiology of solid tumors: opportunities (and problems) for cancer therapy. Cancer Res 1998;58:1408-16.

115. McKeown SR. Defining normoxia, physoxia and hypoxia in tumours-implications for treatment response. Br J Radiol 2014;87:20130676.
116. Thirlwell C, Schulz L, Dibra H, et al. Suffocating cancer: hypoxia-associated epimutations as targets for cancer therapy. Clin Epigenetics 2011;3:9.
117. Reynolds TY, Rockwell S, Glazer PM. Genetic instability induced by the tumor microenvironment. Cancer Res 1996;56:5754-7.
118. Coquelle A, Toledo F, Stern S, et al. A new role for hypoxia in tumor progression: induction of fragile site triggering genomic rearrangements and formation of complex DMs and HSRs. Mol Cell 1998;2:259-65.
119. Bristow RG, Hill RP. Hypoxia and metabolism. Hypoxia, DNA repair and genetic instability. Nat Rev Cancer 2008;8:180-92.
120. Jung HY, Fattet L, Yang J. Molecular pathways: linking tumor microenvironment to epithelial-mesenchymal transition in metastasis. Clin Cancer Res 2015;21:962-8.
121. Graeber TG, Osmanian C, Jacks T, et al. Hypoxia-mediated selection of cells with diminished apoptotic potential in solid tumours. Nature 1996;379:88-91.
122. Ruan K, Song G, Ouyang G. Role of hypoxia in the hallmarks of human cancer. J Cell Biochem 2009;107:1053-62.
123. Barker HE, Paget JT, Khan AA, et al. The tumour microenvironment after radiotherapy: mechanisms of resistance and recurrence. Nat Rev Cancer 2015;15:409-25.
124. Semenza GL. HIF-1 mediates metabolic responses to intratumoral hypoxia and oncogenic mutations. J Clin Invest 2013;123:3664-71.
125. Zhong H, De Marzo AM, Laughner E, et al. Overexpression of hypoxia-inducible factor 1alpha in common human cancers and their metastases. Cancer Res 1999;59:5830-5.
126. Wenger RH, Stiehl DP, Camenisch G. Integration of oxygen signaling at the consensus HRE. Sci STKE 2005;2005:re12.
127. Semenza GL, Wang GL. A nuclear factor induced by hypoxia via de novo protein synthesis binds to the human erythropoietin gene enhancer at a site required for transcriptional activation. Mol Cell Biol 1992;12:5447-54.
128. Jiang BH, Semenza GL, Bauer C, et al. Hypoxia-inducible factor 1 levels vary exponentially over a physiologically relevant range of O2 tension. Am J Physiol 1996;271:C1172-80.
129. Semenza GL. Defining the role of hypoxia-inducible factor 1 in cancer biology and therapeutics. Oncogene 2010;29:625-34.

130. Fan LF, Dong WG, Jiang CQ, et al. Role of Hypoxia-inducible factor-1 alpha and Survivin in colorectal carcinoma progression. Int J Colorectal Dis 2008;23:1057-64.
131. Chen Z, He X, Xia W, et al. Prognostic value and clinicopathological differences of HIFs in colorectal cancer: evidence from meta-analysis. PLoS One 2013;8:e80337.
132. Semenza GL. Oxygen sensing, hypoxia-inducible factors, and disease pathophysiology. Annu Rev Pathol 2014;9:47-71.
133. Tsai YP, Wu KJ. Hypoxia-regulated target genes implicated in tumor metastasis. J Biomed Sci 2012;19:102.
134. Wang H, Flach H, Onizawa M, et al. Negative regulation of Hif1a expression and TH17 differentiation by the hypoxia-regulated microRNA miR-210. Nat Immunol 2014;15:393-401.
135. Kulshreshtha R, Ferracin M, Negrini M, et al. Regulation of microRNA expression: the hypoxic component. Cell Cycle 2007;6:1426-31.
136. Dejean E, Renalier MH, Foisseau M, et al. Hypoxia-microRNA-16 downregulation induces VEGF expression in anaplastic lymphoma kinase (ALK)-positive anaplastic large-cell lymphomas. Leukemia 2011;25:1882-90.
137. Donker RB, Mouillet JF, Nelson DM, et al. The expression of Argonaute2 and related microRNA biogenesis proteins in normal and hypoxic trophoblasts. Mol Hum Reprod 2007;13:273-9.
138. Gee HE, Camps C, Buffa FM, et al. hsa-mir-210 is a marker of tumor hypoxia and a prognostic factor in head and neck cancer. Cancer 2010;116:2148-58.
139. Wu C, So J, Davis-Dusenbery BN, et al. Hypoxia potentiates microRNA-mediated gene silencing through posttranslational modification of Argonaute2. Mol Cell Biol 2011;31:4760-74.
140. Shen J, Xia W, Khotskaya YB, et al. EGFR modulates microRNA maturation in response to hypoxia through phosphorylation of AGO2. Nature 2013;497:383-7.
141. Bandara V, Michael MZ, Gleadle JM. Hypoxia represses microRNA biogenesis proteins in breast cancer cells. BMC Cancer 2014;14:533.
142. Rupaimoole R, Wu SY, Pradeep S, et al. Hypoxia-mediated downregulation of miRNA biogenesis promotes tumour progression. Nat Commun 2014;5:5202.
143. Hammond EM, Denko NC, Dorie MJ, et al. Hypoxia links ATR and p53 through replication arrest. Mol Cell Biol 2002;22:1834-43.

144. Graeber TG, Peterson JF, Tsai M, et al. Hypoxia induces accumulation of p53 protein, but activation of a G1-phase checkpoint by low-oxygen conditions is independent of p53 status. Mol Cell Biol 1994;14:6264-77.
145. Hammond EM, Dorie MJ, Giaccia AJ. ATR/ATM targets are phosphorylated by ATR in response to hypoxia and ATM in response to reoxygenation. J Biol Chem 2003;278:12207-13.
146. Lee SJ, Lim CJ, Min JK, et al. Protein phosphatase 1 nuclear targeting subunit is a hypoxia inducible gene: its role in post-translational modification of p53 and MDM2. Cell Death Differ 2007;14:1106-16.
147. Chandel NS, Vander Heiden MG, Thompson CB, et al. Redox regulation of p53 during hypoxia. Oncogene 2000;19:3840-8.
148. Galban S, Martindale JL, Mazan-Mamczarz K, et al. Influence of the RNA-binding protein HuR in pVHL-regulated p53 expression in renal carcinoma cells. Mol Cell Biol 2003;23:7083-95.
149. Blagosklonny MV, An WG, Romanova LY, et al. p53 inhibits hypoxia-inducible factor-stimulated transcription. J Biol Chem 1998;273:11995-8.
150. Ravi R, Mookerjee B, Bhujwalla ZM, et al. Regulation of tumor angiogenesis by p53-induced degradation of hypoxia-inducible factor 1alpha. Genes Dev 2000;14:34-44.
151. Yu JL, Rak JW, Coomber BL, et al. Effect of p53 status on tumor response to antiangiogenic therapy. Science 2002;295:1526-8.
152. Amelio I, Melino G. The p53 family and the hypoxia-inducible factors (HIFs): determinants of cancer progression. Trends Biochem Sci 2015;40:425-34.
153. Freed-Pastor WA, Prives C. Mutant p53: one name, many proteins. Genes Dev 2012;26:1268-86.
154. Adorno M, Cordenonsi M, Montagner M, et al. A Mutant-p53/Smad complex opposes p63 to empower TGFbeta-induced metastasis. Cell 2009;137:87-98.
155. Montagner M, Enzo E, Forcato M, et al. SHARP1 suppresses breast cancer metastasis by promoting degradation of hypoxia-inducible factors. Nature 2012;487:380-4.
156. Hermeking H. MicroRNAs in the p53 network: micromanagement of tumour suppression. Nat Rev Cancer 2012;12:613-26.
157. Mutharasan RK, Nagpal V, Ichikawa Y, et al. microRNA-210 is upregulated in hypoxic cardiomyocytes through Akt- and p53-dependent pathways and exerts cytoprotective effects. Am J Physiol Heart Circ Physiol 2011;301:H1519-30.

158. Nallamshetty S, Chan SY, Loscalzo J. Hypoxia: a master regulator of microRNA biogenesis and activity. Free Radic Biol Med 2013;64:20-30.
159. Mattagajasingh SN, Yang XP, Irani K, et al. Activation of Stat3 in endothelial cells following hypoxia-reoxygenation is mediated by Rac1 and protein Kinase C. Biochim Biophys Acta 2012;1823:997-1006.
160. Wen Z, Zhong Z, Darnell JE, Jr. Maximal activation of transcription by Stat1 and Stat3 requires both tyrosine and serine phosphorylation. Cell 1995;82:241-50.
161. Tkach M, Rosemblit C, Rivas MA, et al. p42/p44 MAPK-mediated Stat3Ser727 phosphorylation is required for progestin-induced full activation of Stat3 and breast cancer growth. Endocr Relat Cancer 2013;20:197-212.
162. Sakaguchi M, Oka M, Iwasaki T, et al. Role and regulation of STAT3 phosphorylation at Ser727 in melanocytes and melanoma cells. J Invest Dermatol 2012;132:1877-85.
163. Aziz MH, Hafeez BB, Sand JM, et al. Protein kinase Cvarepsilon mediates Stat3Ser727 phosphorylation, Stat3-regulated gene expression, and cell invasion in various human cancer cell lines through integration with MAPK cascade (RAF-1, MEK1/2, and ERK1/2). Oncogene 2010;29:3100-9.
164. Lin GS, Chen YP, Lin ZX, et al. STAT3 serine 727 phosphorylation influences clinical outcome in glioblastoma. Int J Clin Exp Pathol 2014;7:3141-9.
165. Taylor CT, Furuta GT, Synnestvedt K, et al. Phosphorylation-dependent targeting of cAMP response element binding protein to the ubiquitin/proteasome pathway in hypoxia. Proc Natl Acad Sci U S A 2000;97:12091-6.
166. Qin HR, Kim HJ, Kim JY, et al. Activation of signal transducer and activator of transcription 3 through a phosphomimetic serine 727 promotes prostate tumorigenesis independent of tyrosine 705 phosphorylation. Cancer Res 2008;68:7736-41.
167. Doktorova H, Hrabeta J, Khalil MA, et al. Hypoxia-induced chemoresistance in cancer cells: The role of not only HIF-1. Biomed Pap Med Fac Univ Palacky Olomouc Czech Repub 2015;159:166-77.
168. Yang G, Xu S, Peng L, et al. The hypoxia-mimetic agent CoCl(2) induces chemotherapy resistance in LOVO colorectal cancer cells. Mol Med Rep 2016;13:2583-9.

169. Chen J, Ding Z, Peng Y, et al. HIF-1alpha inhibition reverses multidrug resistance in colon cancer cells via downregulation of MDR1/P-glycoprotein. PLoS One 2014;9:e98882.
170. Rohwer N, Cramer T. Hypoxia-mediated drug resistance: novel insights on the functional interaction of HIFs and cell death pathways. Drug Resist Updat 2011;14:191-201.
171. Schnitzer SE, Schmid T, Zhou J, et al. Hypoxia and HIF-1alpha protect A549 cells from drug-induced apoptosis. Cell Death Differ 2006;13:1611-3.
172. Wang J, Biju MP, Wang MH, et al. Cytoprotective effects of hypoxia against cisplatin-induced tubular cell apoptosis: involvement of mitochondrial inhibition and p53 suppression. J Am Soc Nephrol 2006;17:1875-85.
173. Adamski J, Price A, Dive C, et al. Hypoxia-induced cytotoxic drug resistance in osteosarcoma is independent of HIF-1Alpha. PLoS One 2013;8:e65304.
174. Fischer KR, Durrans A, Lee S, et al. Epithelial-to-mesenchymal transition is not required for lung metastasis but contributes to chemoresistance. Nature 2015;527:472-6.
175. Wang J, Wei Q, Wang X, et al. Transition to resistance: An unexpected role of the EMT in cancer chemoresistance. Genes & Diseases 2016;3:3-6.
176. Zheng X, Carstens JL, Kim J, et al. Epithelial-to-mesenchymal transition is dispensable for metastasis but induces chemoresistance in pancreatic cancer. Nature 2015;527:525-30.
177. Arumugam T, Ramachandran V, Fournier KF, et al. Epithelial to mesenchymal transition contributes to drug resistance in pancreatic cancer. Cancer Res 2009;69:5820-8.
178. McConkey DJ, Choi W, Marquis L, et al. Role of epithelial-to-mesenchymal transition (EMT) in drug sensitivity and metastasis in bladder cancer. Cancer Metastasis Rev 2009;28:335-44.
179. Huang J, Li H, Ren G. Epithelial-mesenchymal transition and drug resistance in breast cancer (Review). Int J Oncol 2015;47:840-8.
180. Jackstadt R, Roh S, Neumann J, et al. AP4 is a mediator of epithelial-mesenchymal transition and metastasis in colorectal cancer. J Exp Med 2013;210:1331-50.
181. Hunten S, Kaller M, Drepper F, et al. p53-Regulated Networks of Protein, mRNA, miRNA, and lncRNA Expression Revealed by Integrated Pulsed Stable Isotope Labeling With Amino Acids in Cell Culture (pSILAC) and Next

Generation Sequencing (NGS) Analyses. Mol Cell Proteomics 2015;14:2609-29.

182. Kaller M, Liffers ST, Oeljeklaus S, et al. Genome-wide characterization of miR-34a induced changes in protein and mRNA expression by a combined pulsed SILAC and microarray analysis. Mol Cell Proteomics 2011;10:M111 010462.
183. Yu J, Zhang L, Hwang PM, et al. Identification and classification of p53-regulated genes. Proc Natl Acad Sci U S A 1999;96:14517-22.
184. Pillai RS, Bhattacharyya SN, Artus CG, et al. Inhibition of translational initiation by Let-7 MicroRNA in human cells. Science 2005;309:1573-6.
185. He TC, Chan TA, Vogelstein B, et al. PPARdelta is an APC-regulated target of nonsteroidal anti-inflammatory drugs. Cell 1999;99:335-45.
186. Warfel NA, Dolloff NG, Dicker DT, et al. CDK1 stabilizes HIF-1alpha via direct phosphorylation of Ser668 to promote tumor growth. Cell Cycle 2013;12:3689-701.
187. Livak KJ, Schmittgen TD. Analysis of relative gene expression data using real-time quantitative PCR and the 2(-Delta Delta C(T)) Method. Methods 2001;25:402-8.
188. Jackstadt R, Menssen A, Hermeking H. Genome-wide analysis of c-MYC-regulated mRNAs and miRNAs, and c-MYC DNA binding by next-generation sequencing. Methods Mol Biol 2013;1012:145-85.
189. Menssen A, Epanchintsev A, Lodygin D, et al. c-MYC delays prometaphase by direct transactivation of MAD2 and BubR1: identification of mechanisms underlying c-MYC-induced DNA damage and chromosomal instability. Cell Cycle 2007;6:339-52.
190. Frank SR, Schroeder M, Fernandez P, et al. Binding of c-Myc to chromatin mediates mitogen-induced acetylation of histone H4 and gene activation. Genes Dev 2001;15:2069-82.
191. Cheng CY, Hwang CI, Corney DC, et al. miR-34 cooperates with p53 in suppression of prostate cancer by joint regulation of stem cell compartment. Cell Rep 2014;6:1000-7.
192. Menssen A, Hermeking H. Characterization of the c-MYC-regulated transcriptome by SAGE: identification and analysis of c-MYC target genes. Proc Natl Acad Sci U S A 2002;99:6274-9.

193. Sato T, Stange DE, Ferrante M, et al. Long-term expansion of epithelial organoids from human colon, adenoma, adenocarcinoma, and Barrett's epithelium. Gastroenterology 2011;141:1762-72.
194. Aziz MH, Manoharan HT, Church DR, et al. Protein kinase Cepsilon interacts with signal transducers and activators of transcription 3 (Stat3), phosphorylates Stat3Ser727, and regulates its constitutive activation in prostate cancer. Cancer Res 2007;67:8828-38.
195. Moreno-Bueno G, Peinado H, Molina P, et al. The morphological and molecular features of the epithelial-to-mesenchymal transition. Nat Protoc 2009;4:1591-613.
196. Zgheib C, Zouein FA, Chidiac R, et al. Calyculin A reveals serine/threonine phosphatase protein phosphatase 1 as a regulatory nodal point in canonical signal transducer and activator of transcription 3 signaling of human microvascular endothelial cells. J Interferon Cytokine Res 2012;32:87-94.
197. Haridas V, Nishimura G, Xu ZX, et al. Avicin D: a protein reactive plant isoprenoid dephosphorylates Stat 3 by regulating both kinase and phosphatase activities. PLoS One 2009;4:e5578.
198. Stenvang J, Petri A, Lindow M, et al. Inhibition of microRNA function by antimiR oligonucleotides. Silence 2012;3:1.
199. Krutzfeldt J, Rajewsky N, Braich R, et al. Silencing of microRNAs in vivo with 'antagomirs'. Nature 2005;438:685-9.
200. Broderick JA, Zamore PD. MicroRNA therapeutics. Gene Ther 2011;18:1104-10.
201. Wurzer JC, Tallarida RJ, Sirover MA. New mechanism of action of the cancer chemotherapeutic agent 5-fluorouracil in human cells. J Pharmacol Exp Ther 1994;269:39-43.
202. Bunz F, Hwang PM, Torrance C, et al. Disruption of p53 in human cancer cells alters the responses to therapeutic agents. J Clin Invest 1999;104:263-9.
203. Kahlert C, Lahes S, Radhakrishnan P, et al. Overexpression of ZEB2 at the invasion front of colorectal cancer is an independent prognostic marker and regulates tumor invasion in vitro. Clin Cancer Res 2011;17:7654-63.
204. Siemens H, Neumann J, Jackstadt R, et al. Detection of miR-34a Promoter Methylation in Combination with Elevated Expression of c-Met and beta-Catenin Predicts Distant Metastasis of Colon Cancer. Clin Cancer Res 2013;19:710-20.

205. Leung AK, Sharp PA. MicroRNA functions in stress responses. Mol Cell 2010;40:205-15.
206. Sullivan NJ, Sasser AK, Axel AE, et al. Interleukin-6 induces an epithelial-mesenchymal transition phenotype in human breast cancer cells. Oncogene 2009;28:2940-7.
207. Kawata M, Koinuma D, Ogami T, et al. TGF-beta-induced epithelial-mesenchymal transition of A549 lung adenocarcinoma cells is enhanced by pro-inflammatory cytokines derived from RAW 264.7 macrophage cells. J Biochem 2012;151:205-16.
208. Fan F, Samuel S, Evans KW, et al. Overexpression of snail induces epithelial-mesenchymal transition and a cancer stem cell-like phenotype in human colorectal cancer cells. Cancer Med 2012;1:5-16.
209. Wang H, Wang HS, Zhou BH, et al. Epithelial-mesenchymal transition (EMT) induced by TNF-alpha requires AKT/GSK-3beta-mediated stabilization of snail in colorectal cancer. PLoS One 2013;8:e56664.
210. Bowen KA, Doan HQ, Zhou BP, et al. PTEN loss induces epithelial--mesenchymal transition in human colon cancer cells. Anticancer Res 2009;29:4439-49.
211. Stange DE, Engel F, Longerich T, et al. Expression of an ASCL2 related stem cell signature and IGF2 in colorectal cancer liver metastases with 11p15.5 gain. Gut 2010;59:1236-44.
212. Usami Y, Satake S, Nakayama F, et al. Snail-associated epithelial-mesenchymal transition promotes oesophageal squamous cell carcinoma motility and progression. J Pathol 2008;215:330-9.
213. Wu Y, Zhou BP. TNF-alpha/NF-kappaB/Snail pathway in cancer cell migration and invasion. Br J Cancer 2010;102:639-44.
214. Wang C, Liu X, Huang H, et al. Deregulation of Snai2 is associated with metastasis and poor prognosis in tongue squamous cell carcinoma. Int J Cancer 2012;130:2249-58.
215. Zeindl-Eberhart E, Brandl L, Liebmann S, et al. Epithelial-mesenchymal transition induces endoplasmic-reticulum-stress response in human colorectal tumor cells. PLoS One 2014;9:e87386.
216. De Wever O, Pauwels P, De Craene B, et al. Molecular and pathological signatures of epithelial-mesenchymal transitions at the cancer invasion front. Histochem Cell Biol 2008;130:481-94.

217. Schaafsma HE, Van Der Velden LA, Manni JJ, et al. Increased expression of cytokeratins 8, 18 and vimentin in the invasion front of mucosal squamous cell carcinoma. J Pathol 1993;170:77-86.

218. Dass SD, Cheah PL, Ong DB, et al. E-cadherin downregulation at the infiltrating tumour front is associated with histological grade and stage in colorectal carcinoma of Malaysians. Malays J Pathol 2015;37:19-24.

219. Chen J, Rocken C, Hoffmann J, et al. Expression of carbonic anhydrase 9 at the invasion front of gastric cancers. Gut 2005;54:920-7.

220. Wigerup C, Pahlman S, Bexell D. Therapeutic targeting of hypoxia and hypoxia-inducible factors in cancer. Pharmacol Ther 2016;164:152-69.

221. Chai EZ, Shanmugam MK, Arfuso F, et al. Targeting transcription factor STAT3 for cancer prevention and therapy. Pharmacol Ther 2016;162:86-97.

222. Wang X, Li J, Dong K, et al. Tumor suppressor miR-34a targets PD-L1 and functions as a potential immunotherapeutic target in acute myeloid leukemia. Cell Signal 2015;27:443-52.

223. Cortez MA, Ivan C, Valdecanas D, et al. PDL1 Regulation by p53 via miR-34. J Natl Cancer Inst 2016;108.